ABSTRACT

SHI, YUE. Integrated Volt/Var Control on Smart Distribution Systems. (Under the direction of Dr. Mesut Baran).

This study investigates the integrated Volt/Var Control (VVC) on smart distribution systems with PV penetration.

First, a two-phase VVC method is proposed to solve the Volt/Var Optimization (VVO) problem efficiently by decoupling the VVO problem into voltage problem and Var problem. In Phase I, a search based approach is used to find the optimal tap position setting for voltage regulation devices, such as load tap changer (LTC) and voltage regulator (VR). Phase II adopts the gradient based approach to determine the optimal Var injection of smart PV inverters, or solid state transformers (SST) such that the system power loss is minimized. To facilitate the coordination between the conventional slow-acting VVC devices (e.g. LTC and VR) and the fast-acting VVC devices (e.g. smart inverter and SST), a new coordinated VVC method is proposed based on the two-phase method. The proposed coordinated VVC scheme assigns the voltage problem and Var problem at two control levels. The first level uses LTC and VR to adjust the voltage level on the circuit to keep the voltages along the circuit within the range desired. The second level determines Var support needed from smart inverters or SSTs to smooth the fast voltage variations while providing effective power factor correction to keep the system power losses at minimum. For real-time implementation purpose, a master-slave based decentralized control architecture is introduced to fit the proposed VVC methods.

Case studies of proposed VVC methods show that both two-phase method and coordinated VVC method are very effective in maintaining acceptable voltages on the system under various operating conditions while meeting the operational constrains. The coordinated

VVC is more practical since it can reduce the excess operations of conventional VVC devices due to the variability of PV generation. Simulation results also show the computational efficiency of the methods. In this dissertation, accomplishment of real-time VVC on an Hardware-In-the-Loop system and Green Energy Hub system will also be presented.

Since the proposed methods are model-based approach, load modeling for VVC in smart distribution systems is also discussed in this work. A real-time load parameter estimation approach is proposed to facilitate real-time VVC such that the VVC application has knowledge of a more accurate load model and monitors the real-time performance of VVC.

Case study of load parameter estimation on an IEEE feeder with detailed load modeling for houses show that the proposed real-time estimation approach is effective to reflect the sensitivity of load to voltage change.

Integrated Volt/Var Control on Smart Distribution Systems

by
Yue Shi

A dissertation submitted to the Graduate Faculty of
North Carolina State University
in partial fulfillment of the
requirements for the degree of
Doctor of Philosophy

Electrical Engineering

Raleigh, North Carolina

2018

APPROVED BY:

_____	_____
Dr. Mesut Baran Committee Chair	Dr. Ning Lu
_____	_____
Dr. David Lubkeman	Dr. Thomas Reiland

DEDICATION

TO MY PARENTS

and

MY FAMILY

BIOGRAPHY

Yue Shi was born in Dandong, Liaoning, China. She received her B.Eng. in Electrical Engineering from Tianjin University in 2012 and M.Sc. of in Electrical Engineering from North Carolina State University (NCSU) with thesis *An Investigation of Volt/Var Control on FREEDM Systems* in 2014. She joined FREEDM Systems Center as a research assistant under the guidance of Dr. Mesut E. Baran in 2013, and then started to pursue the Ph.D. degree at NCSU in 2014. She interned at Quanta Technology in 2015, at General Electric in 2016, and ABB in 2017. Currently, she is a consultant at ABB US Power Consulting. Her research interests include power distribution system optimization and control, Volt/Var control, and assessment of smart distribution technologies.

ACKNOWLEDGMENTS

My sincere gratitude goes to the people who made this work possible.

To my advisor, Dr. Mesut Baran, who has continuously guided and encouraged me with his insight and patience throughout the time I was at NC State University.

To my committee members, Dr. Ning Lu, Dr. David Lubkeman and Dr. Thomas Reiland, for their time, valuable suggestions and help.

To my research fellows in the FREEDM Systems Center and colleagues in Quanta Technology, GE and ABB. It is a great pleasure to work with all of you.

To all my friends, for the time we've been through together. I feel so lucky to have you all.

And last and foremost, to my parents, Baode Shi and Zhimin Sun, for their love and support throughout my entire life.

TABLE OF CONTENTS

LIST OF TABLES

LIST OF FIGURES

CHAPTER 1. Introduction

Volt/Var Control (VVC) is the process of managing voltage levels and reactive power (Var) to make the power distribution system work at a desirable operating point. Utilities have been using VVC for many years to maintain acceptable voltages for distribution systems. With the advancement of device technology and analysis methods in power systems, more advanced VVC, named Volt/Var Optimization (VVO), is under development. In this chapter, the motivations, control devices, benefits and challenges of VVO is discussed, and a formulation of VVO problem for a smart distribution system is also presented.

1.1 Overview of Volt/Var Control

For a distribution system with a radial structure, the voltage drops gradually as the distance from the substation increases. The ANSI C84.1 standard [1] specifies the recommended "service voltage" for "range A" as ±5% of the nominal value (i.e., 114 V ─ 126 V for a nominal service voltage of 120 V). Under heavy load conditions, without VVC, a distribution system may experience under-voltage violation as shown by the blue line on Figure 1.1. Since distribution system voltage regulation is a fundamental requirement for all utilities, the primary goal of VVC is to maintain the voltages along a distribution feeder within an appropriate range under all operating conditions.

The means to achieve VVC falls into the two following categories:

1) Voltage regulation by LTC or VR
2) Var compensation by smart inverters, CAPs, etc.

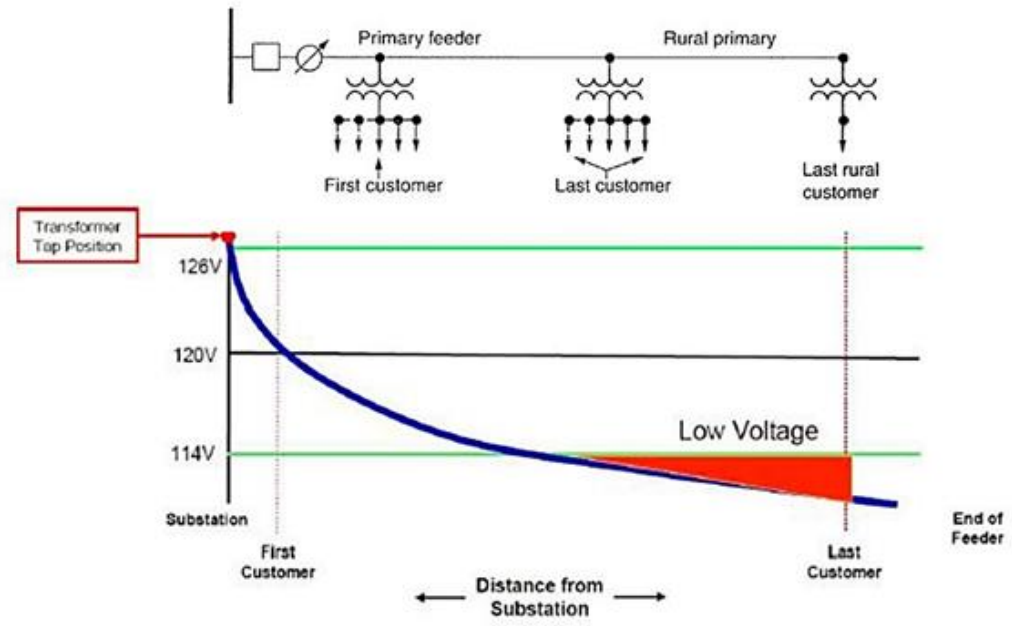

Figure 1.1 Feeder voltage under heavy load condition

In conventional distribution systems, voltage regulators (VRs), load tap changers (LTCs) and capacitor banks (CAPs) are the devices that have been used for Volt/Var control (VVC) purpose. With the increasing penetration level of distributed renewable energy resources (DRERs) on distribution system, PV with smart inverters or solid state transformers (SSTs) are considered as Var control devices [2]. In traditional VVC, VRs and LTCs are controlled based on local measurements, and they are coordinated by differentiating the time-delay setting [3], [4]. In this local control mode, the user can configure the voltage set point of a VR or LTC, and then the controller gives command of increasing/decreasing the tap position to regulate the voltage to the set point by changing the turns ratio. The control of The capacitors is realized by manually switching at the substation or by automatic control, including time-switched, voltage-controlled, voltage-time-controlled, voltage current-controlled and temperature-controlled schemes [3].

With the extension of supervisory control and data acquisition (SCADA) to distribution system, the traditional VVC can be improved to achieve more benefits while keeping the voltages acceptable. More advanced controllers with remote control function enable VR, LTC and Caps to receive command by the SCADA system. In remote control mode, VR and LTC receive command of tap increasing/decreasing from the control center [5], [6], and Cap receive command of on/off. On the other hand, high level of DRER penetration imposes new challenges on traditional VVC. Therefore, researchers started to develop more advanced VVC schemes, Volt/Var optimization (VVO), which is a process of optimally managing voltage levels and reactive power to achieve more efficient gird operation by solving an optimization problem.

Although the primary goal of VVO is to keep voltages within acceptable range, the benefit of VVO falls into the following three aspects:

1) Power quality, such as the improvement of voltage profile and power factor.
2) Energy saving, for example power loss reduction and peak demand reduction.
3) Reduction of control cost.

Among the proposed approaches, [7] uses power loss, and [8] uses control cost minimization as the objective function. Other objectives including demand reduction and power factor correction are mentioned in [9] .

With different formulations of VVO problem, the methods to solve them vary as well. The VVO methods can be divided into two categories: i) centralized VVO, for example in [7], [10] and [11], and ii) decentralized VVO, for example in [12], [13] and [14].

With the promotion of smart grid technology, the planning and operation of distribution systems evolves and VVO should take the challenges associated with the smart features in distribution systems. A traditional distribution system considers discrete control variables (LTC, VR and CAPs) only: LTC and VR change the voltage by moving the taps, and Caps change the reactive power flow by connecting/disconnecting to the feeder. However, in modern distribution system, with the proliferation of DRERs, smart inverters and SSTs reactive power can be injected into the system in continuous amount. Therefore, VVO should be able to handle both continuous and discrete variables. Besides, DRER generation adds more uncertainty to the system net load profile. Traditional VVC runs in an offline manner due to the unavailability of data from real-time monitoring. Even though, with short-term forecasting technology the PV prediction can be updated as frequently as 15 min [15], the actual PV generation may vary in much smaller time interval. In smart distribution system, the SCADA system has the access to real-time data from smart meters at the loads, inverters and/or SSTs at the DRERs, enabling VVO to run in real-time to optimize the system operation timely. However, for a large distribution with many DRERs and loads, a centralized VVO scheme has a high communication requirement due to the large number of real-time data exchanged at the control center. This drives the centralized VVO structure into decentralized VVO structure. To address the issues mentioned above a master-slave based master-slave based decentralized VVO architecture is proposed in Chapter 2.

Nowadays, vendors such as GE Grid Solutions, Eaton and Siemens have developed centralized VVO application (as known as Integrated Volt/Var Control, IVVC) as one of the main functions in their Distribution Management System (DMS) software. To take the IVVC

application from Eaton, as shown in Figure 1.2, as an example, IVVC application utilizes the real-time data from LTC, VR, CAPs and monitoring points such as customer meter and medium voltage sensor to find the optimal operation of VVC devices to minimize the operational cost [16]. In centralized IVVC, each device with communication capability exchanges real-time data directly with the RTU (Remote Terminal Unit, a component of SCADA). And the real-time data collected by the RTUs at different substations and remote locations on the feeder are pooled by the MTU (Master Terminal Unit, a component of SCADA) at control center [17]. In some of the available products, the IVVC function will run periodically at a user adjustable time interval (typically ≥ 15 min), or when a significant change in feeder loading occurs.

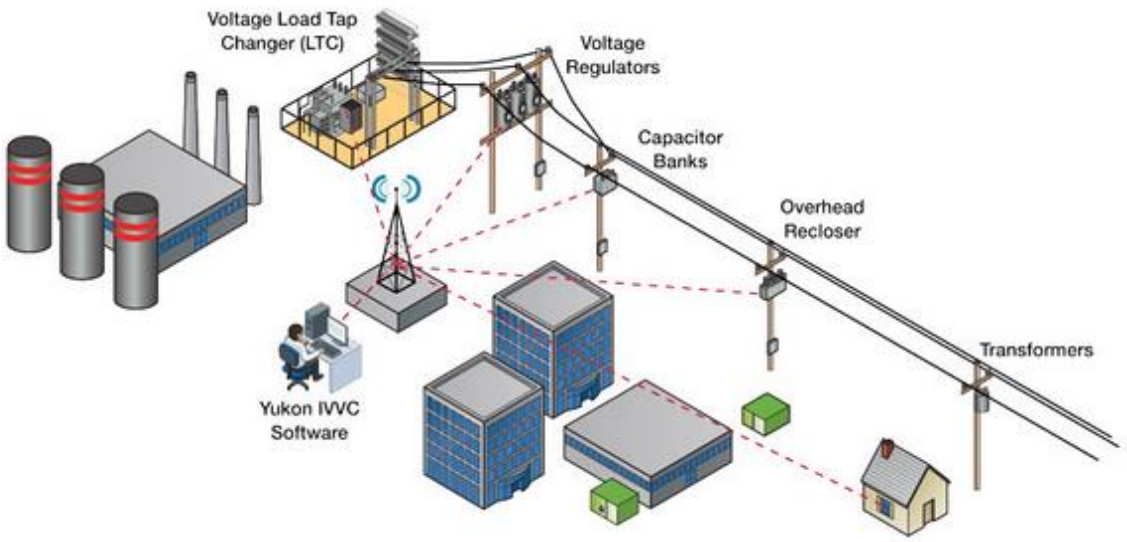

Figure 1.2 Yukon IVVC Application from Eaton [16]

Most of VVC schemes proposed in the literature, aim at determining the set points for the Volt-Var control devices at a given operation point, and thus formulate the VVC as an

optimal power flow problem. To formulate the Volt/Var control as an optimization problem, one needs to determine the objective and then the constraints.

The objective of VVO would be minimizing one or a weighted combination of the following terms:

1) Power loss or energy loss [7]
2) Control cost [13]
3) Voltage variation [18]
4) Peak demand [19]

The constraints of VVO include both equalities and inequalities. The equality constraints represent power flow of the system. Due to the high R/X ratio of distribution networks, the non-linear and non-convex power flow equations is not recommended to be simplified into linear form, which makes it challenging to solve the VVO problem. The inequality constraints include, but are not limited to:

1) Voltage limits
2) Tap position limits of LTC and VR
3) Maximum number of switches for CAPs
4) Line current limits
5) Power factor limit at either substation or other points in the system
6) Three-phase balancing constraints on the main feeder

Based on different selected objective functions and constraints, the VVO problem can be generally classified into the following categories:

1) Linear Programing (LP) problem, where both the objective function and the constraints are linear and the variables are all continuous variables.

2) Mixed Integer Linear Programing problem (MILP), where both the objective function and the constraints are linear, but the variables include both continuous and discrete variables.
3) Non-linear Programing problem (NLP), where either the objective function selected is non-linear or the constraints has non-linear term, and the variables are all continuous variables.
4) Mixed Integer Non-linear Programing (MINLP) problems, where either the objective function selected is non-linear or the constraints has non-linear term, and the variables include both continuous and discrete variables.

The above four types of VVO problem can be solved centrally by directly applying various optimization techniques[20], [21]. An LP VVO can be solved by either simplex method or interior point method, however it applies to a distribution system with continuous control variables only. [10] models the VVO as an MILP problem. Although the accuracy of the MILP model is adequate, the computation time is too long for real-time implementation. In [10], it takes 200-400 s to solve and MILP VVO for a system with 34 nodes. For an NLP VVO, successive linear programing can be used to find the optimal solution. Like the LP approach, this method cannot handle the VVC device operating in a discrete manner, such as Caps and VR. The MINLP VVO is the most difficult one to be solved. [22] uses the mixed integer conic programming technique to solve an MINLP VVO, however it also suffers long computation time, thus not suitable for real-time implementation.

VVO problems can also be solved in a decentralized fashion [14], [23], [24] . The idea is to decompose the original problem into sub-problems and to use the master problem to coordinate the sub-problems. [14] solves a successive linear programing (SLP) based VVO by Dantzig-Wolfe decomposition. Others use heuristic algorithms to realize the decentralized

optimization [22], [23]. However, little research has been done to integrate the decentralized optimization based VVO into the DMS system.

1.2 Proposed Volt/Var Control Schemes

In this work, the Volt/Var Control problem is formulated as an optimization problem aiming at minimizing power loss with operating constraints considered.

In conventional distribution systems, voltage regulators, and load tap changers (LTCs) and capacitor banks (CAPs) are the devices that have been used for Volt/Var control (VVC) purpose. With the increasing penetration of DRERs, smart inverters are encouraged to be used as Var control devices [25], [26]. The main contribution of this work is to propose effective Volt/Var Control schemes which utilize both conventional VVC devices and DRER, especially PV systems.

A general formulation of VVO problem to minimize power loss is shown in formulas (1-1) to (1-4).

$$min \;\; f(x,u) = P_{loss}(x) \qquad (1\text{-}1)$$

$$s.t. \;\; g(x,u) = 0 \qquad (1\text{-}2)$$

$$V^{min} \le V \le V^{max} \qquad (1\text{-}3)$$

$$u^{min} \le u \le u^{max} \qquad (1\text{-}4)$$

where $x = [\theta; V]$ is the state variable which is the vector containing voltage angles and magnitudes, and u are the control variables which will be discussed in detail later. The full expression of power loss function is in the following equation [27]:

$$P_{loss}(V,\theta) = \sum_{i \neq j} g_{ij}\left[V_i^2 + V_j^2 - 2V_iV_j\cos\left(\theta_i - \theta_j\right)\right] \quad i, j \in \mathbb{N} \qquad (1\text{-}5)$$

where g_{ij} is the branch conductance, $\mathbb{N}$ is the set that contains all the nodes in the system.

The equality constraints in (1-2) correspond to power flow equations [27]:

$$g(x,u)=\begin{bmatrix} P_{Gi}-P_{Li}-V_i\sum_j V_j\left(G_{ij}\cos\theta_{ij}+B_{ij}\sin\theta_{ij}\right) \\ Q_{inji}-V_i\sum_j V_j\left(G_{ij}\sin\theta_{ij}-B_{ij}\cos\theta_{ij}\right) \end{bmatrix}=0 \quad i,j\in\mathbb{N} \tag{1-6}$$

where P_{Gi} is the real power generation from the PV at node *i*, P_{Li} is the real power consumption at node *i*, Q_{inji} is the reactive power injection at node *i*, $\theta_{ij}=\theta_i-\theta_j$ is the voltage angle difference between node *i* and node *j*, $G_{ij}+jB_{ij}=Y_{ij}$ is the element of Y-bus matrix.

This work focuses on developing an effective Volt/Var Control scheme for smart distribution systems with DRERs, especially PV systems. PV systems generating DC power need inverters or SSTs to connect to the grid. These devices have the capability to act as a reactive power sources or sink. Therefore, the dispatchable Var from DRER will be considered as one of the control variables to realize the goal of VVC.

The VVO for smart distribution systems aims at minimizing power loss while keeping feeder voltages acceptable under all operating conditions. The FREEDM Notional Feeder, as shown in the dashed box in Figure 1.3, is used to illustrate how the VVO problem is formulated. In a FREEDM System, SST is used to convert DC voltage of PV into AC voltage and to boost the voltage to grid voltage level. As Figure 1.3 shows, there are nine SSTs in the Notional Feeder system, and each of them has both load and PV connected. With the Load and PV profile shown in Figure 1.4, the SSTs are sufficient to main the feeder voltages

within acceptable range. Therefore, on this test feeder there is no need to install VR, LTC or Cap. The objective of the VVO problem on the FREEDM Notional Feeder system is to minimize the power loss as shown by equation(1-5). The voltage magnitude on the feeder is restricted by the constraint in (1-3). Constraint (1-4) indicates that the reactive power from SST should be limited by the capacity of SST. The solution u^* of the VVO problem represented in (1-1) – (1-4) is the optimal reactive power injection $Q_{inj}{}^*$ of the nine SSTs on FREEDM Notional Feeder.

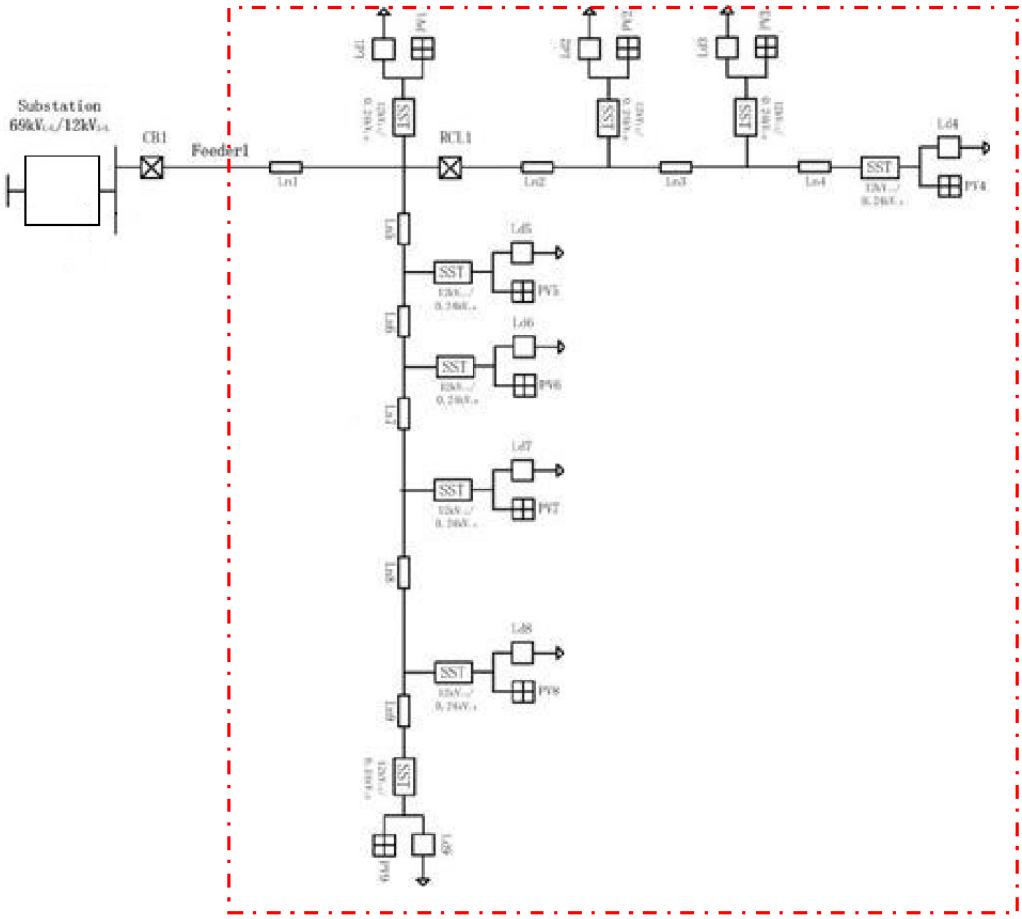

Figure 1.3 Simple diagram of FREEDM Notional Feeder

In a large FREEDM system, for example the FREEDM IEEE 34 System, both voltage regulating devices (LTC and/or VR) and SSTs are using as VVC devices. The solution of VVO u^* should give the optimal tap position of each voltage regulating device and the optimal reactive power injection of each SST. The inequality constraint in (1-4) should be expanded into the following inequalities.

$$Q^{min} \le Q_{inj} \le Q^{max} \quad (1\text{-}7)$$

$$Tap_{LTC}^{\min} \le Tap_{LTC} \le Tap_{LTC}^{\max} \quad (1\text{-}8)$$

$$Tap_{VR}^{\min} \le Tap_{VR} \le Tap_{VR}^{\max} \quad (1\text{-}9)$$

where Q_{inj} is continuous variable, Tap_{LTC} and Tap_{VR} are discrete variables representing the tap positions of LTC and VR. (1-7) indicates that the reactive power injection should be limited by the reactive power capacity of SSTs. The tap position limitations of LTC and VR are represented by the inequalities in (1-8) and (1-9) .

Hence, to be general, the VVO problem for FREEDM System is a non-linear optimization problem with both discrete and continous variables. The discrete variables correspond to voltage control devices, LTC and VR. The continous variables correspond to Var control devices, SST. The solution of the VVO problems should the give the optimal setting of all VVC devices. In reality, LTC and VR are remotely controlled by command of tap increasing/decreasing, therefore the tap postion in the solution of VVO, Tap^*, needs to be converted into tap change, ΔTap^*, in implementation to model the control of actual VR and

LTC. The SST in the FREEDM system has a local controller to process the command, Q_{inj}^{*}, therefore no conversion is needed.

In order to solve the optimization problem above efficiently, a two-phase method is proposed in Chapter 2.

1) Phase I: Voltage Problem
2) Phase II: Var Problem

By decompsing a MINLP problem into an integer problem and an NLP problem, the proposed two-phase method is comuputationally efficient to be implemented in real-time VVO. The proposed method can be applied to a master-slave based decentralized control scheme to realized power loss minimization and acceptable feeder voltage. Details of this VVC scheme can be found in Chapter 2.

Case studies of the two-phase methods shows a significant tap changes of LTC and VR throughout day. Therefore, to mitigate the excessive operation of these electric-mechanical devices, a coordinated Volt/Var Control scheme is proposed based on the methodology of two-phase method. The slow acting devices like VR and LTC are controlled in a slow loop, while the faster acting devices such as SST and inverter are controlled in a fast loop. Details of this VVC method are presented in Chapter 3.

Chapter 2. Two-phase Volt/Var Control Scheme

Since the IVVC designed for smart distribution systems should be able to react to load and DRER generation change in real-time, a Mixed-Integer Programing solver is not recommended to be used due to long runtime when discrete variables involved. In this chapter, a two-phase decoupled VVO method is proposed and implemented as a master-slave based VVC architecture. The effectiveness of the proposed VVC scheme is verified by case studies on two FREEDM Systems, FREEDM Notional Feeder and FREEDM IEEE 34 System.

2.1 A Two-phase VVO Method

Based on the linear model of VR in [7], the power loss change due to VR depends on voltage magenitude change only [7]. Pratically, VR in the system keeps the voltages on the feeder within a tight limits, therefore within the small voltage range power loss change due to VR is small. With voltages regulated in a small, the power loss change is mainly due to CAP's Var support. Hence, a VVO problem presented in section 1.3 can be decoupled into two problems, Voltage problem (to adjust VR to limit the voltage to a tight range) and Var problem (to change the Var compensation to minimize the power loss [7]. Since a well-regulated voltage profile is required for decoupling the original VVO, Voltage problem needs to run before solving the Var problem. Figure 2.1 shows a diagram of the two phased method. Phase I – Voltage problem gives the solution of discrete control variables, the tap positions for LTC and VR. Phase II – Var problem gives the optimal reactive power injection from SSTs.

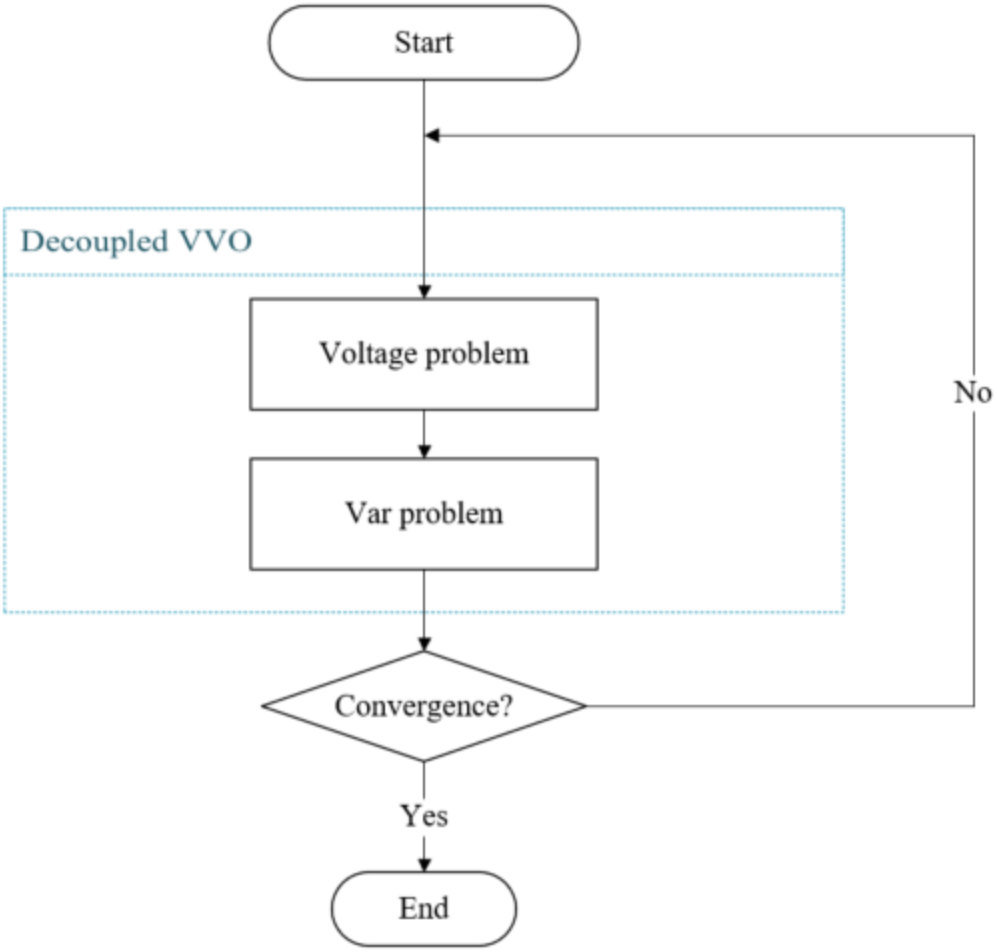

Figure 2.1 Decoupled Volt/Var Optimization

Phase I Voltage Problem

Since the ANSI C84.1 standards [1] specify a required voltage range for distribution feeders. The goal of the voltage control problem here is to maintain voltages within the range of 0.95 p.u.- 1.05 p.u.. Since 1) the control variables of the voltage problem, the VR and LTC tap positions, are discrete, and 2) the combination of tap positions of LTC and VRs that satisfy the voltage requirement is not unique, a complete search approach, in which all

combinations are visited in the search, can be adopted to search for the possible tap position combinations of LTC and VRs.

LTC or VR usually has usually 33 taps, including the zero-tap position, and each tap corresponds to a 0.00625 p.u. of turns ratio change. The LTCs are typically three-phase controlled and installed at the substations. In this work, since we use the secondary side voltage of LTC as the slack bus to solve the power flow, the secondary side voltage of LTC can be represented by a set of discrete voltage values in p.u., which indicates the tap position of LTC. Therefore, In the examples and simulation results in this chapter, the tap position of LTC is represented by voltage in p.u.. The tap positions of VR are still represented by integer numbers. For VRs, the three phases are usually controlled independently. For example, a system with one LTC and one VR has possible tap position combinations of $33 \times 33 \times 33 \times 33 = 1{,}185{,}921$. Therefore, the complete search is not an efficient way to obtain the solution of Phase I problem.

For an operating distribution system, voltages change after the change of system load and/or the output of DG and/or storage devices, therefore VVC devices are expected to make adjustment to follow such changes to achieve feasible voltages. In the proposed two-phase VVO, Phase I brings the system voltages to a small range within 0.95-1.05 p.u. by increasing/decreasing the tap of LTC and/or VR. In addition to the computation inefficiency of a complete search, drastic change of the states of the tap position due to the next run of VVO should be avoided. And due to the limited life span of taps, excessive movement in a

time interval is not desired as well. Considering the practical operation of VR and LTC, a complete search on all taps is not necessary.

To avoid such huge number of searches, a searching approach based on [28] is proposed. Instead of searching all possible 33 taps, [28] considers initial tap and two taps up and down for LTC and VR: $\Delta Tap = \{0, \quad \pm 1, \quad \pm 2\}$. In this way, the system in the previous example has a possible tap position combinations of $5 \times 5 \times 5 \times 5 = 625$, which is a significantly smaller number. The proposed search method can narrow down the searching further by applying additional rules to determine ΔTap.

In this work a backward-forward distribution power flow solver, DPF[29], is utilized to provide power flow solution to evaluate the feasibility of the tap position combinations found. To start the Phase I –Voltage problem, an initial tap position should be given. The search always starts from the substation and moves towards the downstream devices. This is to mimic the time setting to coordinate multiple voltage regulating devices in the system. In the proposed method, the following rules for VR are used to reduce the number of search:

Starting from the voltage control device closest to the substation (e.g. LTC), run DPF for each possible tap position of that device while keeping the taps constant for any other downstream voltage control devices.

1) If no voltage violation occurs, a full search for downstream devices in which $\Delta Tap_{VR}^{p} = \{\pm 1, \quad \pm 2\}$ is conducted.
2) If voltage violation occurs, for the downstream devices
   i) If $V_p^{min} < 0.95$, $\Delta Tap_{VR}^{p} = \{+1, \quad +2\}$ is conducted, where *p* represents phase a, b or c, V_p^{min} is the minimum system voltage in phase p.

ii) If $V_p^{max} > 1.05$, $\Delta Tap_{VR}^{p} = \{-1, \quad -2\}$ is conducted, where p represents phase a, b or c, V_p^{max} is the maximum system voltage in phase p.

The idea of the rules is to avoid searching the increasing taps when over-voltage violation occurs and to avoid searching the decreasing taps when under-voltage violation occurs. Figure 2.2 summarizes the rules above.

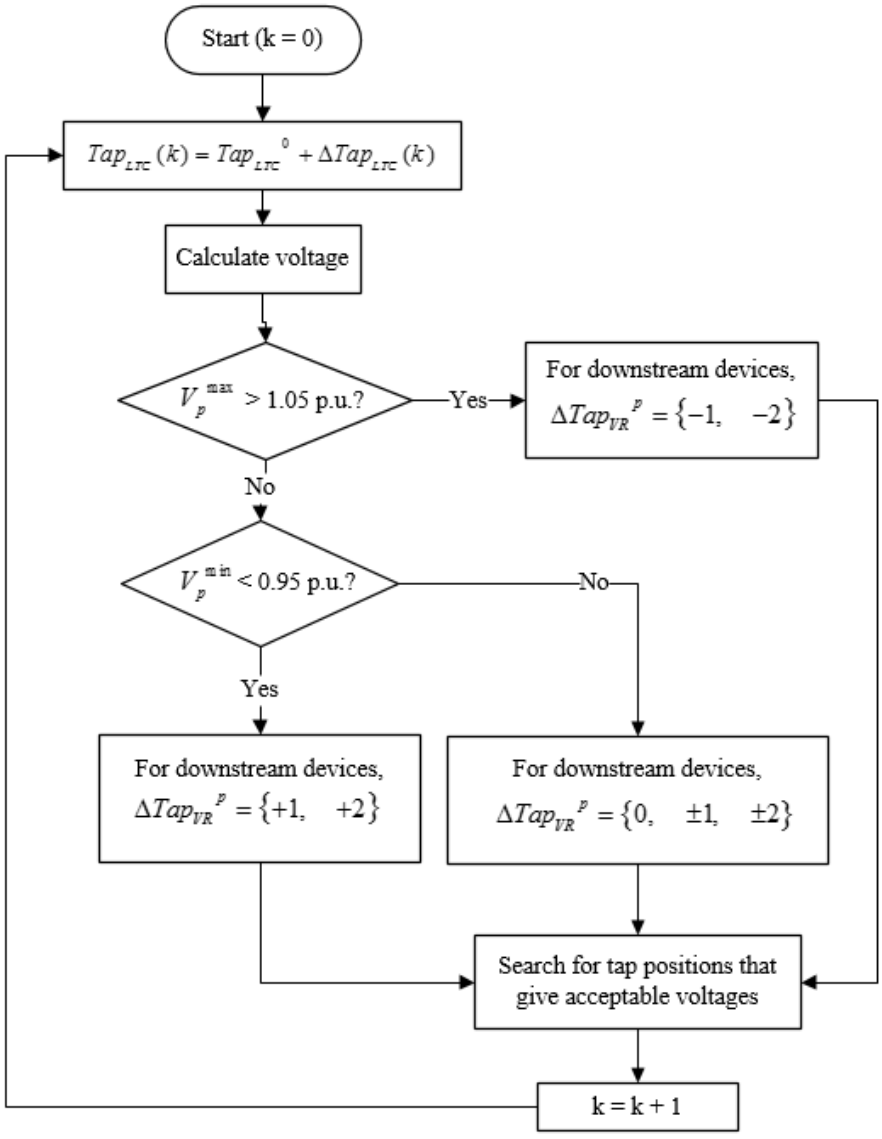

Figure 2.2 Search method for Phase I

Consider the following case as an example:

- Voltage control devices in the system: 1 LTC (three-phase controlled) at substation and 1 feeder VR (single-phase controlled)
- Initial tap positions: $Tap_{LTC} = 1.05$ p.u. and $Tap_{VR} = [7 \quad 5 \quad 6]$
- Initial power flow: $V_b^{min} < 0.95\ p.u.$ and $V_c^{min} < 0.95\ p.u.$.
- Load condition: heavy load

The first step in the proposed search method is to determine the possible tap position combinations. The next step is to use power flow solver to find the feasible combinations.

In this example, the initial setting of LTC is 1.05 p.u. Since 1.05 p.u. hits the upper voltage limit of the ANSI requirement [1], LTC tap positions higher than 1.05 p.u. (increasing tap positions) will not be considered. Therefore, only three tap position settings for LTC are considered. The original search method in [28] gives $5 \times 5 \times 5 = 125$ VR tap position combinations for LTC tap position = 1.05 p.u.. With the proposed scheme, phase b and c have low voltage violation, therefore only the VR taps that help raise the voltage are considered, as shown in Table 2.1. Hence, the number of possible combination when LTC is set as 1.05 p.u. becomes $5 \times 2 \times 2 = 20$, which is much smaller than 125. The above procedure should be repeated on the other two possible LTC tap positions as well.

Table 2.1 Possible VR tap positions when LTC tap = 1.05 p.u

ΔTap	-2	-1	0	+1	+2
Tap_{VR}^{a}	5	6	7	8	9
Tap_{VR}^{b}				6	7
Tap_{VR}^{c}				7	8

In the second step, power flow results of all the possible combinations are compared with the voltage upper and lower limits to find the feasible solutions for Phase I problem. Since the solution from Phase I is not unique, a criterion is needed to determine the best solution to initialized Phase II problem. Since Phase II is to minimize the power loss, in order to save the computation effort in Phase II, the tap position combination with least power loss can be selected as the criterion. Solution with the least voltage variance can also be used to initialize Phase II, because power loss with small voltage variance is very close to the minimum power loss.

Phase II Var Problem

The VVO scheme in this work is designed for the smart distribution systems which have DRERs accommodated by either SSTs or smart inverters. This section will use FREEDM system to illustrate the proposed VVC scheme. In FREEDM systems, SST can provide sufficient reactive power for the purpose of VVO. Therefore, capacitors are not necessary in the FREEDM systems and the control variables in the Var problem are the reactive power injection by SSTs, which are continuous variables. With the best solution from Phase I, the Var problem can be obtained from the original problem defined in (1-1) to (1-4) with fixed

tap positions. Therefore, the Var problem only involves continuous and therefore it becomes an NLP optimization problem.

This NLP problem can be solved approximately by a sequential line search method [20], [21] , or Successive Linear Programming (SLP) method. In SLP method, the optimal of an NLP problem is found by solving a sequence of first-order approximations (i.e. linearizations). In [30] , the Var problem is solved by a SLP method. However, the SLP based method takes much time to update linear model and the determination of linear trust region is challenging for a complicate problem like Var optimization.

In this work, a gradient based method is adopted to solve the Var problem. Although, second order methods, such as Newton and quasi Newton, converge faster than gradient method, for the proposed online VVC architecture with a 5 min control interval, the performance of gradient method is quite satisfying (see case study results of runtime in Chapter 2 and Chapter 3). Essentially, the proposed gradient based method is a sequential line search method along the direction of steepest descent. The steepest descent (negative gradient) of the objective function with respect to the control variables, $-\nabla f_u$, provides an effective direction for updating the control command [31]. To obtain the optimal solution of the NLP problem, the gradient should be updated iteratively, and an optimal step-size needs to be determined in each steepest descent direction. Figure 2.3 shows how a sequential line search approach based on steepest descent (updated gradient method) is applied to solve the Var problem. In this figure, the iterator *i* is for the outside loop to update the gradient.

In each search along the steepest descent, the gradient $\nabla f_u(i)$ is calculated first (details of calculating ∇f_u is given in Appendix A) and then the control variable is updated as

$$u(i) = u(i-1) - \beta^*(i) \cdot \nabla f_u(i) \qquad (2\text{-}1)$$

In each gradient update, the challenge is to determine the best step size $\beta^*(i)$ such that the objective function (power loss) is minimized without violating voltage constrains. The best-step size can be found by an inner loop search as shown in Figure 2.4. The power loss shown in Figure 2.3 and Figure 2.4 comes from the power flow solver, DPF, instead of the summation of objective functions for each phase.

As the figure shows, β is updated as

$$\beta(k+1) = \beta(k) \cdot \gamma \qquad (2\text{-}2)$$

for some $\gamma > 1$. The largest $\beta(k)$ which achieves the maximum power loss reduction without violating the voltage constraints is selected as $\beta^*(i)$. There're also other methods such as Armijo's rules [21] to determine $\beta^*(i)$. However, to use Armijo's rules, an effective (neither too large nor too small) $\beta(0)$ should be selected based on Lipschitz constant which is usually unknown for a complicate function like power loss function in VVO [20], [21]. In the proposed method, the initial value $\beta(0)$ is selected such that the minimum change for the control (SSTs) $|\Delta u|^{\min}$ is some small value, for example 0.01 kVar. In the proposed gradient method, a larger $\beta(0)$ or γ can reduce the number of iterations to get $\beta^*(t)$, thus speeding up the convergence. However, larger $\beta(0)$ results in reluctance of SST to respond to system change and larger γ results in more inaccuracy of the solution.

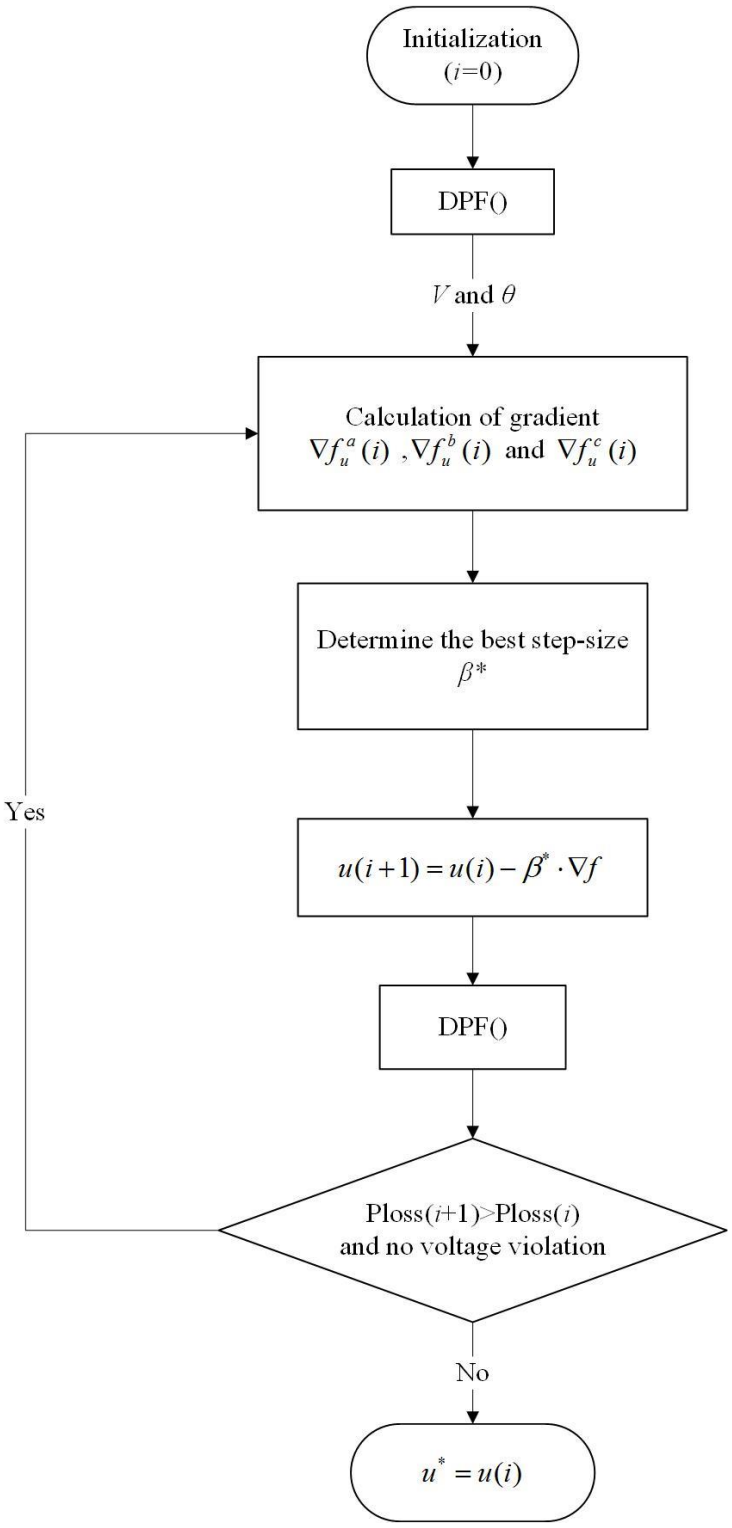

Figure 2.3 Updated gradient based Volt/Var optimization

In the proposed method, the gradient is calculated phase by phase, which means problem modeled in equation (1-1) – (1-4) is formulated for each phase. Although, setting total power loss of three phases as the objective and using three-phase power flow equations can be more accurate, the single-phase formulation reduces the dimension of the matrices involved (e.g. Jacobian matrix of power flow equations) in gradient calculation by 2/3.

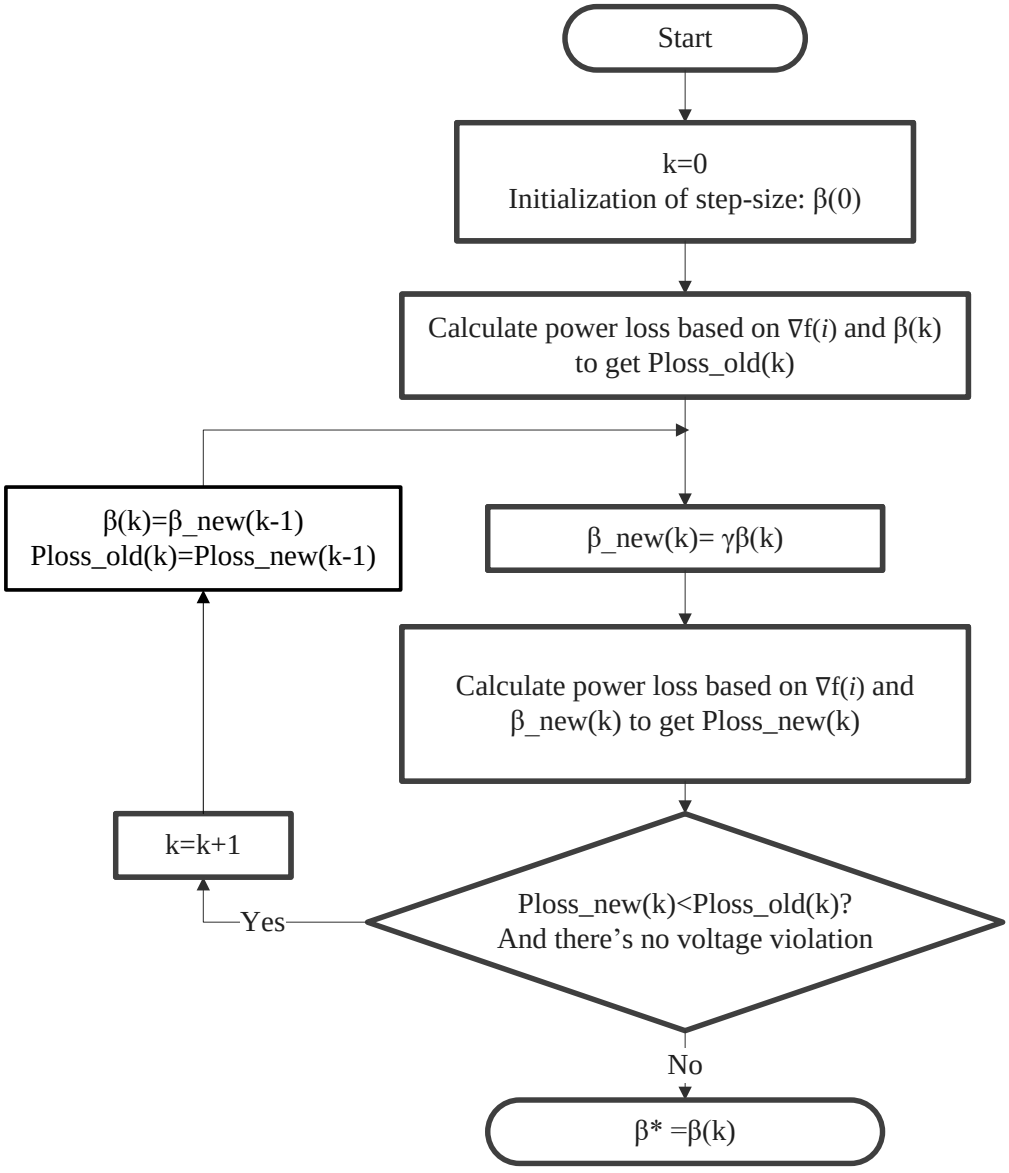

Figure 2.4 An iterative step-size searching method

Real-time implementation of VVO involves updating the control every 5-10 minutes. In each control updating period, an $u^*$is determined by the proposed VVO method. The simulation results in section 2.3 shows that in some situations the proposed gradient approach performs better than the SLP method to solve the Var problem.

2.2 Master-slave based Volt/Var Control Scheme

In conventional distribution systems, there's no processing capability at the substation. The VVO problem is solved at the control center managing multiple substations. In centralized VVO scheme, the SCADA system at the control center receives data from all intelligent devices at feeder level. "Centralized" here refers to the topology of the communication network. Real-time centralized VVO places heavy communication burden on the control center in a system with large number of remote monitoring devices.

Distributed Volt/Var control on smart inverters or SSTs is effective to avoid voltage violation [26], [27]. In this approach, the control is generated locally at the inverter or SST and no centralized communication to the control center is needed. However, such distributed Volt/Var control scheme mainly focus on voltage issue without considering other benefits of VVO, such as power loss reduction. Due to approximations of system models, this approach is lack of system level optimization.

Recent efforts have been made to develop decentralized VVO and there're several reasons as listed below:

1) Communication requirement is high for centralized VVO scheme
2) The size of a centralized VVO problem can be very large
3) Smart distribution systems enable communication and processing capability at the feeder level

For a large distribution system with a great number of smart inverters or SSTs, the VVO problem can be very large, which needs more computation efforts. Therefore, researches have been conducted to apply decentralized computation techniques to the VVO problems. Decentralized optimization techniques [20], [23], [24] , in which a large problem are

decomposed into smaller sub-problems, have been proposed to solve a large NLP problem. [11] and [14] implement the Dantzig-Wolfe decomposition to decompose the SLP based VVO problem into sub-problems coordinated by the master problem. However, this decomposition technique solves a LP problem at the cost of more iterations to update the master and sub-problems [20] and it has the same drawbacks as the SLP based VVO. Therefore, the proposed two-phase VVO method is computationally more efficient to be considered for real-time implementation for smart distribution systems.

In a smart distribution system, multiple intelligent agents (for example the DGI nodes in FREEDM systems) in the network can compute and communicate. This enables the implementation of a decentralized control architecture.

Hence, as a trade of between centralized and purely decentralized approach, a master-slave based decentralized VVC architecture is proposed for implementation in smart distribution systems. In the proposed master-slave VVC architecture, intelligent agents at the feeder level can utilized the real-time data to generate the control for the VVC devices in the system. Therefore, there's no need to send those real-time data to the control center to utilize the DMS system to run VVO. The proposed master-slave VVC architecture can greatly reduce the data exchange at the control center.

Grouping of the VVC devices

Since a distribution feeder line section can be rather short, the distance between SSTs can be short. And therefore, sensitivity of the power loss to Q_{inj} for the SSTs that are close to each other will be very similar. Indeed, when we examine the gradient ∇f_u we can see that it

is the case. This observation indicates that we can group the SSTs that are close to each other together and put them under a local "slave controller", so that all the SSTs in this group can be controlled together. This is the approach used to group the SSTs on a feeder into smaller clusters and develop a decentralized scheme based on this clustering. The grouping results of FREEDM IEEE 34 systems later in section 2.4 can also be verified by applying data mining techniques to power loss sensitivity of each nodes (see in Appendix B).

Master-slave based decentralized VVC architecture

To coordinate the control among the groups, a "master controller" is used to act as a supervisory controller feeding the updated signals to slave units based on the gradient method. In the master, the two-phase approach can solve the VVO problem more efficiently than using MINLP optimization techniques, which enables the proposed VVO to run in real-time. After the solution in Phase II is obtained by the gradient method, the solution vector u^* is partitioned according the grouping of SSTs, and then sended to the corresponding slave units, as shown in Figure 2.5. Figure 2.6 shows the participation. The index *mi* refers to index of VVO slaves, and Δu_{mi}^* corresponds to all SSTs managed by slave *mi*.

After receiving the message for the gradient, each slave allocates the reactive power injection based on the capacity of reactive power support of SSTs. For each SST under a VVO slave,

$$u_i = \left(\sum_{i=1}^{i\max} u_i^* \right) \cdot \frac{Q_i^{\max}}{\sum_{i=1}^{i\max} Q_i^{\max}} \qquad (2\text{-}3)$$

Where *i max* is the total number of SSTs under the slave, *i* is the index of SST and $Q_i^{\max}$ is the reactive power capacity of SST *i*. In real-time VVO, u_i is determined in very control period, for example every 5 minutes.

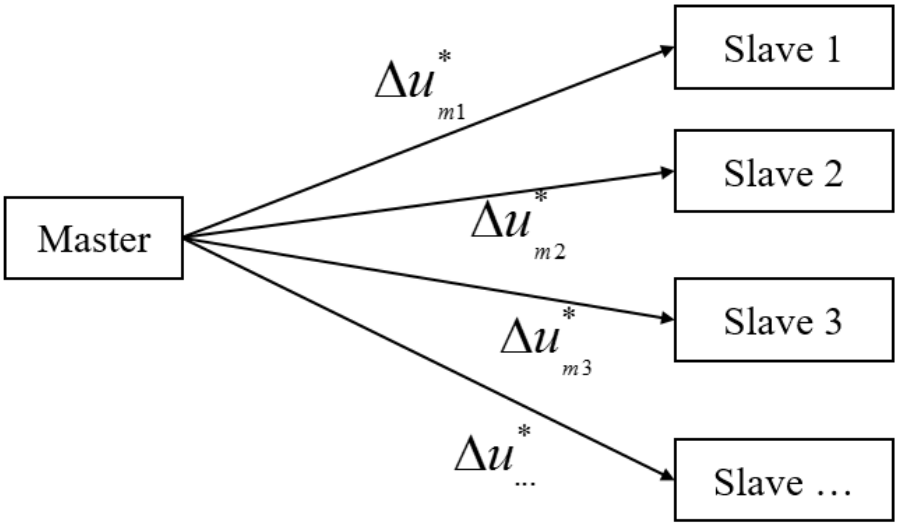

Figure 2.5 Interaction between master VVO and slave VVO

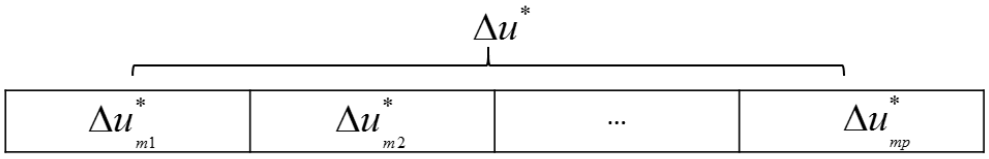

Figure 2.6 Partition of the solution in Phase II

2.3 FREEDM Notional Feeder Results

As shown in Figure 1.3, there is no voltage regulator or shunt capacitor on FREEDM Notional Feeder system. Therefore, without any voltage regulating devices, the VVO problem becomes an NLP problem, and Phase I is skipped since the SSTs regulate the system voltages well. An SLP based centralized VVO is also simulated to be compared with the proposed decentralized VVO scheme.

2.3.1 Initial System Operating Condition

As mentioned in the previous chapter, SST can automatically work at a unity power factor. Therefore, in the initialization of the algorithm, we set $Q_{inj} = 0$, which means the SSTs provide the reactive power demanded by the loads. The loads in the system are set to their peak load values. The substation voltage is assumed to be 1.0 p.u.. Feeders in the FREEDM Notional Feeder systems, are all three-phase and loads are three-phase unbalanced. Figure 2.7 shows the feeder voltage in phase A at the original system operating condition.

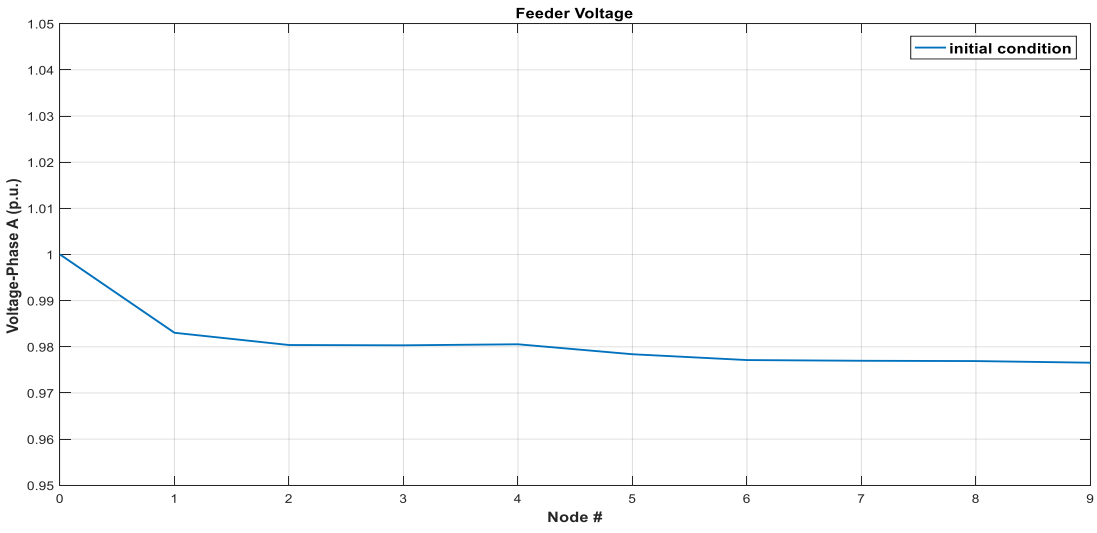

Figure 2.7 Feeder phase A voltage on FREEDM Notional Feeder

The lowest voltage in phase A in the system occurs at feeder end Node 9. The power flow results of this feeder show that voltages on the primary side are between 1.0052 p.u. and 0.9603 p.u. Therefore, there is no voltage issue on this feeder. The voltages form Node 0 to Node 4 is not monotonically decreasing because of the unbalance of the loads and the coupling effect of three-phase feeder lines. The power loss can be calculated from the power flow results by subtract the total loads from the power at the substation. Under the initial condition above, system has a power loss of 126.7053kW.

2.3.2 VVO Simulation Results on the FREEDM Notional Feeder

Based on the sensitivity test results, the nine SSTs in the system are divided into three groups, shown in Figure 2.8.

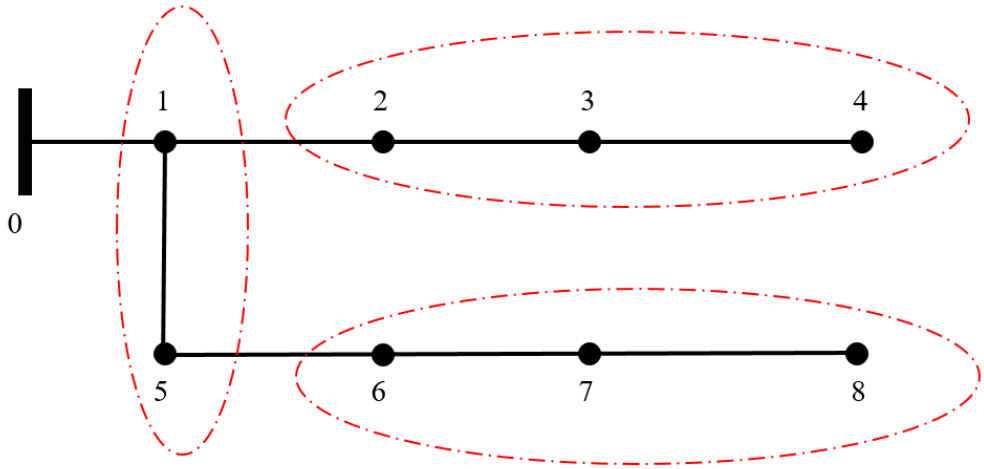

Figure 2.8 Simple one-line diagram of the FREEDM Notional Feeder

Since there's no voltage control devices in this system, and the voltage profile under the initial condition is satisfactory, we will skip Phase I and go directly to Phase II.

For simplicity, the "updated gradient approach" refers to the sequential line search based on steepest descent. The initial step-size to search for β^* in each line search is selected such that the minimum change for the control (SSTs) $|\Delta u|^{\min}$ is 0.1 kVar. The detailed convergence information is shown in Table 2.2. The initial system power loss is 126.705 kW. After the first line search along the steepest descent, the power loss is reduced to 122.789 kW. The optimal step-size for the first line search is obtained after 29 inner loop iterations. From the results in the table, the first line search has a power loss reduction of about 4 kW, which is significantly larger than the power loss reduction in other line searches. This verifies the fact that the performance of gradient method gets worse when getting close to the optimal point [20]. The "NA" in the last row of the table means that in the last line search the power loss cannot be further reduced by a small change of control based on initial step-size $\beta(0)$. It takes four sequential line searches (i.e. gradient is updated four times) to converge to the optimal solution. Figure 2.9 shows that the power loss decreases as the gradient is updated, and a total power loss reduction of 4.99 kW is achieved after convergence. Figure 2.10 shows that the minimum voltage is always greater the 0.95 p.u., meanwhile the maximum voltage is always 1.05 p.u.. This indicates the voltages are kept feasible during the Var optimization process. Figure 2.11 shows the path of the reactive power injection of SST4 phase A to reach the optimal.

The master finds the optimal control for each SST, u^*, and send the partitions to the slaves. Based on the allocation rule in (2-3), the power loss after decentralized control is

121.711 kW which is very close to the optimal power loss 121.704 kW calculated by the VVO master. The minimum voltage after decentralized control is 0.977 p.u. From Figure 2.12, we can observe a slight voltage rise within the feasible range in [1] due to the decentralized gradient based VVO.

Table 2.2 Convergence information of the gradient based decentralized VVO

Iteration for gradient updating	Power loss (kW)	Vmin (p.u.)	Iteration for step-size search
0	126.7053435	0.960272	29
1	122.7890484	0.977779	24
2	122.5769644	0.976918	25
3	121.7705037	0.979355	21
4	121.7038926	0.977848	NA

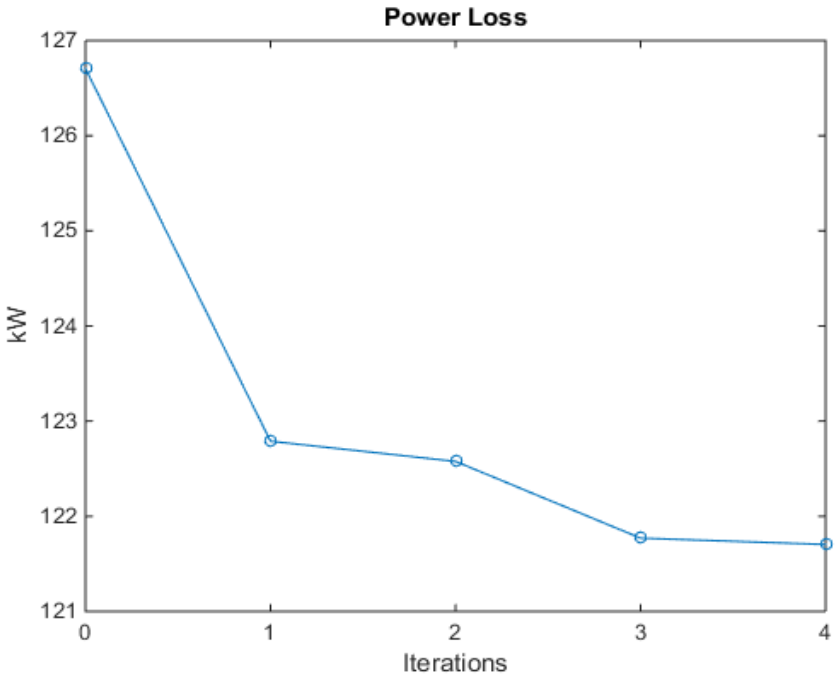

Figure 2.9 Power loss during the gradient based decentralized VVO

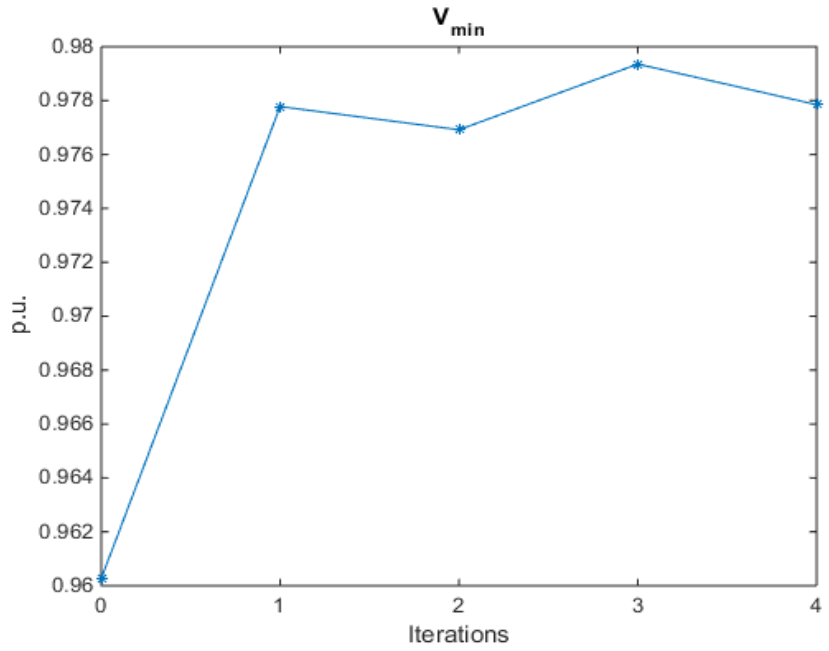

Figure 2.10 System minimum voltage during the gradient based decentralized VVO

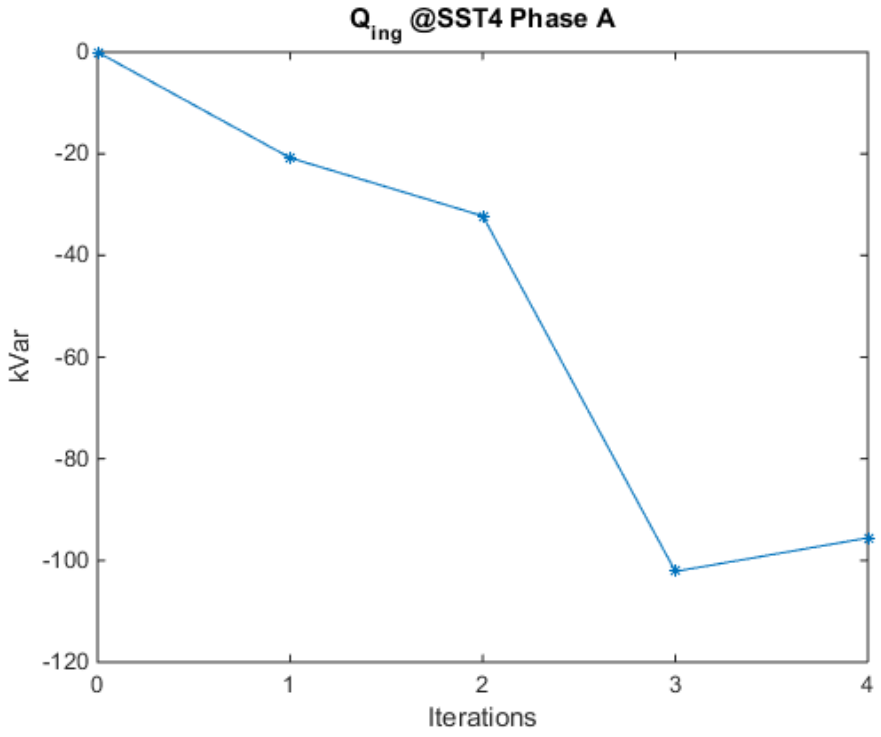

Figure 2.11 Q_{inj} at SST4 during the gradient based decentralized VVO

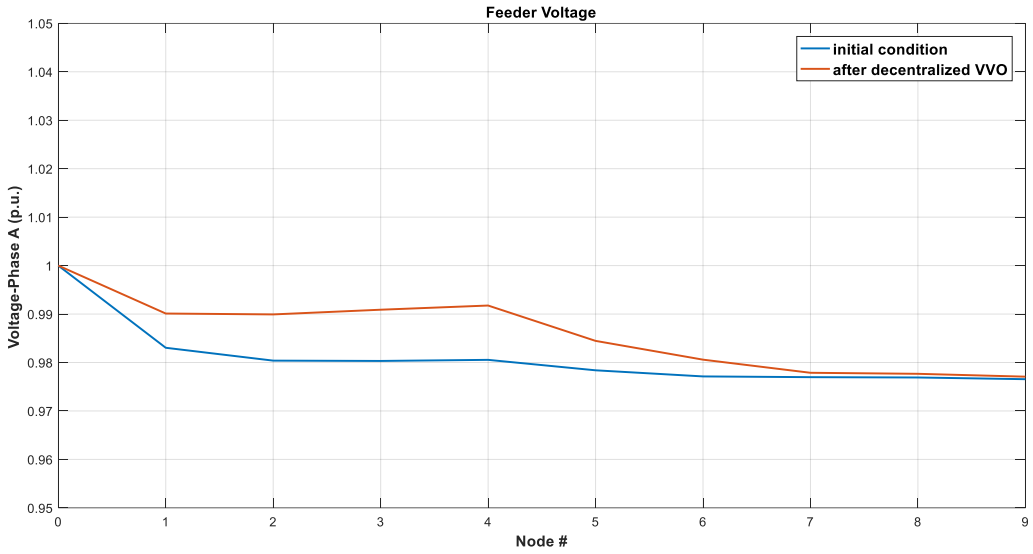

Figure 2.12 Primary feeder voltage on FREEDM Notional Feeder

To verify the effectiveness of the proposed decentralized VVO on various load conditions, the following 8 load samples in Figure 2.13 are considered in the case studies. A SLP based centralized VVO is also simulated to compare the performance. Case 6 is the peak load condition mentioned in section 2.3.1. Figure 2.14 shows the power loss reduction of the two VVO schemes. The power loss reduction is calculated by subtracting the power loss after VVO is applied from the power loss at Q_{inj} = 0 kVar at all SSTs. The results show that the proposed decentralized VVO can effectively reduce the power loss for all load cases. In load case #1, #2, #3, #5 and #8, the proposed VVO performs better than the SLP based centralized VVO.

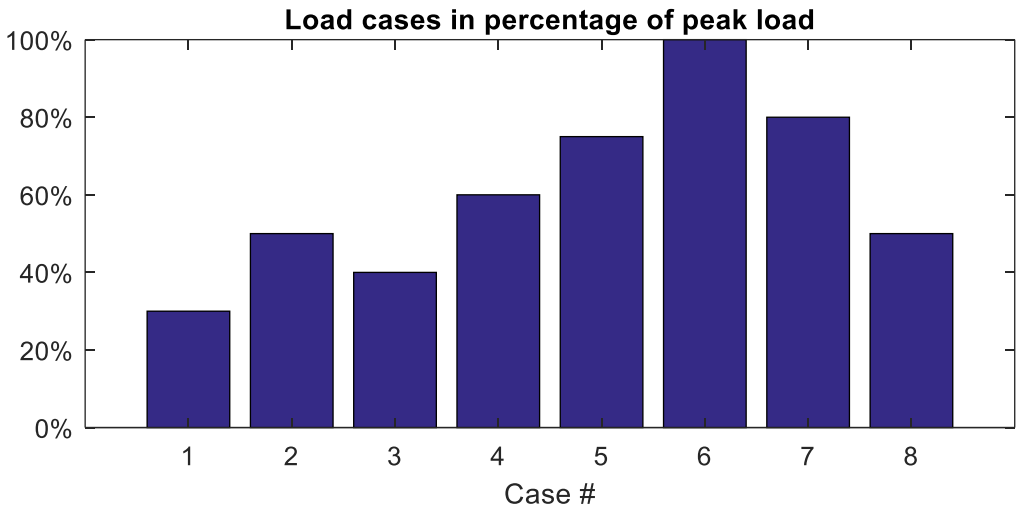

Figure 2.13 Load level tested on FREEDM Notional Feeder

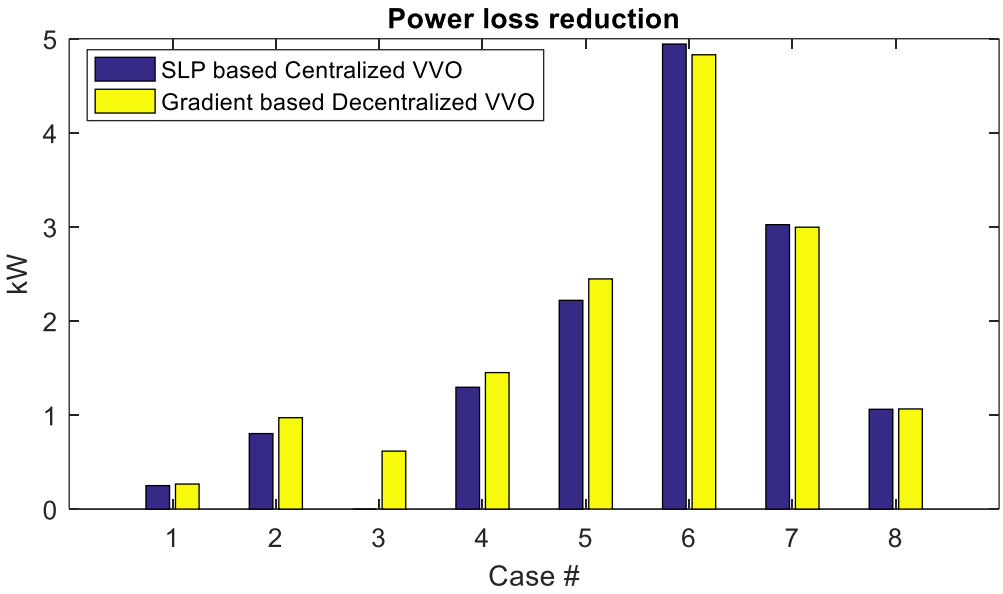

Figure 2.14 Performance of VVO on FREEDM Notional Feeder for different load cases

2.4 FREEDM IEEE 34 Test System Result

IEEE 34 node test feeder is an actual feeder with a nominal voltage of 24.9 kV, as shown in Figure 2.15. It is characterized by its long line length and heavy peak load. An in-line distribution transformer, between node 832 and 888, steps down the voltage to 4.16 kV for a short section of the feeder. Besides, there are two VRs connected between node 814-850 and node 852-832, and two capacitor banks connected at node 844 and 848 separately [32]. These Var compensation and voltage regulation devices are needed to maintain a good voltage profile under all operating conditions. The voltage regulators have ± 16 tap position range with $\pm 10\%$ of maximum voltage change. And the three phases of the VRs are controlled separately. The original IEEE 34 system does not have any DRER.

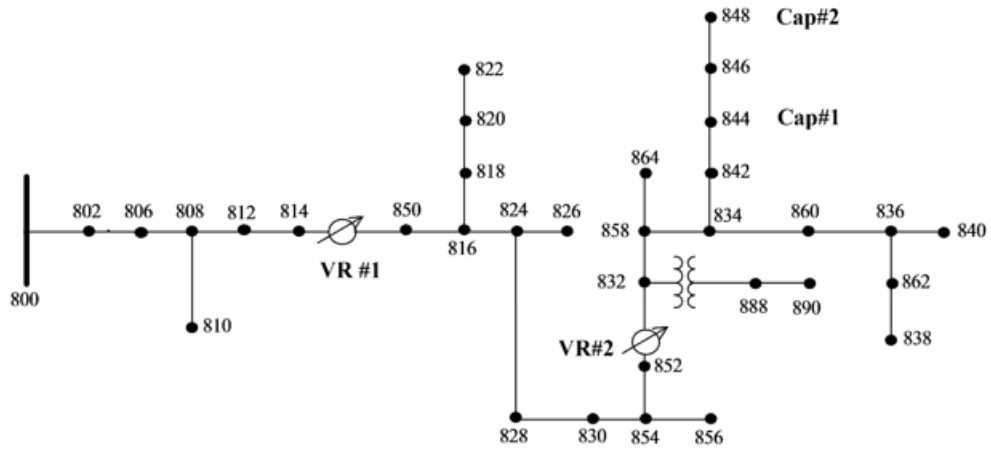

Figure 2.15 Simple diagram of the original IEEE 34 Test System [32]

In the FREEDM IEEE 34 system, all traditional distribution transformers are replaced by SSTs and all SSTs have both load and PV connected. There is no transformer between the node 832 and 888. In this system, A three-phase controlled LTC at the substation and a VR is sufficient to maintain feasible feeder voltages. Therefore, only one VR is kept in the

FREEDM IEEE 34 system and it is put in the same place as VR1 in the original system. The LTC is assumed to have the same tap range and ratio range as the VRs. However, since the feeder voltage should be between 0.95 p.u. and 1.05 p.u. [1], only taps with voltage in this range is feasible for the LTC. All shunt capacitors are removed as well, since SSTs can provide sufficient reactive power for the purpose of VVC. Figure 2.16 shows the diagram of FREEDM IEEE 34 test system.

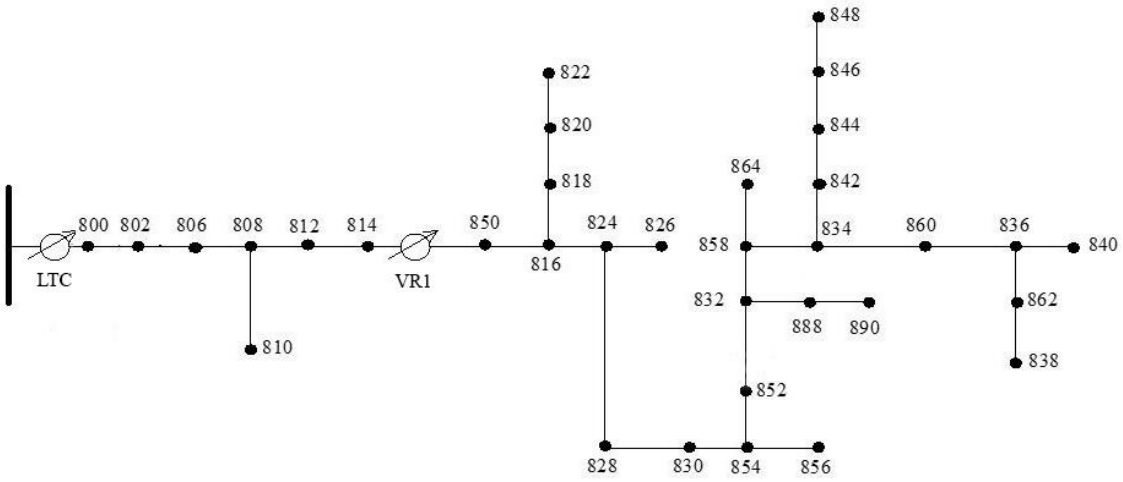

Figure 2.16 Simple diagram of FREEDM IEEE 34 Test System

It is possible to use SSTs only to regulate the voltages to an acceptable range. However, the VVO solution in this case [11] results too much reactive power goes into the substation (The direction of reactive power at the substation is reversed and the value is large, which is bad power factor issue.). This is an over compensated situation in which the current going through the feeder lines is high resulting in high power loss. Therefore, voltage regulating devices are needed in the FREEDM IEEE 34 system. With LTC, VR and SSTs as the VVC devices, the VVO problem here is a MINLP problem which can be solved by the proposed two-phase method. To test the effectiveness of the proposed VVO scheme, single operating

point for peak load condition is simulated. A 24-h simulation is also performed to verify that the proposed method is suitable for real-time implementation. Since results in section 2.3 show that the first line search can provide a solution very close to the optimal, in the following case studies the sequential line search method simplified into single line search along the steepest descent.

2.4.1 Initial System Operating Condition

As stated before, one of the main features of SST is that it can automatically work under unit power factor. Similar as in section 2.3, the system is initialized with the peak load condition and unity power factor. The initial tap positions for LTC is 1.05 p.u. and VR at position 6 for all three phases. Figure 2.17 shows the feeder voltage in phase A under the operating condition above. The maximum voltage in the system is 1.05 p.u., and the system minimum voltages is 0.9520 p.u.. The power loss calculated from the power flow results is 214.6791 kW.

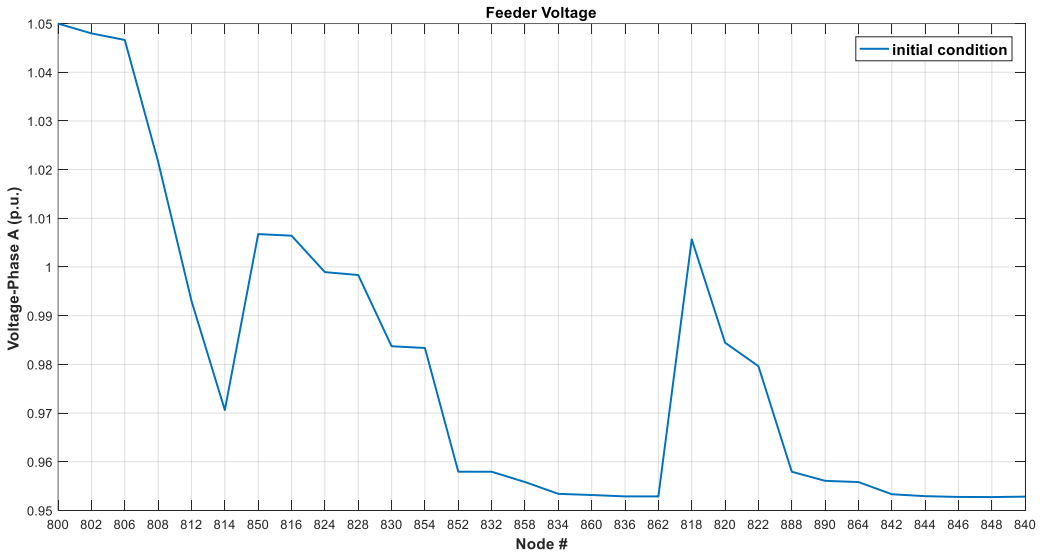

Figure 2.17 Primary voltage on FREEDM IEEE 34 System

2.4.2 VVO Simulation Results on FREEDM IEEE 34 Test System

Phase I – Voltage Problem

The number of the possible LTC and VR tap combinations is $3\times5\times5\times5=375$ using the method in [28]. By applying the reduced search approach proposed in section 2.1, the number of possible combinations is 168. Since the feasible tap position combination is not unique, Phase II - Voltage Problem returns a list of all feasible tap position combinations. Since the DPF runs for every possible tap position combination, the power loss which comes from DPF results for all feasible combination is also available. It may happen that the reducing search method proposed finds less number of feasible tap position combinations than the original method in [28]. Thus, the proposed method has the potential to miss the feasible combination with the least power loss, which means a global optimal is not guaranteed. However, it should always finds a solution good enough to initialized the Var Optimization as long as the system is well-designed.

Table 2.3 shows the results of Phase I of the two searching methods, method in [28] and the proposed reducing search method. The results show that the proposed searching method is able to find all feasible combinations and has more than 50% runtime improvement. The runtime results is abtained by running the two methods on the same PC (Intel® Core™ i7-6600U CPU @2.60GHz 2.81GHz, RAM 16.0 GB, 64-bit OS). Since the searching method gives a list of feasible combinations, some criteria are needed to determine which combination is the one to intialized the Var Optimizaiton process. In this case, the combination with the least power loss is selected as the best solution to initialize Phase II. Other possible criteria can be voltage varience (variation from the mean of voltage

magnitude) or the metrics proposed in [33]. Results show that the two searching methods give the same feasible solutions.

Table 2.3 Phase I results on FREEDM IEEE 34 System

	Original Method in [28]	**Proposed method**
Number of possible solutions	375	168
Number of feasible solutions	64	64
Best solution found	VR=[8 8 8]	VR=[8 8 8]
Power loss associated with the best solution (kW)	211.742	211.742
Runtime (s)	4.479	2.021

Phase II – Var Optimization

Figure 2.18 shows how the SSTs are grouped based on the approach in section 2.2 (see validation using k-means method in Appendix B). As the figure shows, in this case 20 SSTs are divided into 6 groups. Managing this small number of groups becomes easier than the individual SSTs for VVO using a centralized approach.

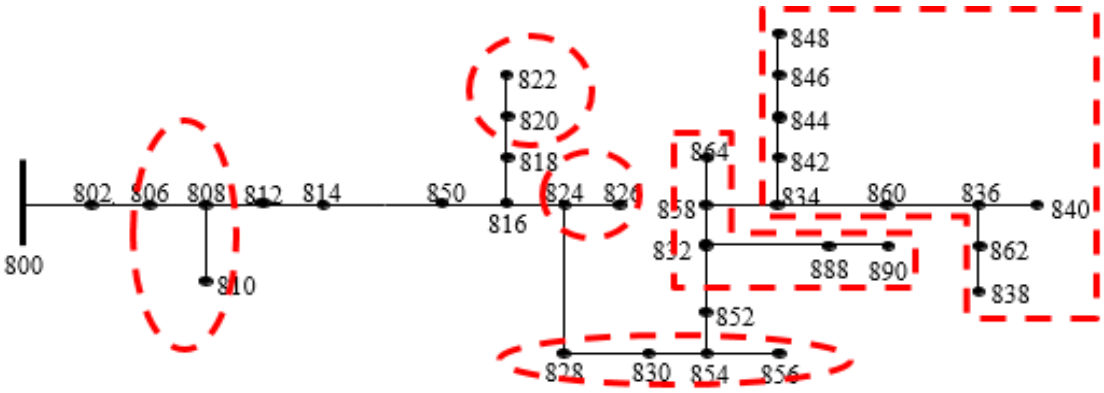

Figure 2.18 Grouping of SSTs in FREEDM IEEE 34 System

The updated gradient approach is not adopted to the Var problem on this feeder for the ease of implementation, since the first iteration of the updated gradient approach gives a much more significant power loss reduction compared with the next few iterations. The initial step-size to search for β^* is selected such that the minimum change for the control (SSTs) $|\Delta u|^{\min}$ is 0.02 kVar. Figure 2.20 shows power loss for the optimal step-size search. As the figure shows, the power loss decreases gradually until it reaches the 16th iteration. After the 16th iteration, power loss starts to increase. And a total power loss reduction of 1.665 kW is achieved at the 16th iteration. Figure 2.21 shows the reactive power injection at Node 840 Phase A of each iteration. As Figure 2.20 and Figure 2.21show, after 16th iteration, increasing the Var support won't further reduce the power loss, which means the step-size search stops at the 16th iteration. The minimum voltage before Var Optimization runs is 0.9654 p.u.; after convergence the minimum voltage is 0.9721 p.u.. Figure 2.22 shows the reactive power injection of all phase A SSTs after convergence. The voltage profile before and after VVO is shown in Figure 2.23. As the figure shows, the VVO helps also raise the voltage profile.

Figure 2.19 shows typical convergence profile of the steepest descent method: good monotone convergence during the first few iterations and then convergence slows down as the solution gets close to the optimal point. This indicates that in practice only a few iterations are needed to get a good solution. Therefore, the SLP based centralized VVO in section 2.1 is used to compared with the fixed gradient approach (single line search method). Table 2.4 shows that the proposed scheme can obtain a solution very close to the optimal solution obtained by the SLP VVO.

Runtime of the proposed VVO for the above case is 0.97s and considerably less than the 3.38s runtime of the SLP based VVO (same PC). This is not only because the gradient based approach has less iterations, but also because each iteration of SLP VVO takes more time to update and solve the LP problem.

Table 2.4 Convergence information of Phase II optimization for FREEDM IEEE 34 System

	Iterations	**Vmin (p.u.)**	**Vmax (p.u.)**	**Loss (kW)**	**Loss Reduction(kW)**
Before Phase II		0.965	1.05	211.742	
Gradient Method	16	0.972	1.05	210.077	1.665
SLP Method	21	0.973	1.05	209.992	1.750

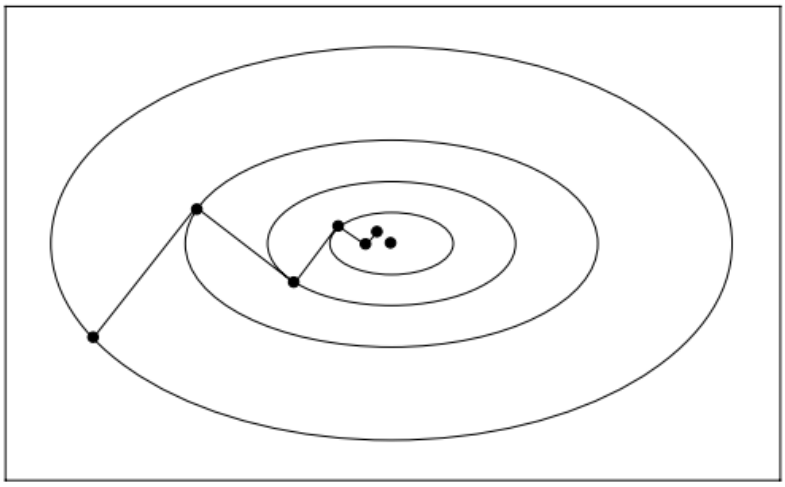

Figure 2.19 Convergence profile of steepest descent method [21]

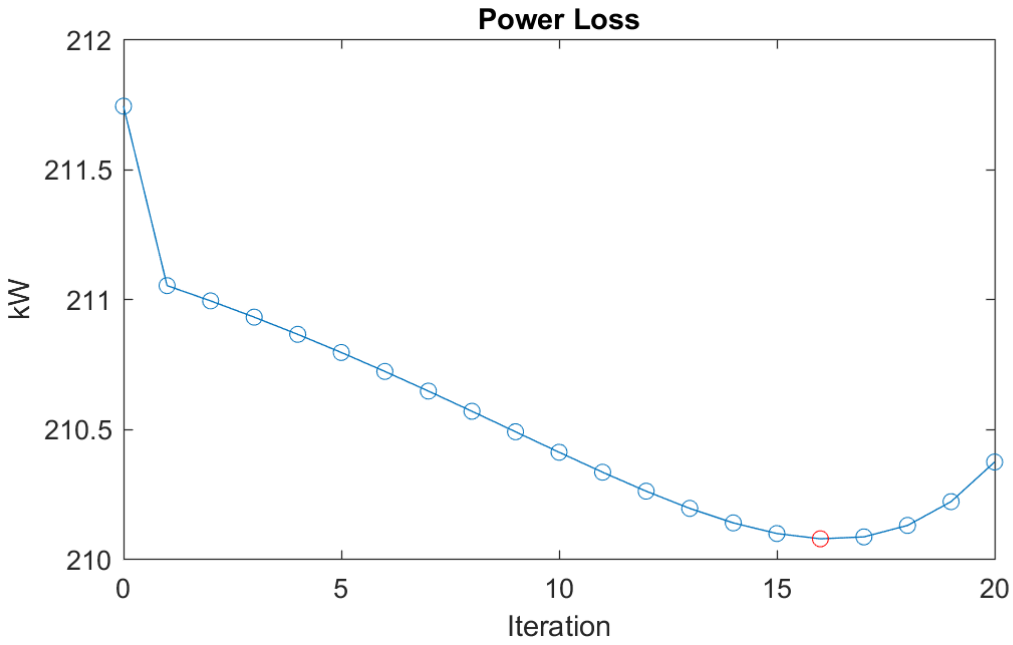

Figure 2.20 Power loss of gradient based decentralized VVO

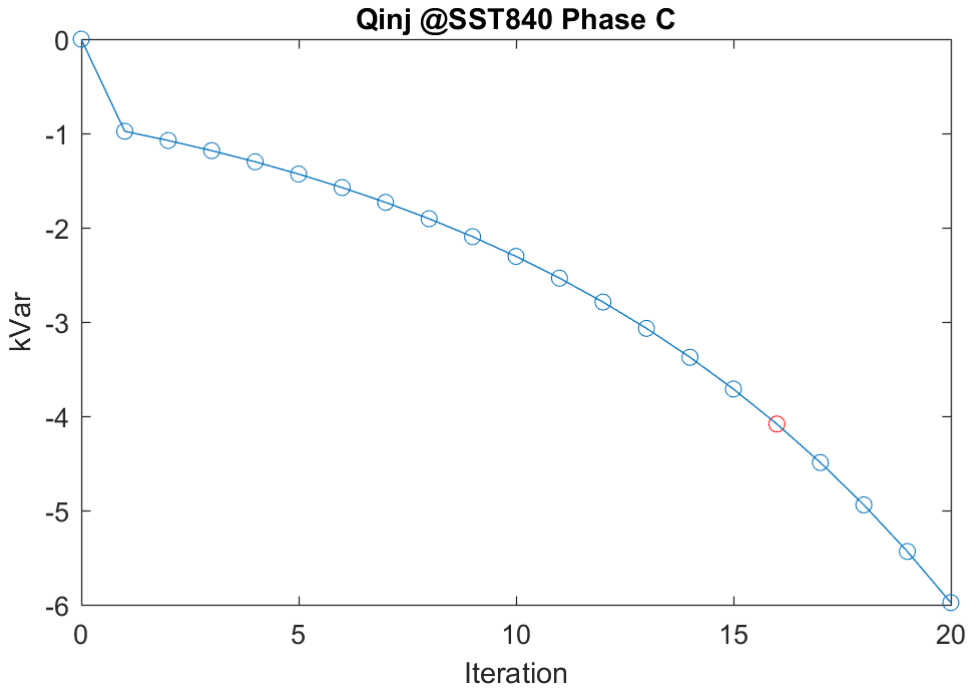

Figure 2.21 Reactive power injection of SST at Node 840 Phase C

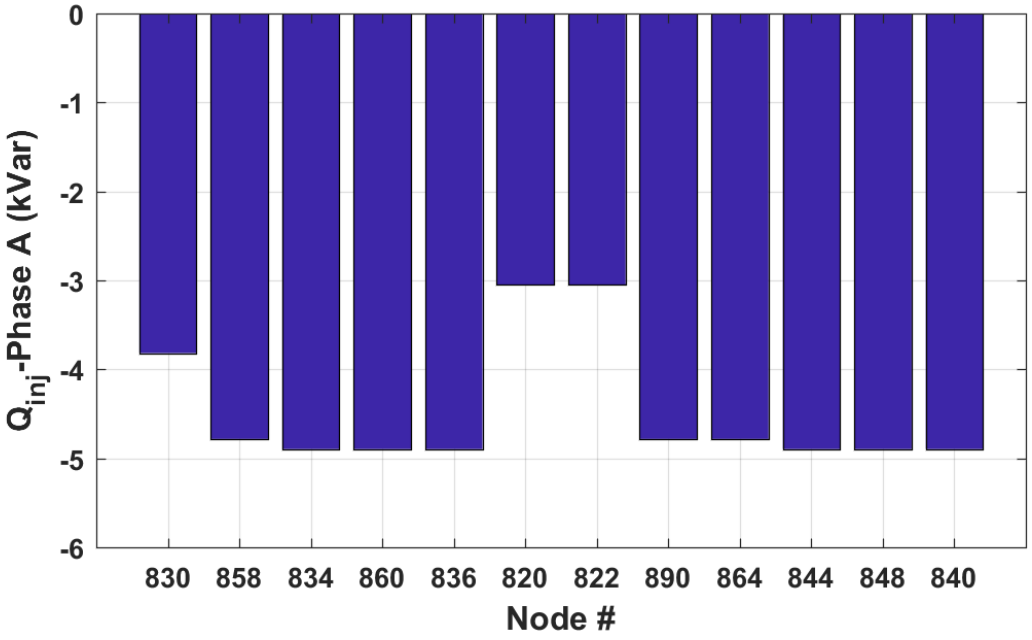

Figure 2.22 Reactive power injection at Phase A SSTs

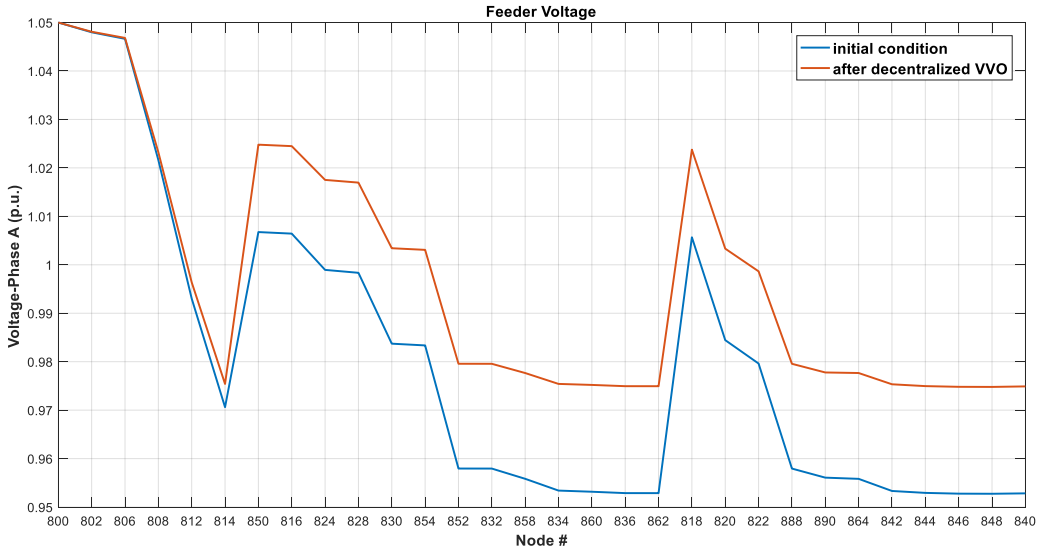

Figure 2.23 Primary feeder voltage in FREEDM IEEE 34 System

VVO results of a 24-hour simulation

To simulate the operation of the test feeder on a typical day, a 24-hour PV and load profile with a 5-min resolution, shown in Figure 2.24, is used. The goal of this simulation is to test the effectiveness of the proposed VVO in adjusting reactive power injection of SST as the system net load changes.

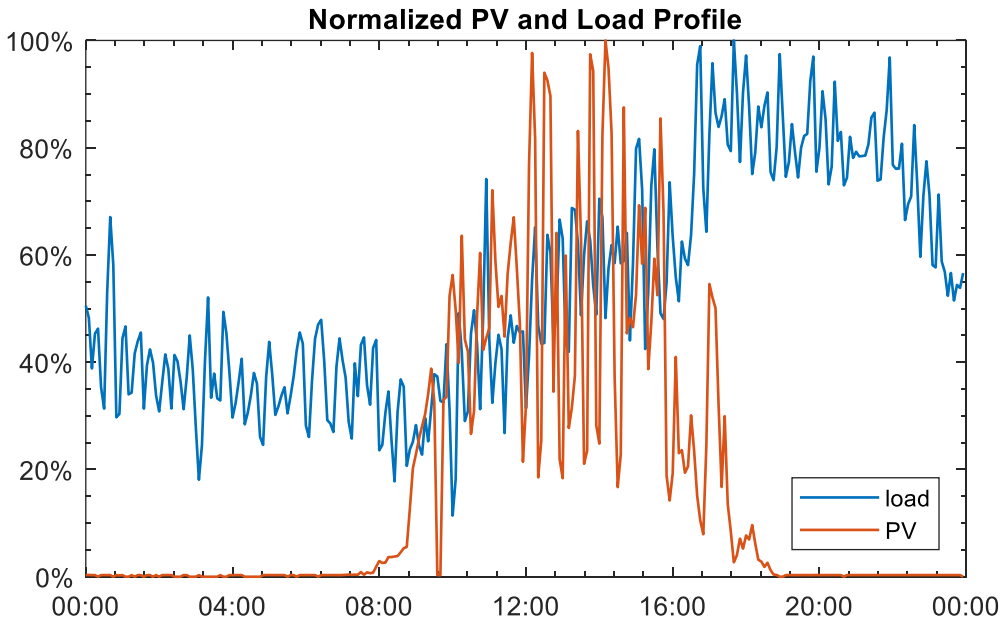

Figure 2.24 PV and load profile in 24 h

For each load case, Phase I -Voltage Problem runs first to obtain the best tap position setting to be passed to Phase II -Var Problem. In this simulation, the feasible tap position combination with least voltage variance is selected to be the best one in Phase I. Because in some cases, the tap positions that has the least power loss lead to convergence problem of Phase I in the next control period in which the system load has a significant change. This is due to the incomplete searching mechanism. The feasible solution with least voltage variance usually has a power loss very close to the least power loss and therefore good enough to

initialize Phase II. In Phase II, the proposed decentralized VVO runs to minimize the power loss and provide additional voltage boost/buck if needed.

In single operating point simulation, the VVO is initialized by a unity power factor at SSTs and certain tap positions of LTC and VR. For a 24-hour simulation, in each control period the VVO is initialized by the present net load condition and the VVC device status returned by the VVO in previous control period. Due to non-convexity of the VVO problem, the line-search method provides solution to a local optimal. For the same peak load condition, in this 24-hour simulation the VVO results is different from the results of the single operating point simulation shown previously, because the same VVO problem is initialized differently.

24-hour simulation of the same VVO problem solved by centralized SLP based method is also presented to compare the performance. It takes 969 s (same PC) for the proposed VVO to solve the 24-hour load profile shown in Figure 2.24 (288 load cases in total). In average, in each control period (5 min) it takes 3.4 s to generate the optimal control of the VVC devices. Therefore, the proposed VVO method is good for real-time implementation. Figure 2.25 shows how the LTC tap changes during the day. Figure 2.26 shows how the VR phase A tap adjust the positions during the day. Results for other phases of the VR can be found in Appendix C. For time *t(k)*, the VVO control command is generated based on the control at time *t(k-1)*. Therefore, Phase I results for both centralized and decentralized VVO can be different at some load cases. Figure 2.27 shows how the power loss is minimized as VVO adjusts the reactive power injection of the SSTs during the day. The two VVO schemes have very close power loss results as shown by Figure 2.27. Although the maximum power loss in the centralized VVO is slightly lower than that in the decentralized scheme, the daily power

loss energy is slightly higher than that in the decentralized scheme. Figure 2.28 shows the reactive power injected by SST 840 Phase C at each control period. As the figure confirms, with small load variation at each step, variations of $Q_{inj\ 840C}$ are small, although the magnitude of $Q_{inj\ 840C}$ can be considerable especially during the high load conditions. Figure 2.29 shows that the proposed VVC scheme keeps the node voltages within the acceptable range of 0.95-1.05 p.u..

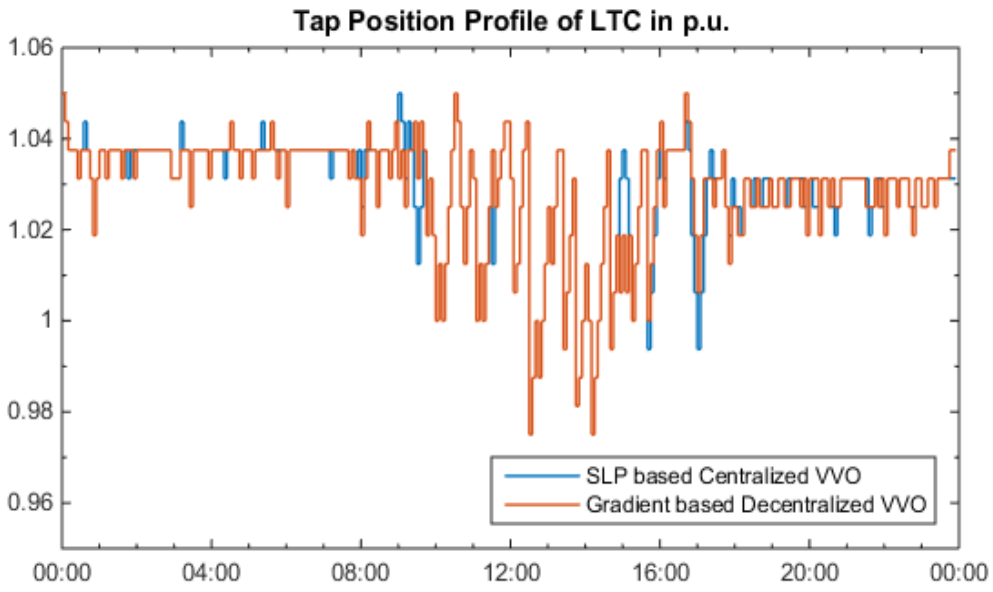

Figure 2.25 LTC position during 24 hours

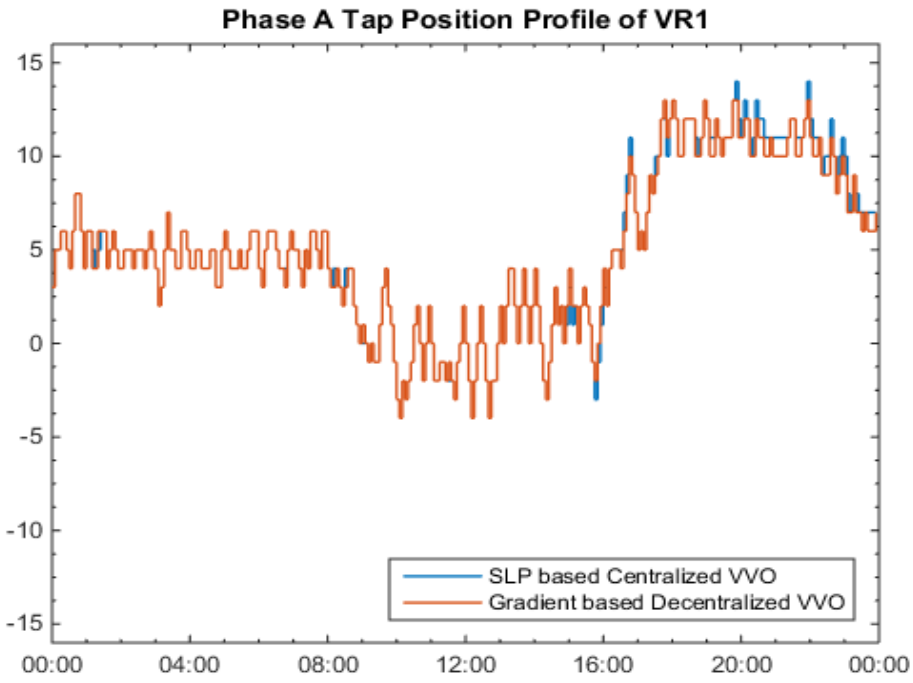

Figure 2.26 VR phase A tap positions during 24 hours

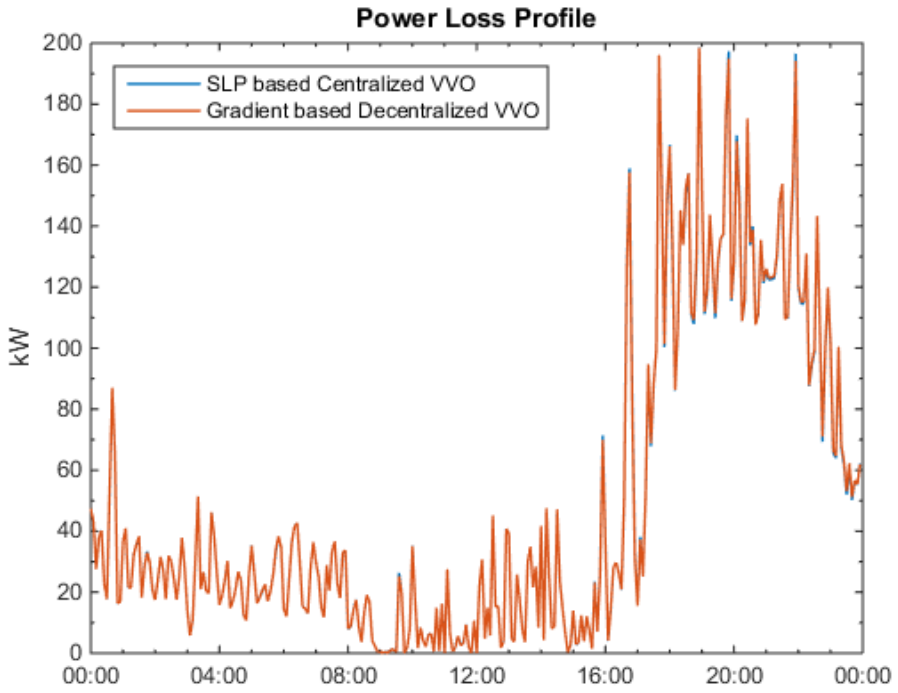

Figure 2.27 Power loss profile for FREEDM IEEE 34 System

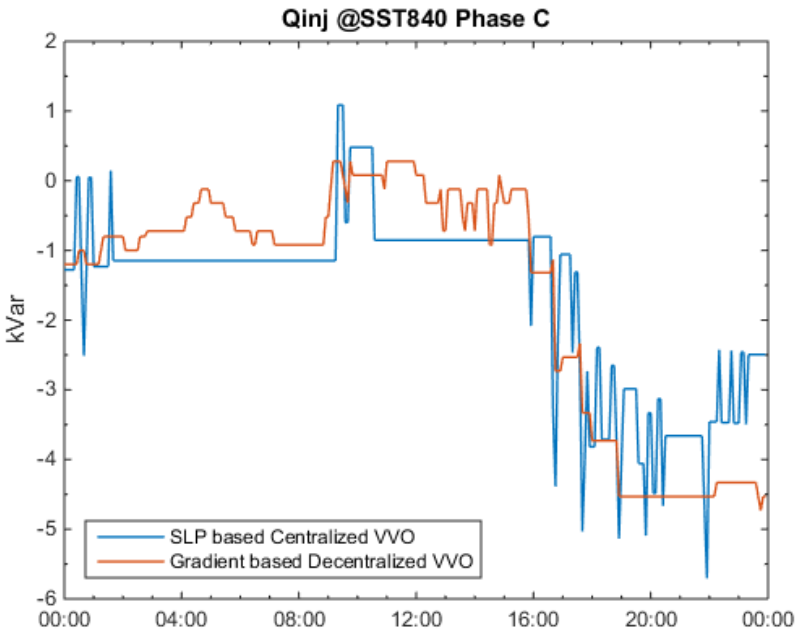

Figure 2.28 Reactive power injection at Phase C SST840 profile

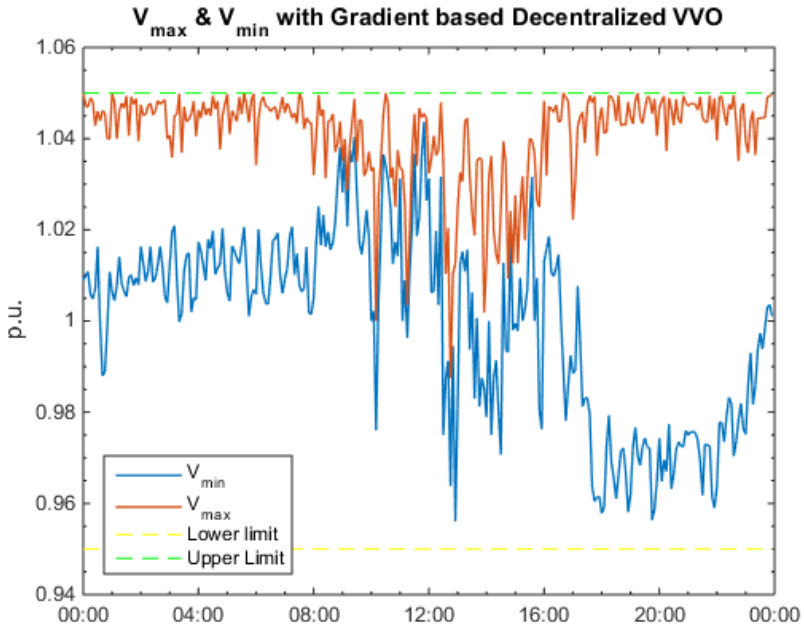

Figure 2.29 V_{max} and V_{min} profile of FREEDM IEEE 34 System

Partial SST deployment

Previous simulations show the test results of systems in which all loads and PV are accommodated by SSTs. However, practically SSTs are installed only at some locations. Therefore, the proposed VVO scheme are test on a modified FREEEDM IEEE 34 system with a few SSTs. In Figure 2.30, locations with SSTs are circled in red. Node 822 has phase A only. Node 844, Node 860, Node 836 and Node 890 have three-phase SSTs.

At peak load condition after Phase I, the system voltage as still within the range of 0.95 p.u. – 1.05 p.u. as shown in Table 2.5. And a total power loss reduction of 10.24 kW is achieved after convergence. Figure 2.31 shows the power loss decreases monotonically and the search stops at the 72nd iteration. The 3-D plots, Figure 2.32 and Figure 2.33 show the initial Q_{inj} and the Q_{inj} after the gradient based method converges. The black line segments on z = 0 plane represents the actual feeder topology. The stems represent the Q_{inj} of at the locations with loads. After Phase II converges, the Q_{inj} at locations with SSTs become negative, which means SSTs are providing extra reactive power support for the system to minimize power loss.

Table 2.5 Convergence information of Phase II optimization for modified FREEDM IEEE 34 System

	Iterations	**Vmin (p.u.)**	**Vmax (p.u.)**	**Loss (kW)**	**Loss Reduction(kW)**
Before Phase II		0.957	1.05	221.169	
Gradient Method	72	0.969	1.05	210.930	10.240

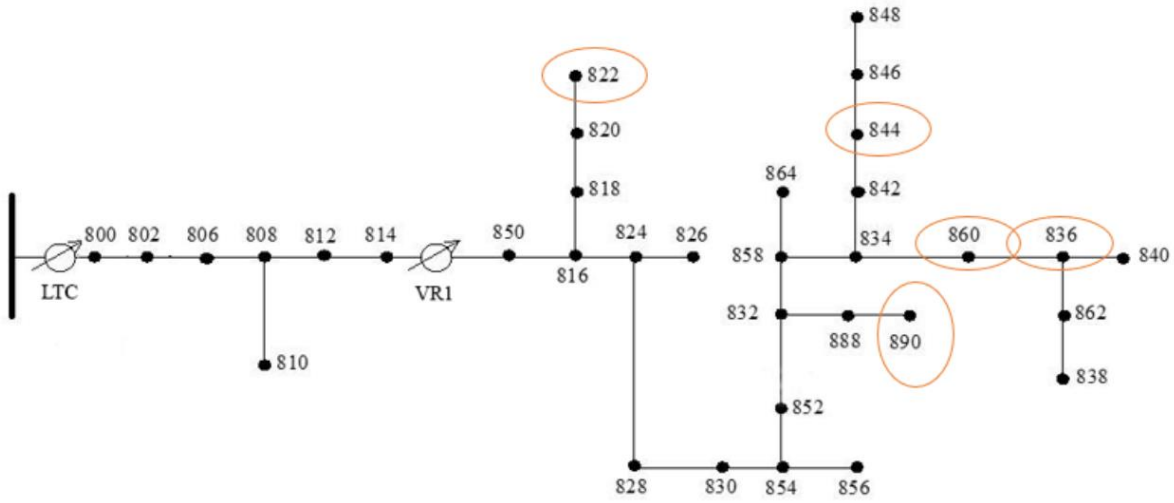

Figure 2.30 Modified FREEDM IEEE 34 Test System

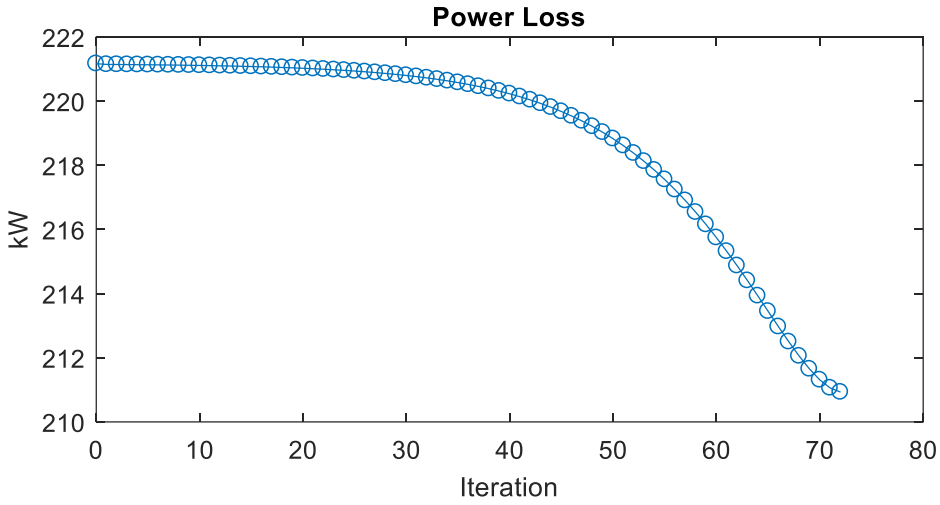

Figure 2.31 Power loss of gradient based VVO

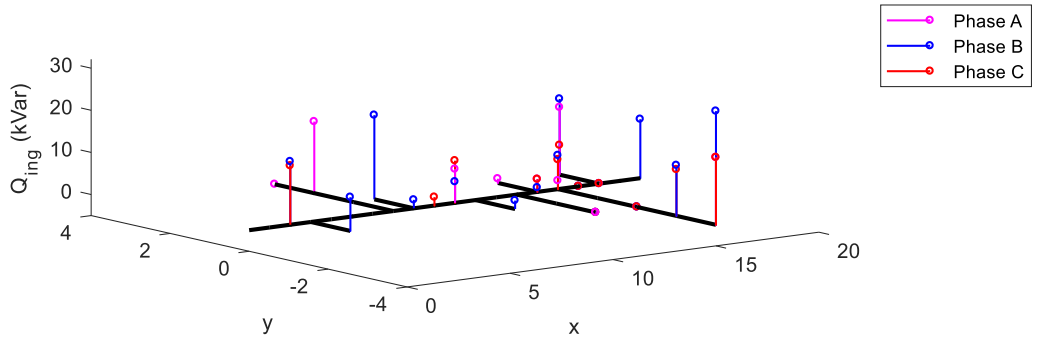

Figure 2.32 Q_{inj} on modified FREEDM IEEE 34 system before Phase II

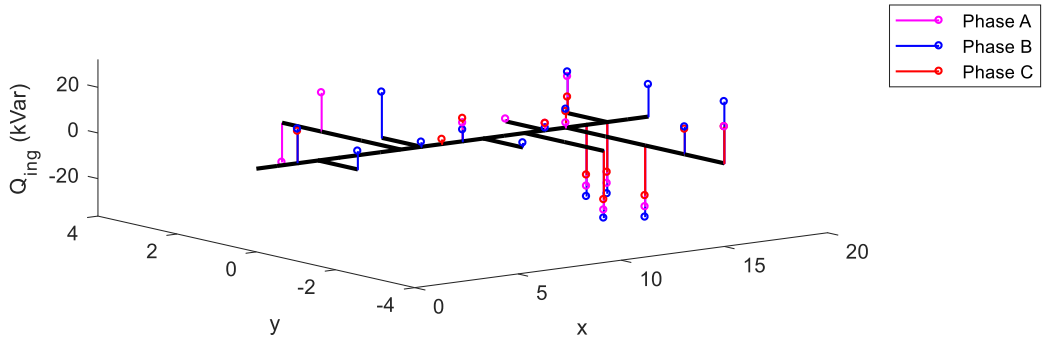

Figure 2.33 Q_{inj} on modified FREEDM IEEE 34 system after Phase II

2.5 Conclusions

In this chapter, a two-phase decentralized Volt/Var optimization scheme is proposed. Two FREEDM test feeders are used to test the proposed scheme. Based on the simulation results, the proposed scheme can effectively reduce power loss while maintaining voltages within feasible region. The two-phase method decouples the MINLP problem into an integer problem and an NLP problem, greatly reducing the computation time. Therefore, the proposed VVO method is applicable to real-time implementation. Since the VVO problem is solved by the intelligent agents at feeder level, the master-slave decentralized control scheme can greatly alleviate the communication load at the control center. The test results of partial SST deployment case show that the proposed method also works in a more practical case. However, this two-phase VVC method results in frequent tap change as shown in Figure 2.25 and Figure 2.26, which is the main reason to develop the new VVC scheme in next chapter.

Chapter 3. Coordinated Volt/Var Control Scheme

Adoption of Photovoltaics (PV) based systems at both residential and commercial scale has accelerated recently. As more PV systems are integrated into a distribution feeder, they will start affecting the voltage control on the feeder, and when the voltage variations become excessive, some mitigation is needed. Conventional Volt/Var control (VVC) devices on the circuit, Load Tap Changer (LTC), Voltage Regulators (VRs), and capacitor banks (Caps), are slow-acting devices. The variability of PV output can also cause excessive operation of traditional VVC devices when PV penetration gets high on the circuit [34], which is also verified by the results shown in previous chapter. This chapter presents a two-level VVC architecture which coordinates the slow-acting devices with the fast-acting devices, providing effective voltage control and mitigating excessive operation of LTC and VRs.

3.1 Two-level coordinated Volt/Var Control

As indicated above, the goal for VVC is to track both the slower load variations and the faster PV variations on a feeder with the goal of minimizing voltage variations while avoiding the excessive operation of Voltage Regulators (VRs) and Cap Banks which may occur due to high variability in PV output. To achieve this, we make use of the fact that the conventional VVC devices are intended to operate at a much slower pace than the smart inverters or SSTs. Also, the VRs are mainly designed to adjust the voltages, Cap Banks and Smart Inverters are mainly reactive power support devices for power factor correction (and thus helps lowering the power losses). These features of VVC devices helps us to decompose the problem [7]. This paper adopts this approach and decomposes the VVO problem into two loops, a slower voltage control loop and a faster Var compensation loop. The first level –

Voltage Control loop – uses LTC and VRs to adjust the voltage level on the circuit to keep the voltages along the circuit within the desired limits. The second level is the reactive power compensation loop which determines reactive power output of inverters needed to smooth the fast voltage variations while providing effective power factor correction to keep the power losses at minimum. Figure 3.1 shows the proposed architecture. The proposed coordinated two-level VVC scheme is computationally efficient, easy for practical implementation, and accommodates the operating constraints.

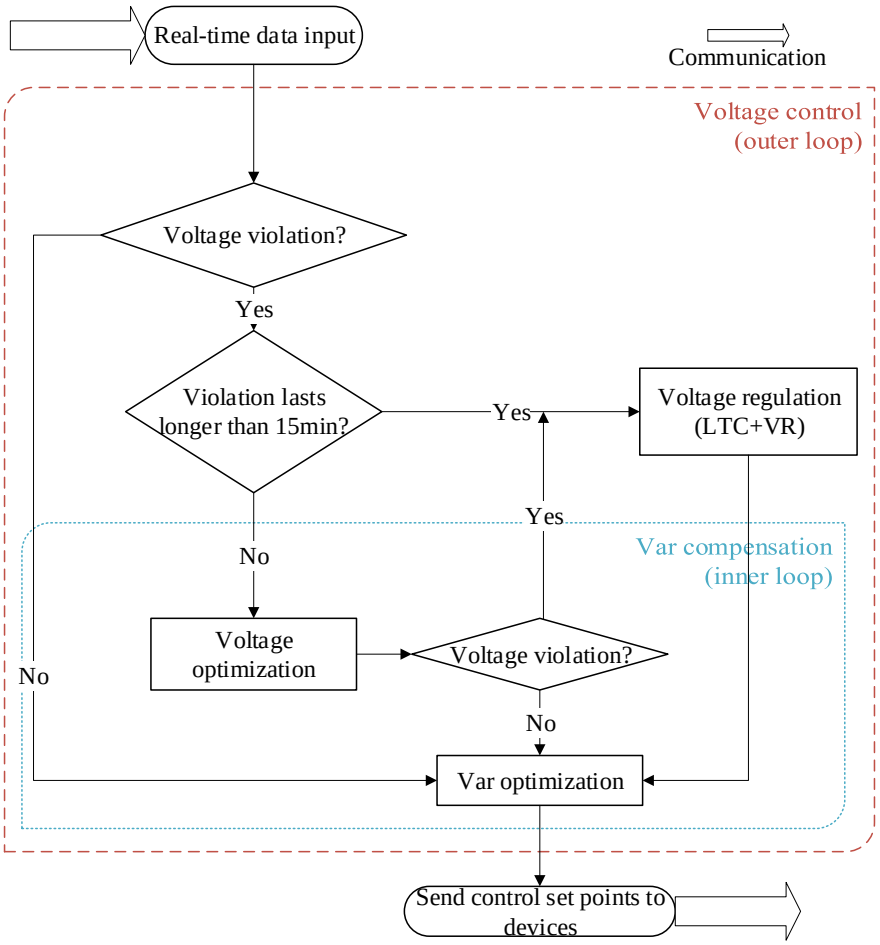

Figure 3.1 Two-level coordinated Volt/Var Control

Voltage Control Loop

The voltage control devices, LTC and VRs, are very effective in adjusting the voltage along the feeder, but they are slow acting devices. Hence, the goal in voltage control loop is to monitor the net load variations along the feeder, filter out the fast variations and have the voltage control devices respond only to slow variations. This prevent excessive device operation. This loop is slow, (which is chosen as 15 min in this paper) and provides the supervisory set points for the LTC and VRs. Details of the method adopted for this module has been presented in previous chapter.

However, the searching increases exponentially as voltage regulation devices increase. In a system with 3 single-phase controlled three-phase VR, ±2 tap range would result in $5^9 = 1953125$ searches, which will increase the computation effort significantly. To resolve this, the topology information of the test feeder is used to reduce the searches.

Practically, the backbone of a feeder has no more than 2 single-phase controlled VRs and other VRs are placed at the beginning of the laterals connected to the backbone, which means there is no more than 2 VR zones from the source of the feeder to one end of the circuit. When a voltage violation is detected, the VVO start to trace voltage regulation device and the phase of taps that are upstream of the nodes of violation. Then only VRs that are upstream of the violation nodes react to the violation with tap changes on respective phases. Figure 3.2 shows this voltage control loop logic.

For a system with 3 single-phase controlled three-phase VR, if an under-voltage violation occurs on only Phase C down stream of VR3, assuming VR1 is the upstream VR of all the other VRs. Table 3.1shows number of search comparison with the previous method.

Table 3.1 Tap search comparison for example case

Method	Previous	Improved
Number of searches	$3^9 = 19{,}683$	$3^2 = 9$

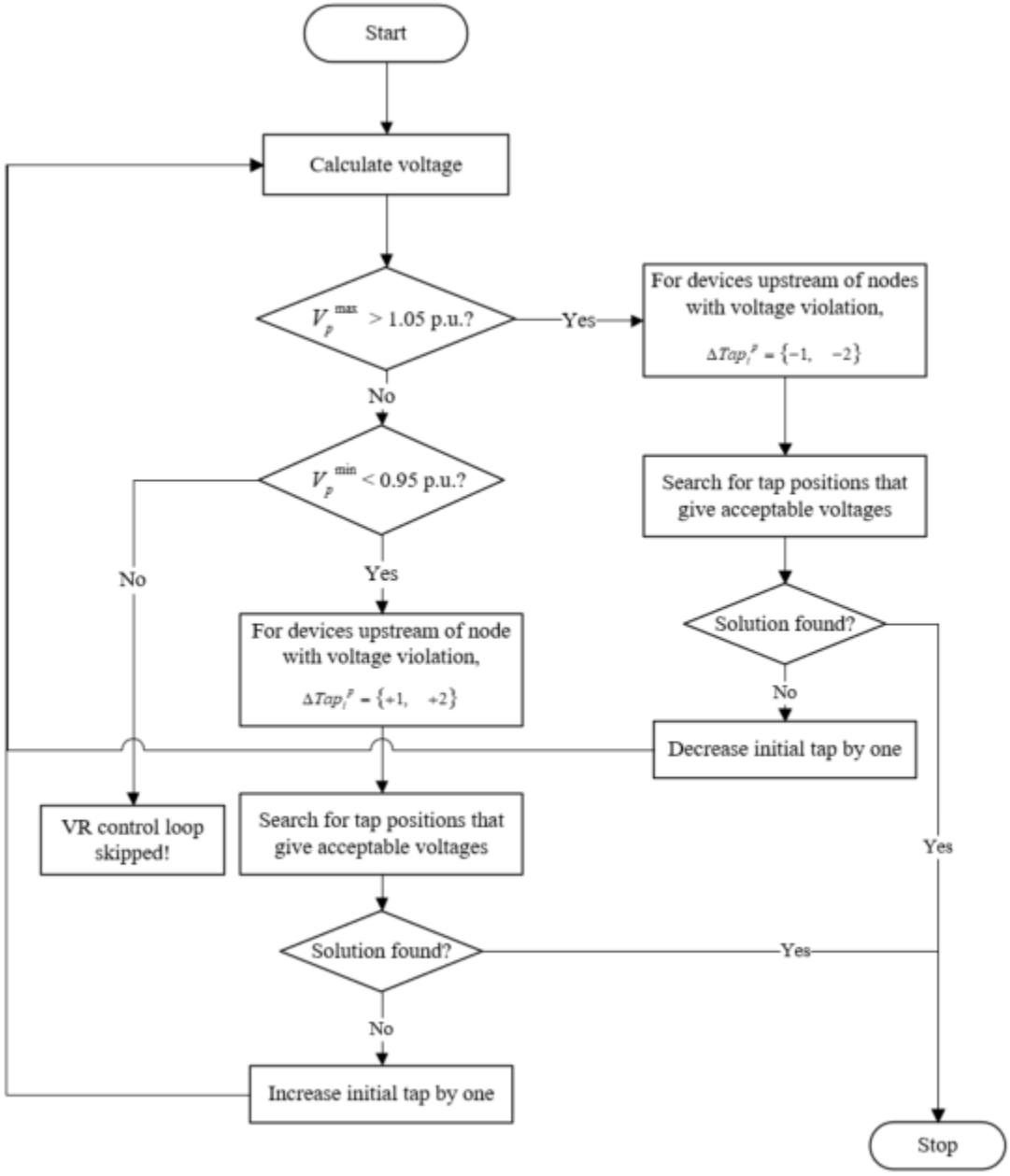

Figure 3.2 Search method for voltage control loop

Var Compensation Loop

As indicated above, this module uses an optimization method to determine the proper Var support needed from inverters or SSTs in the system. The objective of Var compensation, under normal conditions, is to improve system efficiency by reducing power loss on the system. However, when there is need for extra Var support to correct voltage violations, the module determines this extra Var support first. In the latter case, the problem formulation is the same as Phase II problem in (1-1) – (1-4), but with a different objective function as shown in (3-1).

$$f(x) = \sum_{i=1}^{n} \left\{ \omega_i \cdot \left(V_i - 1.0 \right)^2 \right\} \qquad (3\text{-}1)$$

where $\begin{cases} \omega_i = 0 \ \textit{if} \ V_i \in \left[0.95, \quad 1.05 \right] \\ \omega_i = 1 \ \textit{otherwise} \end{cases}$

which aims at determining the minimum Var support needed to bring the node voltages within the limits (which are taken as 0.95 to 1.05 p.u.[1]).

3.2 FREEDM IEEE 34 Test System Result

To demonstrate the effectiveness of the proposed VVC scheme in a more practical case, we assume that smart inverters with a lower cost than SSTs accommodate all PV systems on 34 node system. In previous tests, the SST rating is oversized with 25% more than peak load, i.e. $S_N = 1.25 \times S_{\max}^{load}$. In the following case studies, the rating of the smart inverters is oversized with 25% more than peak generation, i.e. $S_N = 1.25 \times P_{\max}^{PV}$. The available reactive power varies as the PV output changes:

$$Q^{\max}(t) = \sqrt{S_N{}^2 - P_{PV}(t)^2} \qquad (3\text{-}2)$$

In this chapter, the proposed coordinated VVC method is tested on two smart distribution systems, 1) FREEDM IEEE 34 Test System with PV systems at all locations, and 2) a modified IEEE 123 System with PV at some locations. The performance of the coordinated VVC method for both a heavy load day and light load day are presented as well.

Voltage Optimization by Var compensation

To test the effectiveness of the gradient based method to determine Var support to resolve voltage violation, a light load condition where voltage violation occurs due to sudden change in PV output (event corresponds to 10:05 am in Figure 2.24) is tested. In this case, LTC and VR do not respond to this event, but the Var support module reacts and determines extra Var support needed from the inverter to eliminate the voltage violation. Here, the updated gradient method is adopted, because as the indicator variables w_i changes the gradient vector changes significantly. Figure 3.3 shows how the node voltages change during the iterations

of the method. As the figure shows, the node voltages move towards the acceptable ranges quite rapidly and it takes only a few iterations to bring the voltages within 0.95 – 1.05 p.u..

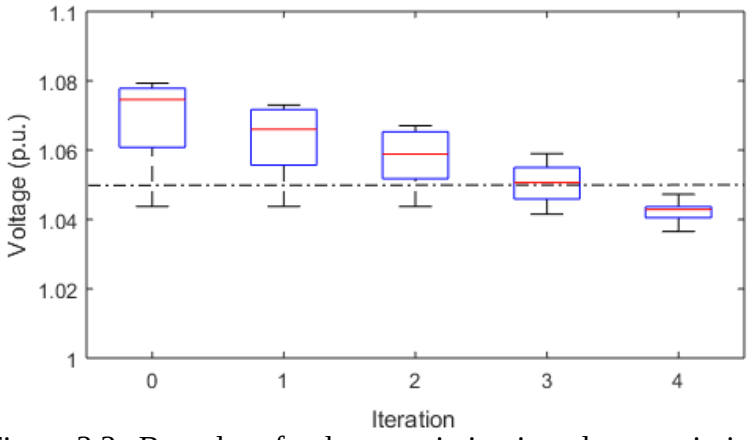

Figure 3.3 Box plot of voltage variation in voltage optimization

Case 1: Heavy load day

The goal of this simulation is to test the effectiveness of the proposed VVO in adjusting reactive power injection of smart inverters as the system net load changes in a heavy load day. Figure 2.24 represents a heavy load day which is used to create the PV generation and load profile.

Figure 3.4 shows how the voltage control devices, LTC and VR, are controlled. From the results we can see that there is no excessive operation of the devices. Figure 3.5 illustrates the reason for each operation. Markers " * " indicates the LTC/VR operation under normal conditions, i.e. the net load change in 15-min period is large enough to warrant adjustment of tap settings. Markers " o " indicate the tap adjustment needed when there is not enough Var support from inverters to keep the voltages within limit, therefore these operations can mainly be considered as the extra operations due to power variability caused by PVs. Markers " + " on the figure indicate Var support from inverters when voltage violation

occurs due to sudden change in PV output. These points thus show that indeed Var support helps to respond the sudden voltage violations quickly and this in turn reduces the excessive operation of voltage regulation devices.

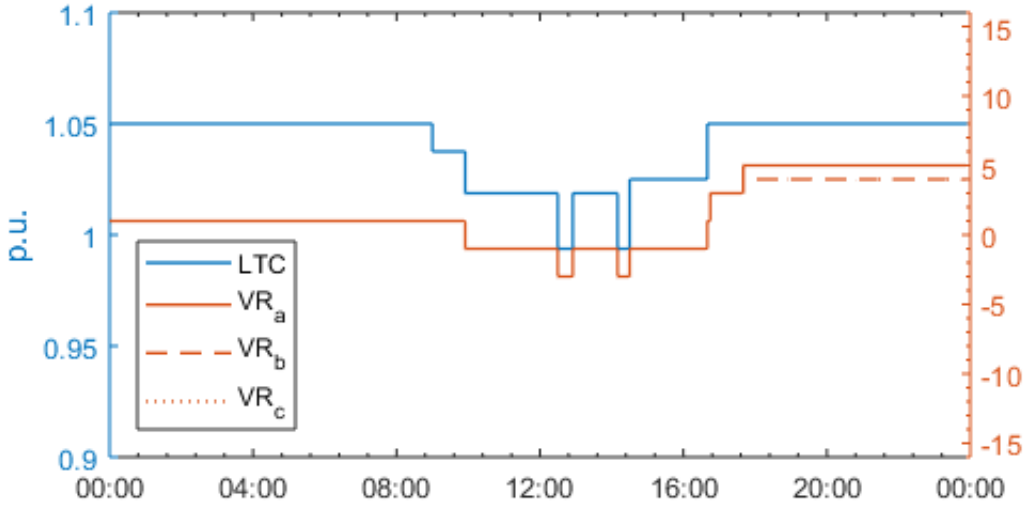

Figure 3.4 LTC and VR tap positions for a heavy load day

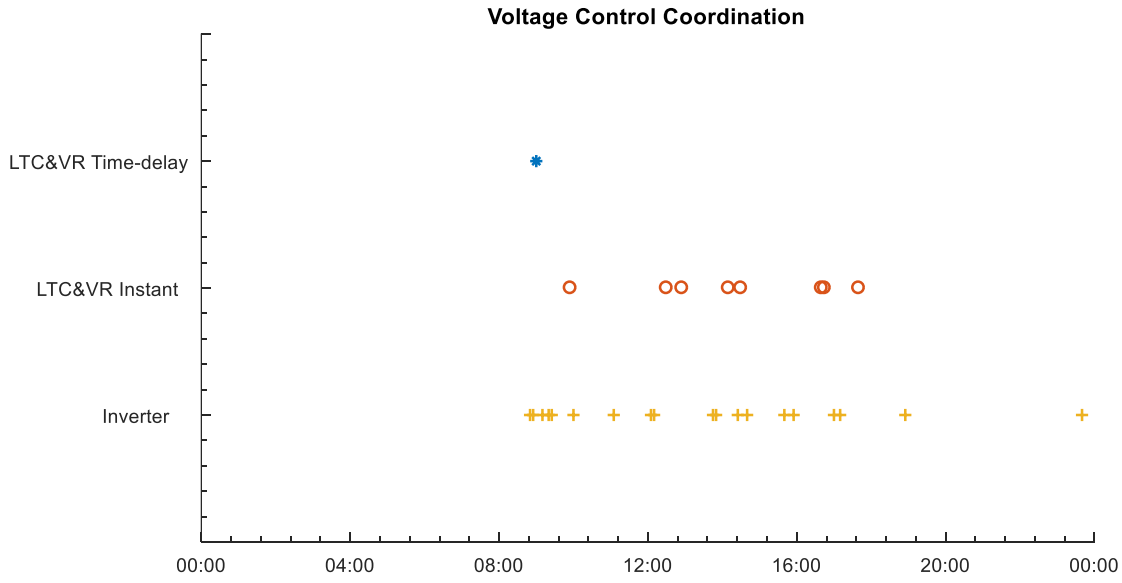

Figure 3.5 Operation sequence of VVC devices in a heavy load day

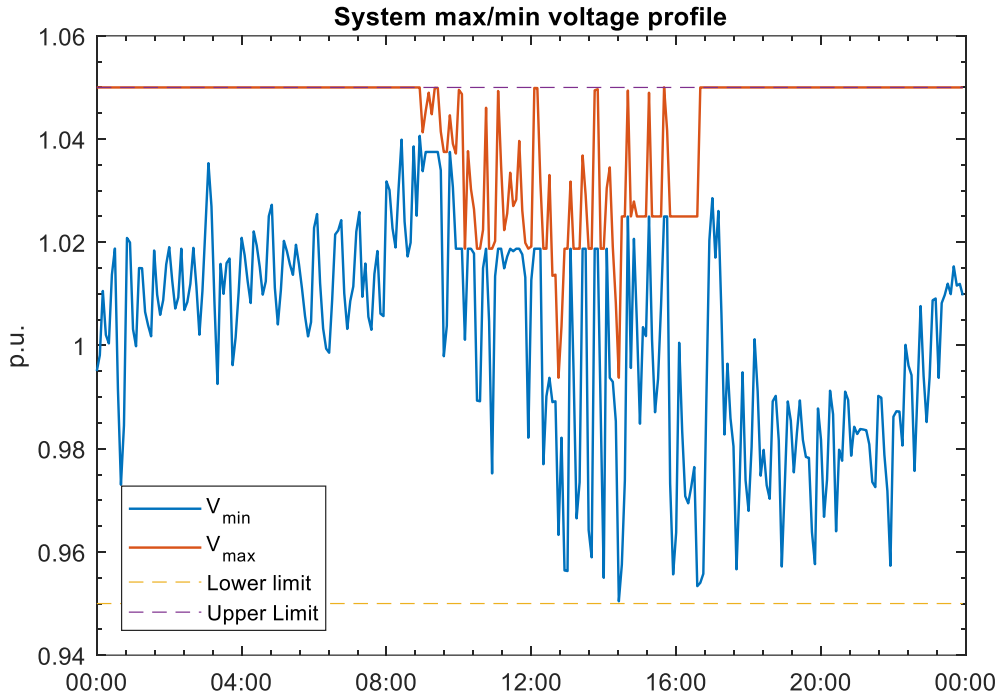

Figure 3.6 V_{max} and V_{min} profile in a heavy load day

Figure 3.6 confirms that the system maximum and minimum voltages are always kept within the range 0.95 – 1.05 p.u.. In the original IEEE 34 system with conventional control scheme, there's over voltage violation during the day time with high PV generation [33] and under voltage violation during the time with heavy load[32]. Compared with the conventional VVC (used on the IEEE 34 node test feeder), the proposed coordinated VVC scheme provides an effective voltage regulation. Figure 3.7 shows the Var support from the inverter at Node 840 phase A. Figure 3.8 shows the apparent power at the same inverter. The simulation indicates that Var support is adjusted throughout the day for both loss reduction as well as for voltage control without violating the rating of the inverter. Majority of the smaller adjustments are for loss reduction under normal conditions (ie. no extra var support for voltage control).

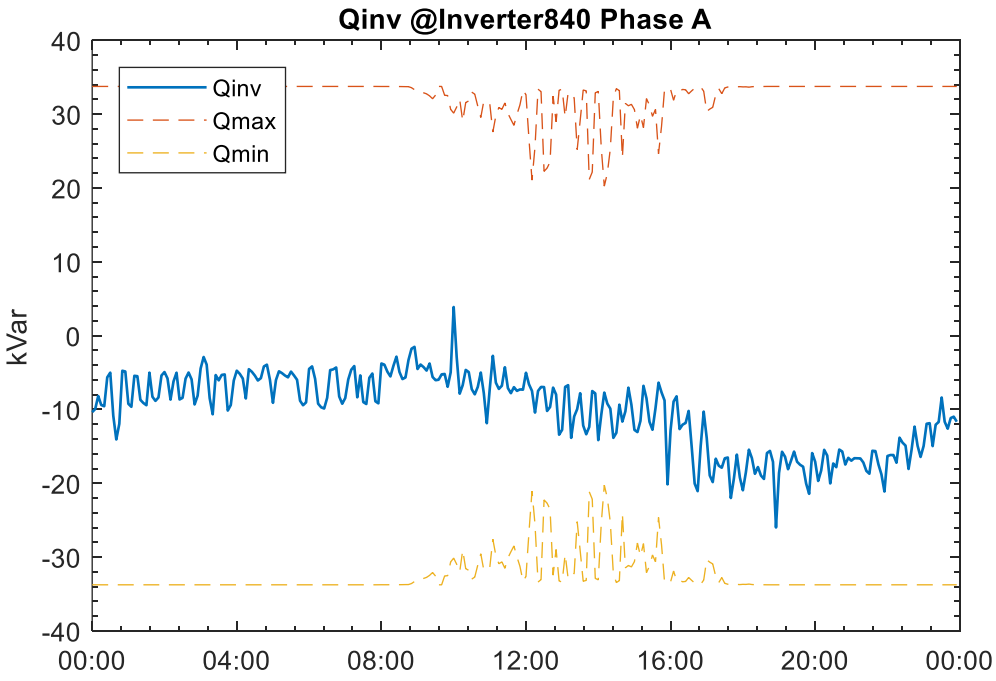

Figure 3.7 Reactive power at Inverter 840 A in a heavy load day

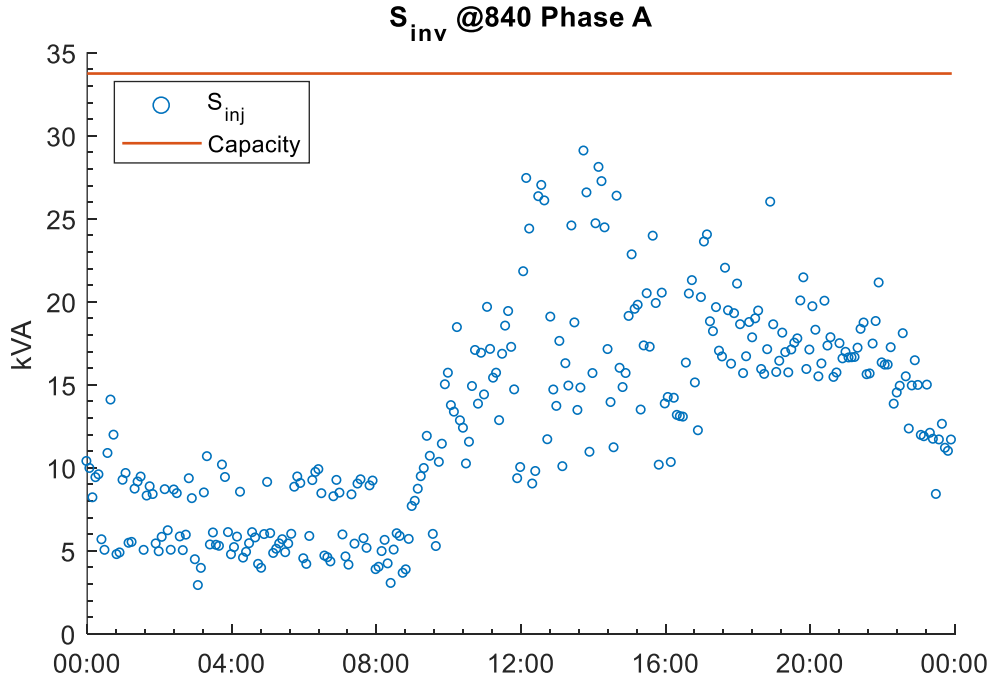

Figure 3.8 Apparent power at Inverter 840 A in a heavy load day

Figure 3.9 shows the power loss profile under both the proposed method and the conventional VVC (used on the IEEE 34 node test feeder) during the day. The results indicate that the proposed VVC provides considerable power loss reduction compared to the conventional VVC scheme: the total energy loss during the day in this case is 36.7% lower than that of the conventional VVC scheme. Figure 3.10 shows the Phase A tap operations of two VRs in the original system. As expected, with variability of system PV output and load, as shown in Figure 2.24, conventional VR control results in excessive tap operations. Compared with Figure 3.4, the proposed coordinated VVC scheme reduces the operation of VR and LTC significantly.

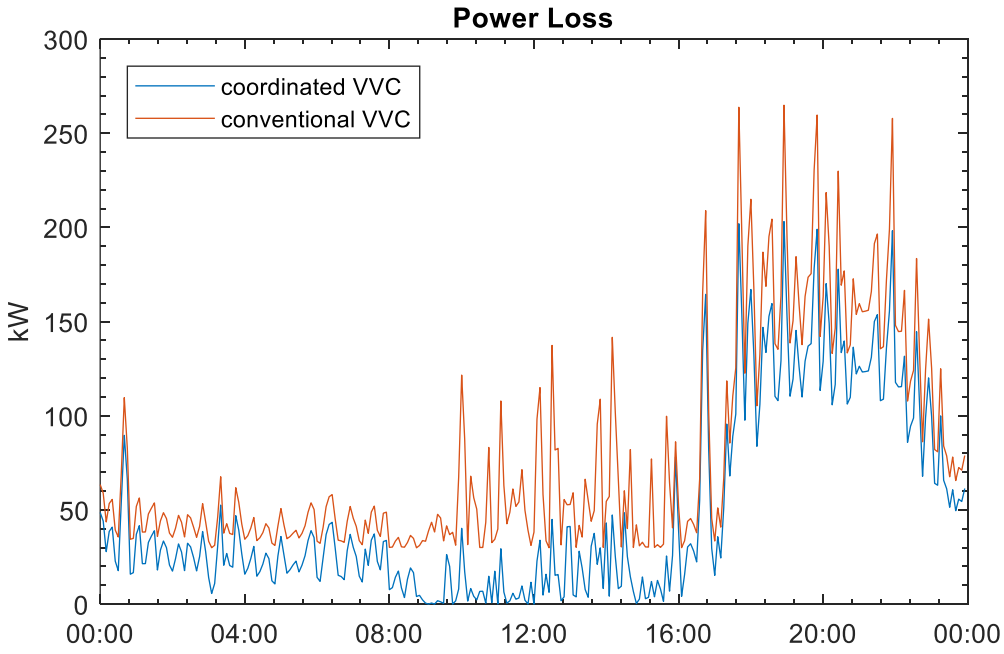

Figure 3.9 Power loss profile in a heavy load day

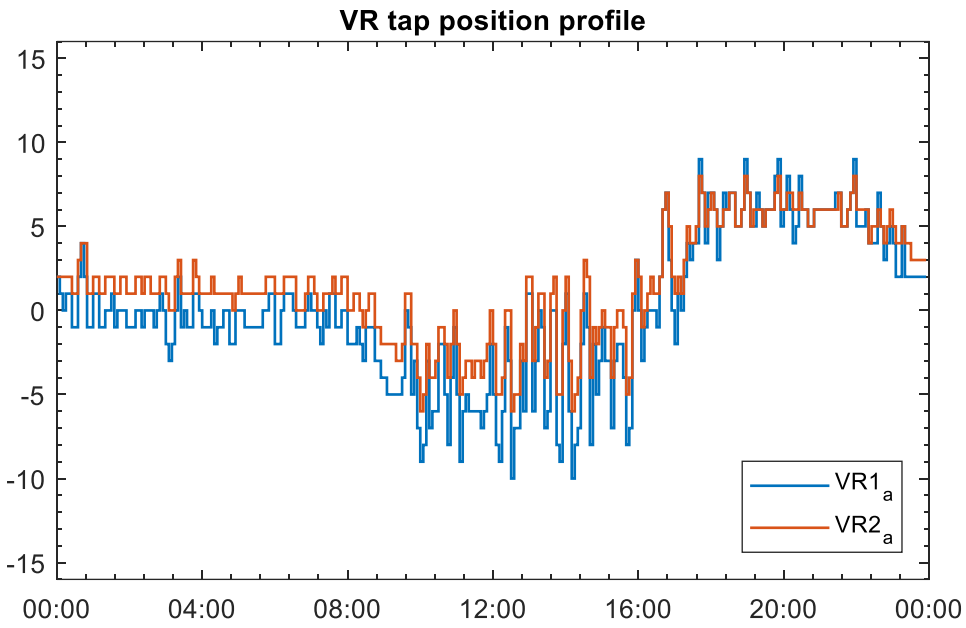

Figure 3.10 VR tap operation profile under conventional VVC

To verify the effectiveness of the proposed voltage control scheme, the 24-h simulation is repeated with a different voltage control scheme. In this case, an exhaustive search method employed for determining the optimal tap settings for voltage control devices when they need to respond to slow load changes. Figure 3.11 and Figure 3.12 show the LTC and VR Phase A tap profiles for the two methods. The two figures show that the exhaustive search method moves the taps more often with finer adjustments, as expected. The main benefits of these adjustments are better loss reduction, as shown in Figure 3.13. However, the cost associated with excessive tap operation may outweigh the additional improvement in power loss reduction.

Finally, the computation time of the proposed coordinated VVC method is quite low, 288 executions of the program (during 24-h simulation) takes 47.4s (0.16s per operating point on

average, with same PC Tech Spec as simulations in Chapter 2). This clearly indicates the feasibility of the method in practice.

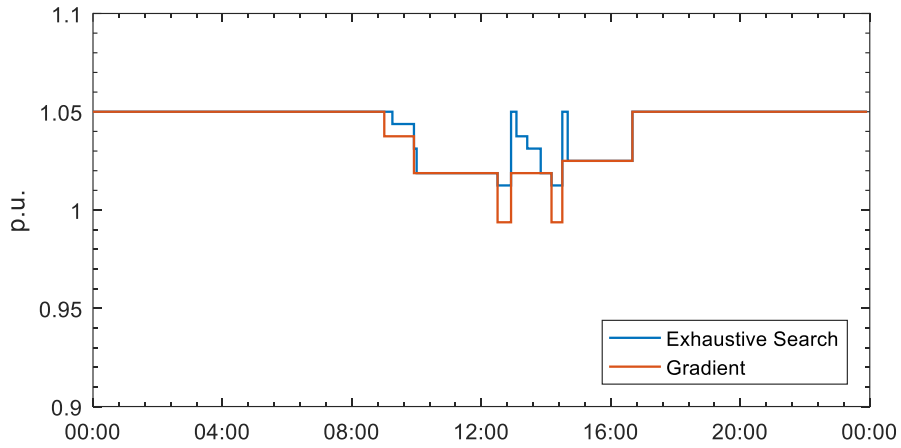

Figure 3.11 Comparison of LTC tap position profile in a heavy load day

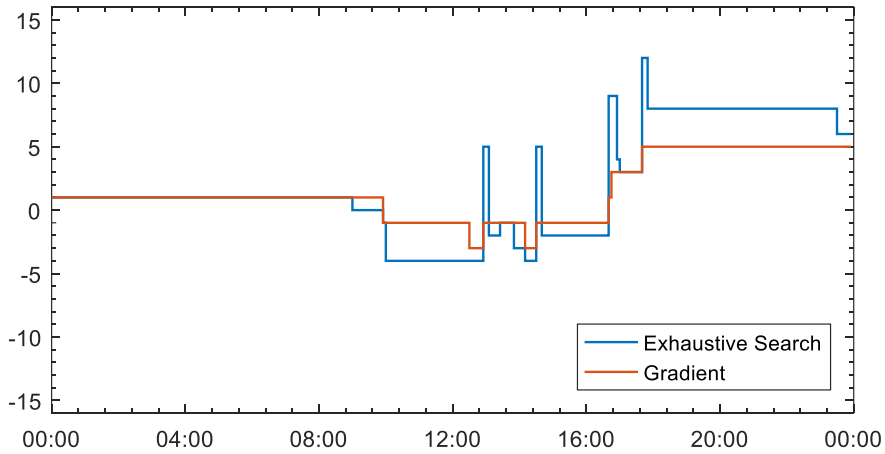

Figure 3.12 Comparison of VR phase A tap position profile in a heavy load day

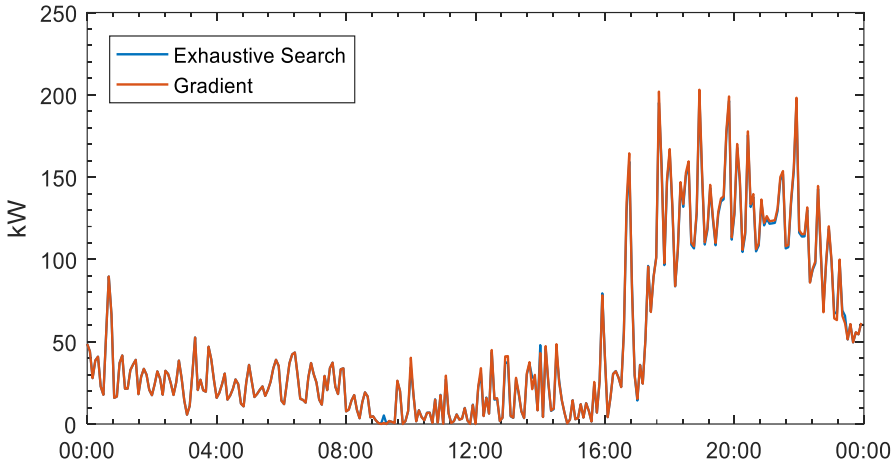

Figure 3.13 Comparison of power loss profile in a heavy load day

To observe the proposed coordinated VVC's performance on the actual circuit, OpenDSS is used as a simulator of a real system. Feeding the control from VVC application in Matlab to OpenDSS circuit, a time-series simulation in is performed to obtain the actual systems response. Figure 3.14 shows a comparison of the power loss expected within the VVC application and the actual power loss of OpenDSS circuit. The box plot of absolute error between two curves in Figure 3.14 is presented in Figure 3.15. The errors are due to the feeder model difference in Matlab and OpenDSS.

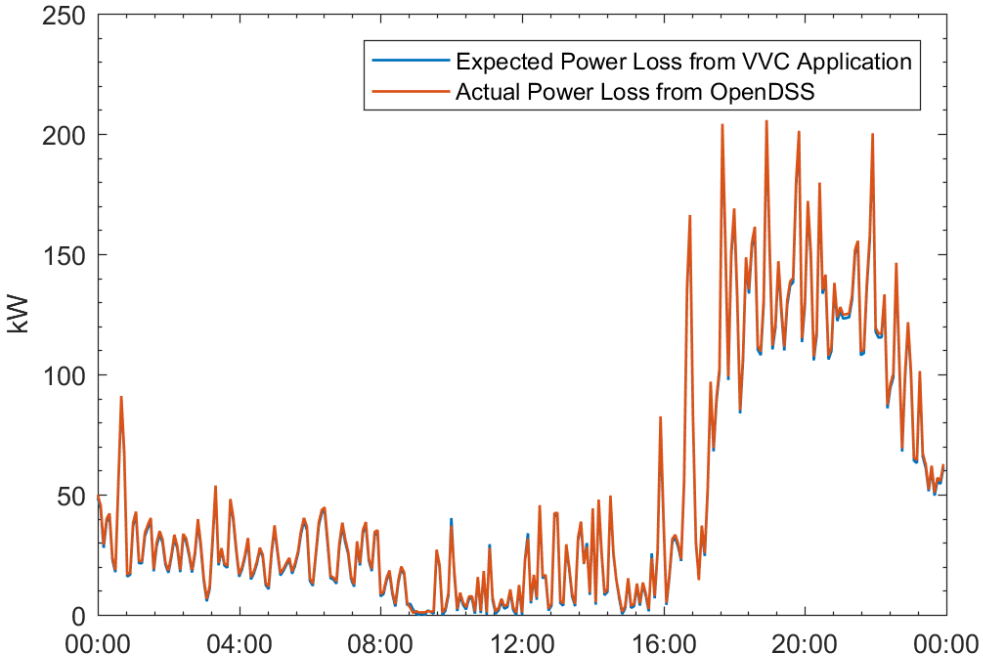

Figure 3.14 Comparison between expected power loss and actual power loss

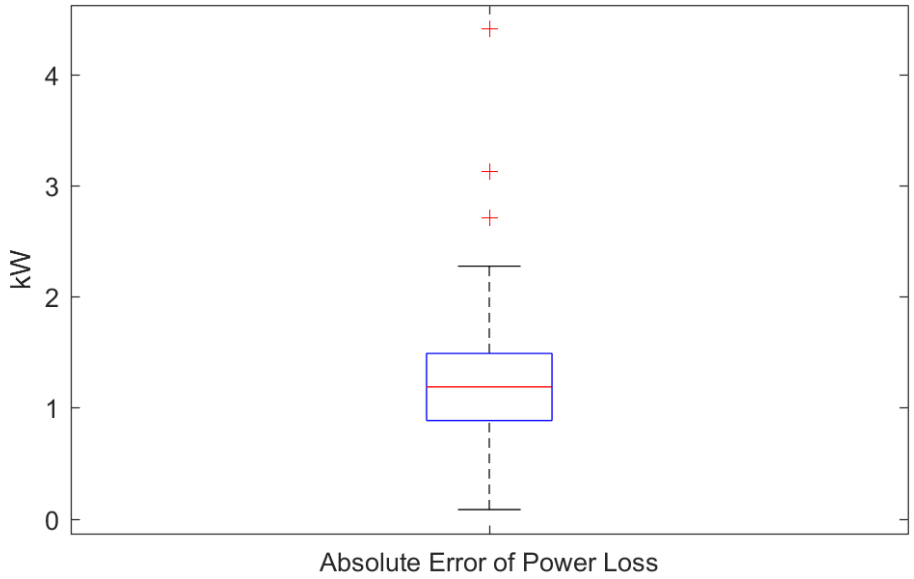

Figure 3.15 Boxplot of absolute error of expected power loss in VVC

Case 2: Light load day

The goal of this simulation is to test the effectiveness of the proposed VVO in adjusting reactive power injection of smart inverters as the system net load changes in a light load day. Figure 3.16 represents a light load day which is used to create the PV generation and load profile.

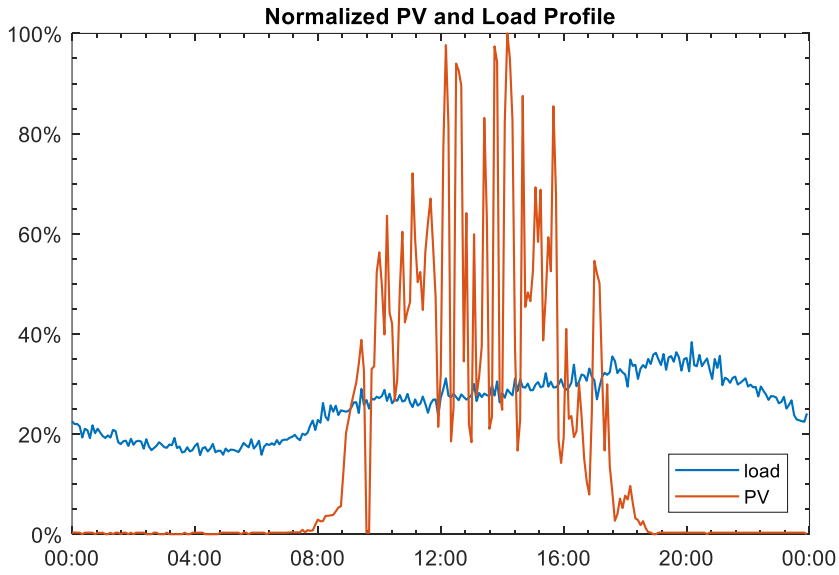

Figure 3.16 PV and load profile in a light load day

Figure 3.17 shows how the voltage control devices, LTC and VR, are controlled. From the results we can see that there is no excessive operation of the devices. Figure 3.18 illustrates the reason for each operation.

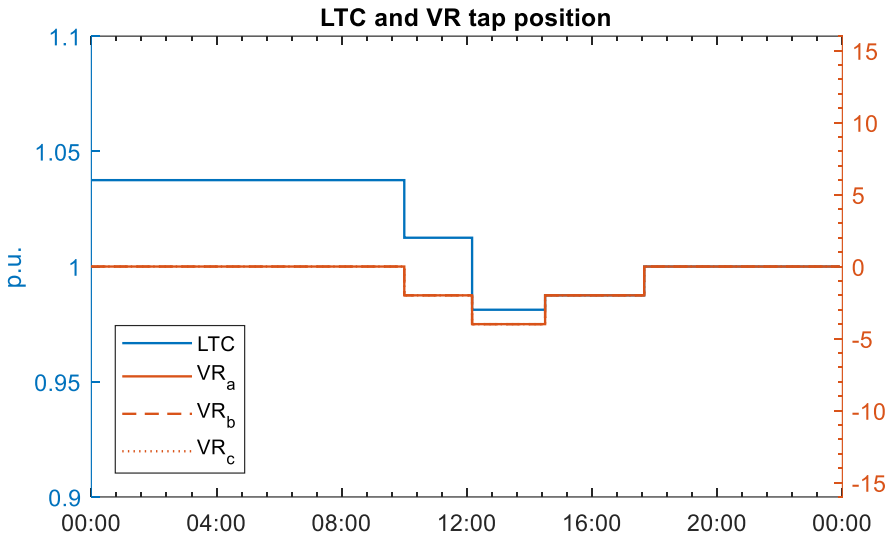

Figure 3.17 LTC and VR tap positions in for light load day

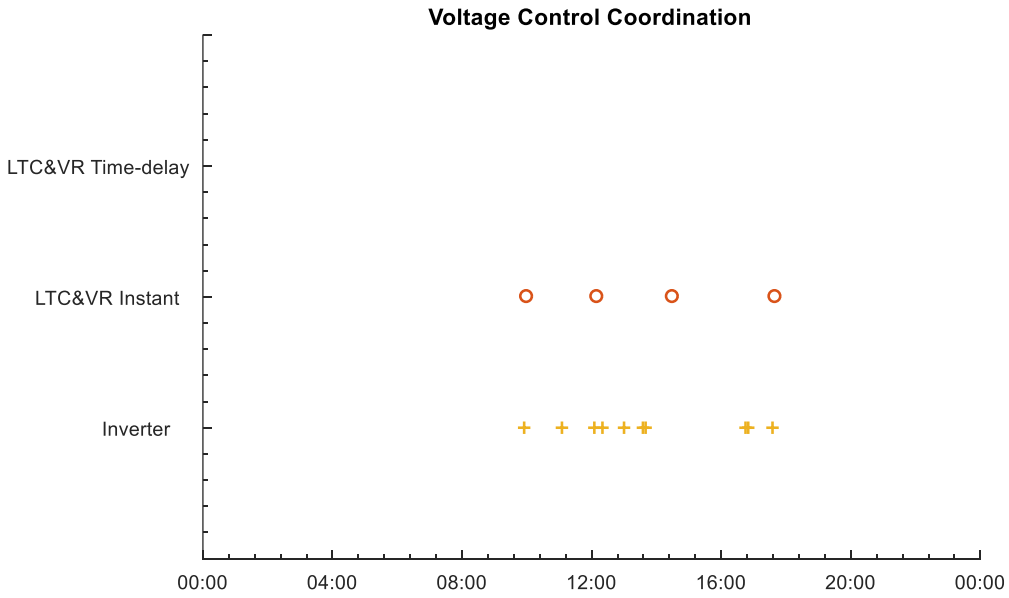

Figure 3.18 Operation sequence of VVC devices

Figure 3.19 confirms that the system maximum and minimum voltages are always kept within the range 0.95 – 1.05 p.u. Figure 3.20 shows the power loss profile under both the proposed method and the conventional VVC (used on the IEEE 34 node test feeder) during the day. The results indicate that the proposed VVC provides considerable power loss

reduction compared to the conventional VVC scheme: the total energy loss during the day in this case is 71.6% lower than that of the conventional VVC scheme. Figure 3.21 shows the Phase A tap operations of two VRs in the original system. As expected, with variability of system PV output and load, as shown in Figure 3.16, conventional VR control results in excessive tap operations. Figure 3.22 shows the Var support from the inverter at Node 840 phase A. The simulation indicates that Var support is adjusted throughout the day for both loss reduction as well as for voltage control, without violating the rating of the inverter as shown in Figure 3.23.

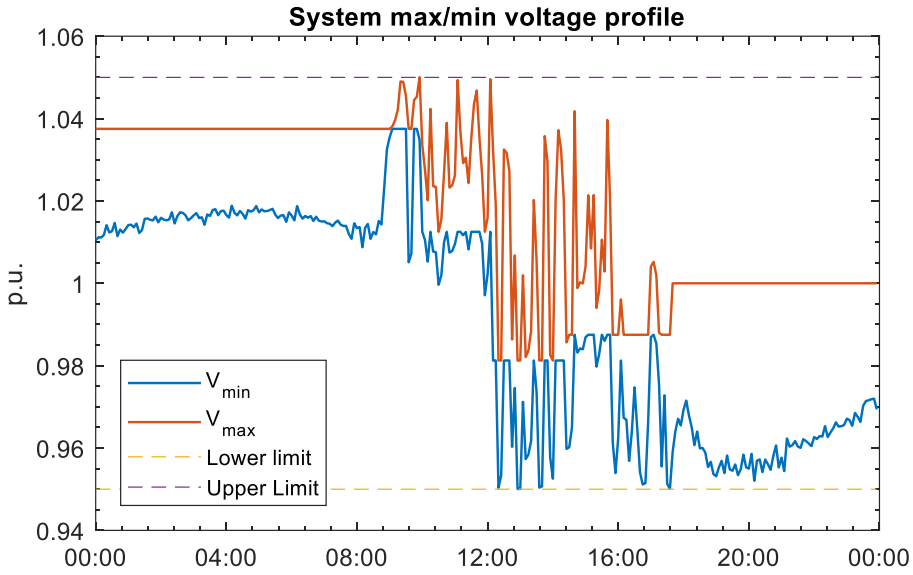

Figure 3.19 Vmax and Vmin profile in a light load day

Finally, the computation time of the proposed coordinated VVC method is quite low, 288 executions of the program (during 24-h simulation) takes 32.3s (0.11s per operating point on average, with same PC Tech Spec as simulations in Chapter 2).

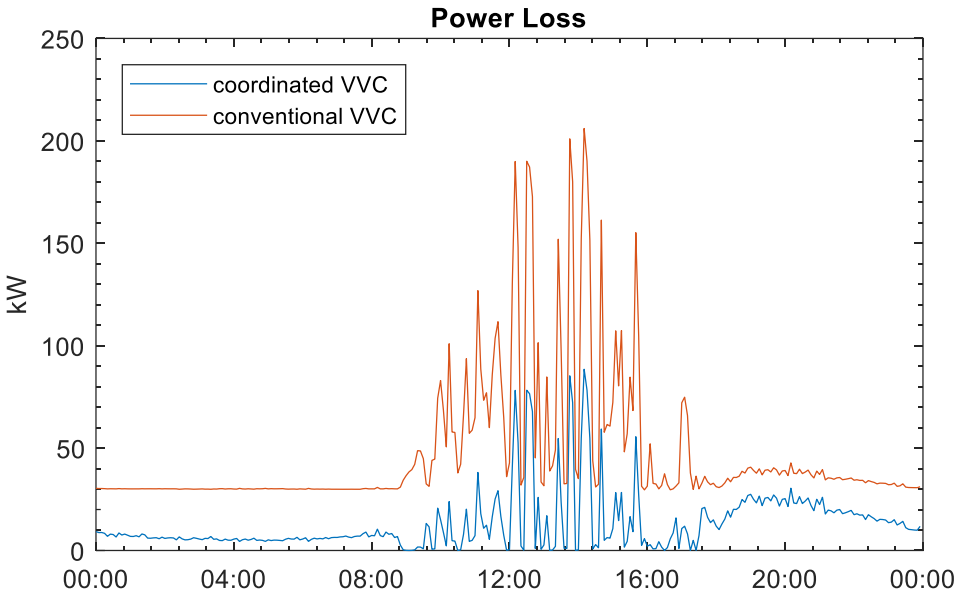

Figure 3.20 Power loss profile in a light load day

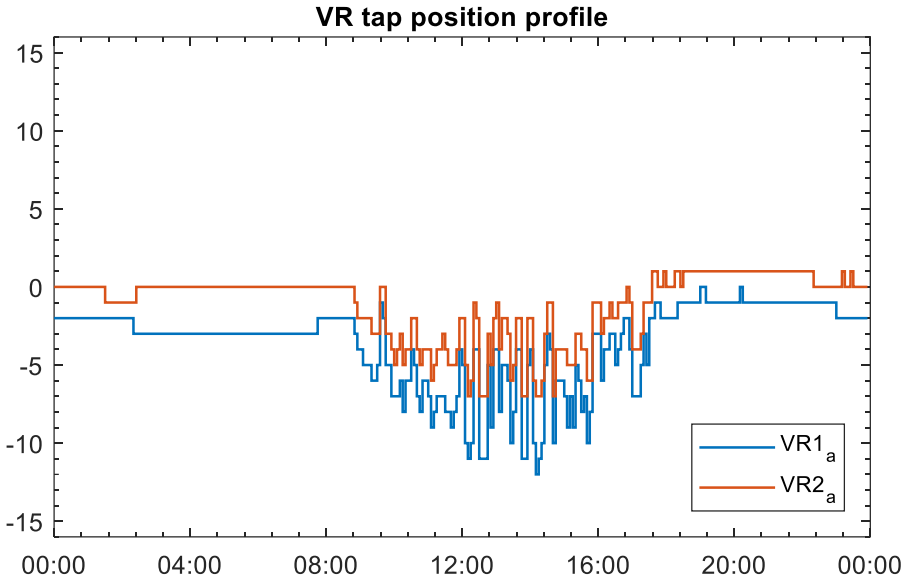

Figure 3.21 VR tap operation profile under conventional VVC

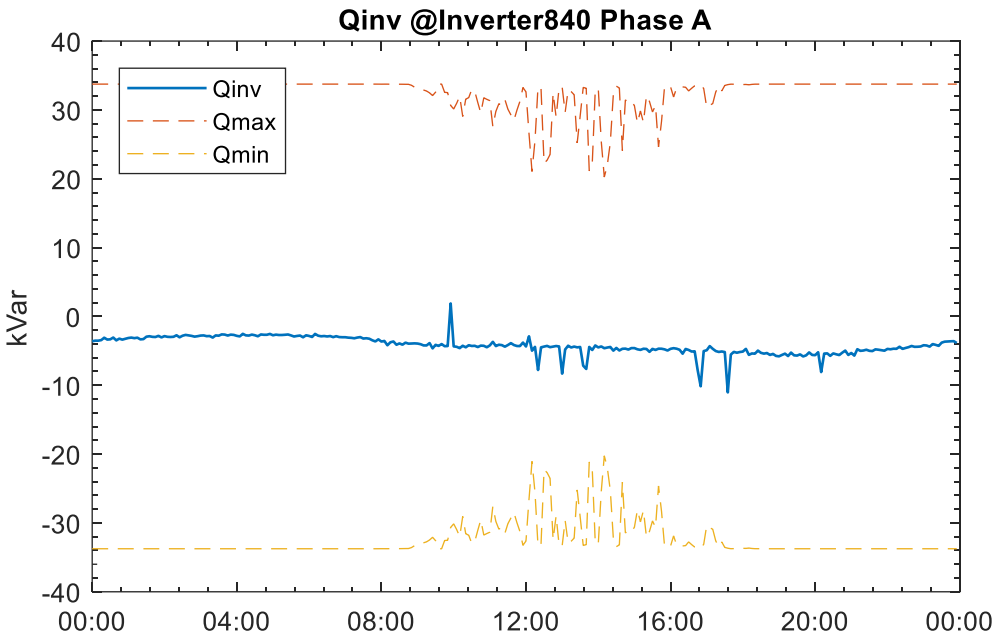

Figure 3.22 Reactive power at Inverter 840 A in a light load day

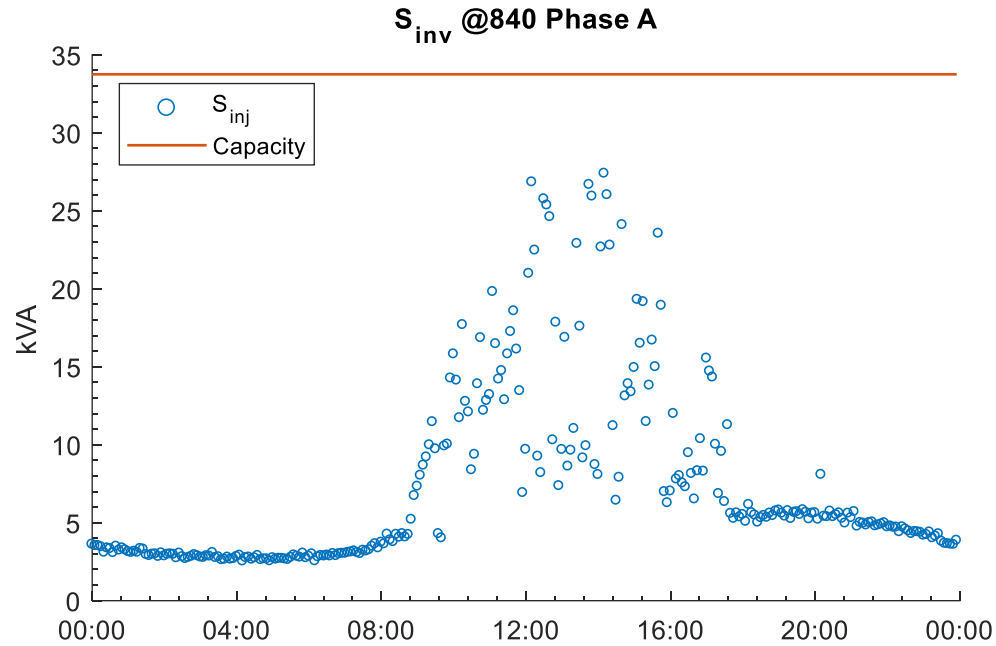

Figure 3.23 Apparent power at Inverter 840A in a light load day

3.3 IEEE 123 Test System Results

IEEE 123 node test feeder is an feeder with a normal voltage of 4.16 kV, as shown in [35]. It is characterized by its many laterals and unbalance. A distribution transformer, between node 61 to 610, step down the voltage to 480V. Besides, there are four VRs as marked in Figure 3.24. There are also 4 shunt capacitors at Node 83, Node 88, Node 90 and Node 92. With the switch status setting as [35], the circuit is a radial system with unbalanced line segments and load. These VVC devices are needed to maintain a good voltage profile under all operating conditions. The VRs have ±16 tap position range with ±10% of maximum voltage change. VR1 is a regulator, with three-phase control. The other VRs are single phase controlled. The IEEE 123 system does not have any DRER.

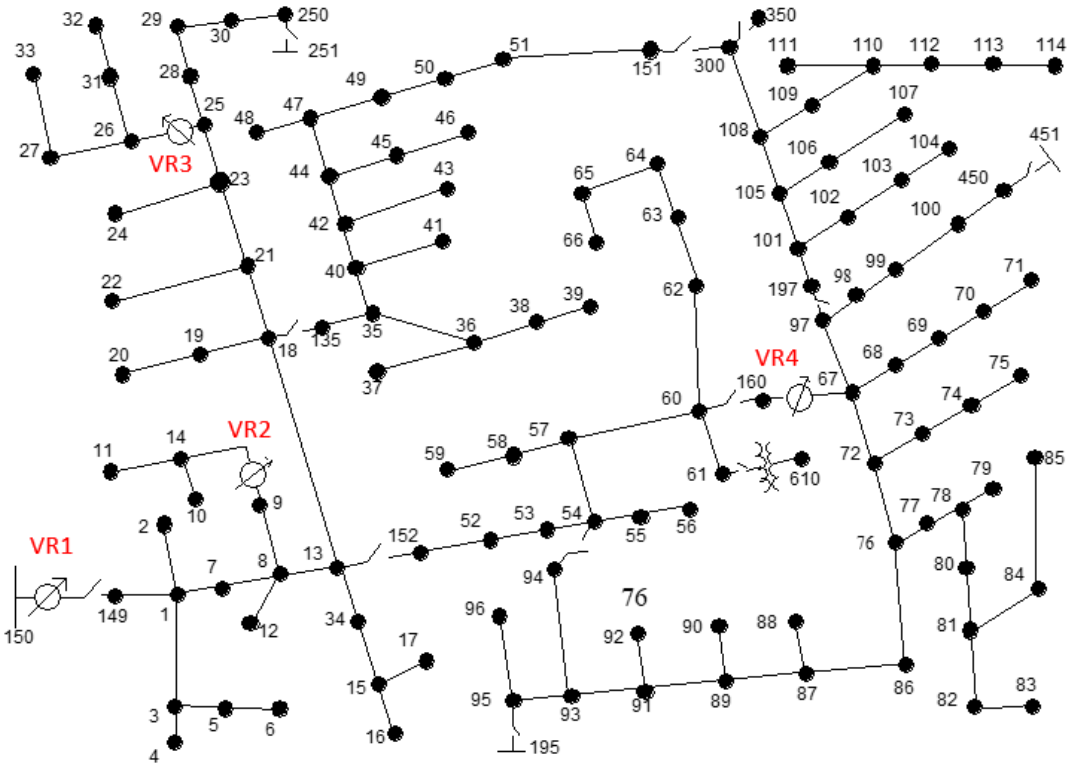

Figure 3.24 Simple diagram of the IEEE 123 Test System [35]

To verify the proposed coordinated VVC's effectiveness on more practical smart distribution system. The following changes are applied to IEEE 123 node test feeder:

1) Load are increased by 10% to create a more severe voltage drop.
2) PV systems with smart inverters are placed at 20% of locations as shown in Table 3.2, and the peak generation is 80% of peak load.
3) All VRs are single phase controlled.
4) All CAPs are removed, since the smart inverters can provide sufficient reactive power for VVC.

Table 3.2 Nodes with PV systems

	Node ID
Phase A	9, 48, 49, 52, 65, 76, 82, 109, 113
Phase B	48, 49, 65, 76
Phase C	48, 49, 65, 76

Case 1: Heavy load day

Figure 3.25 shows the profile of total load (real power) and total PV generation in modified IEEE 123 system in a heavy load day.

Figure 3.26 shows how the taps of VR4 changes in a heavy load day. From the results we can see that there is no excessive operation of the devices. Figure 3.27 illustrates the reason for each operation. Since most of the time, the smart inverters can provide sufficient reactive power to control voltage. The tap changes are very limited.

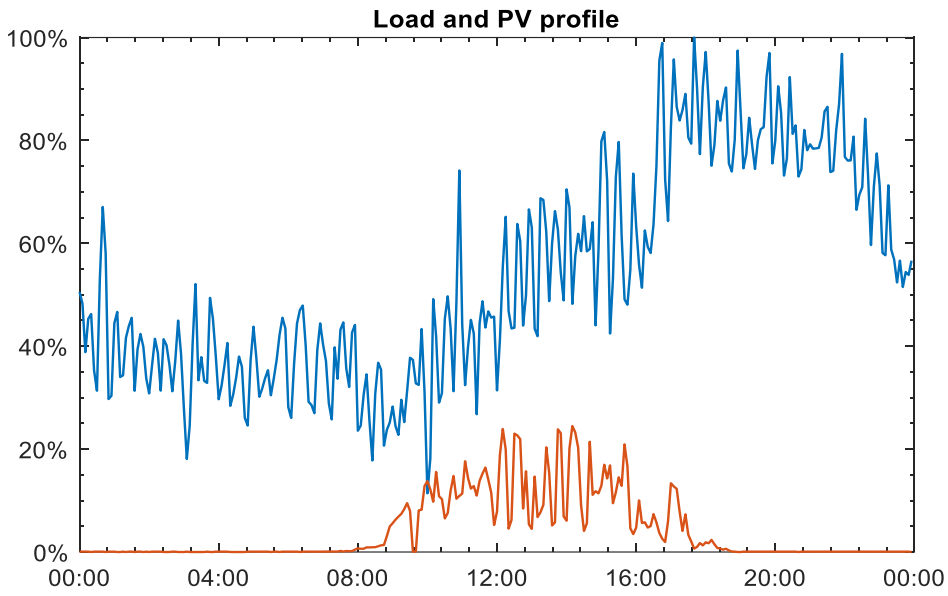

Figure 3.25 Normalized load and PV profile in a heavy load day

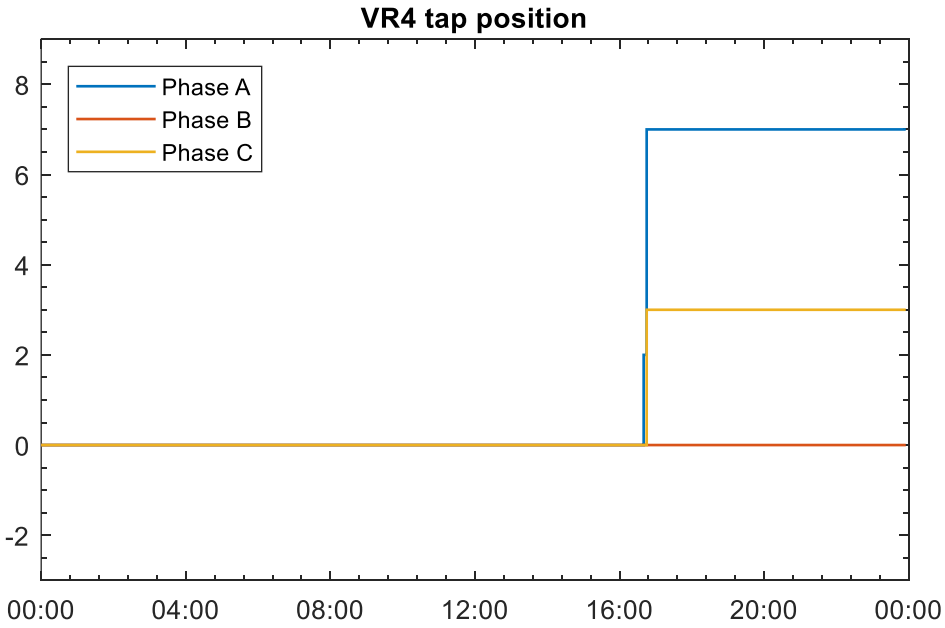

Figure 3.26 VR4 Tap positions for a heavy load day

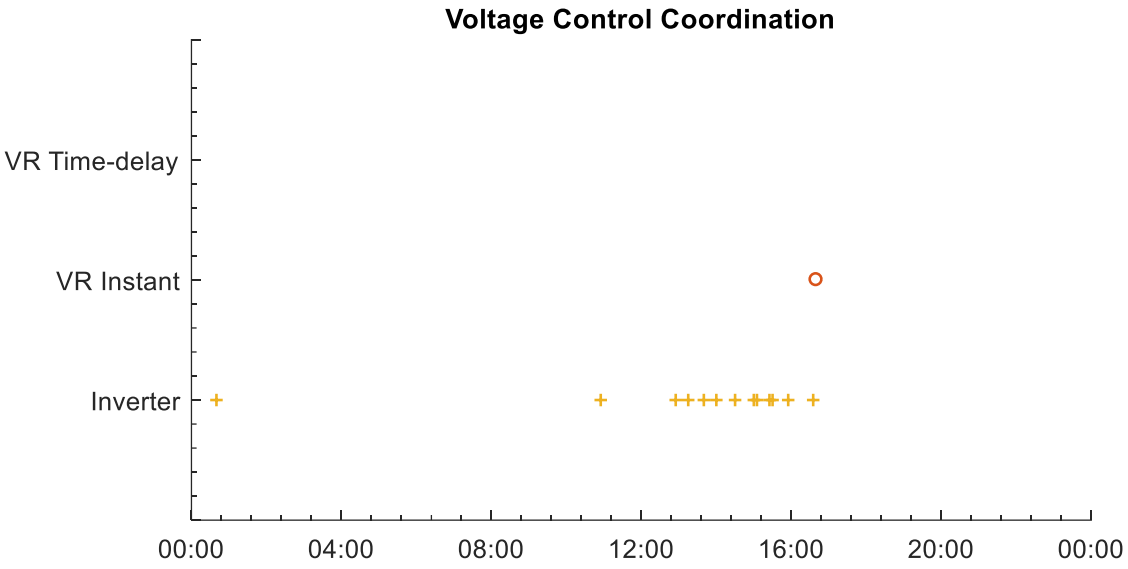

Figure 3.27 Operation sequence of VVC devices in a heavy load day

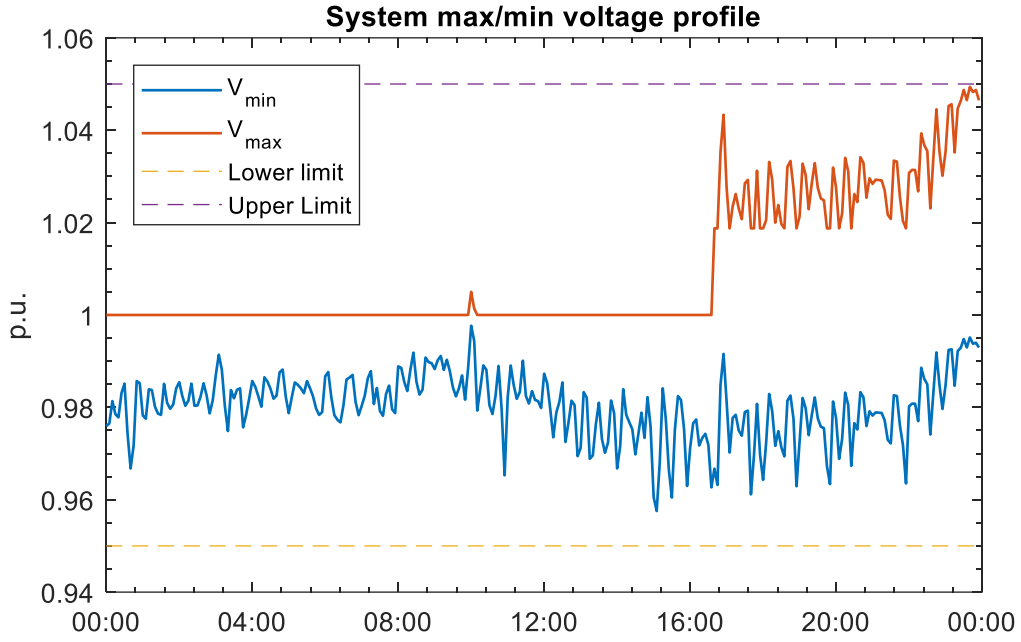

Figure 3.28 V_{max} and V_{min} profile in a heavy load day

Figure 3.28 confirms that the system maximum and minimum voltages are always kept within the range 0.95 – 1.05 p.u.. For this modified IEEE 123 node system, with the

conventional control scheme in [35], system has voltage violation during peak load due to the coupling of unbalanced phases.

Figure 3.29 shows the Var support from the inverter at Node 76 phase A. Figure 3.30 shows the apparent power at the same inverter. The simulation indicates that Var support is adjusted throughout the day for both loss reduction as well as for voltage control without violating the rating of the inverter.

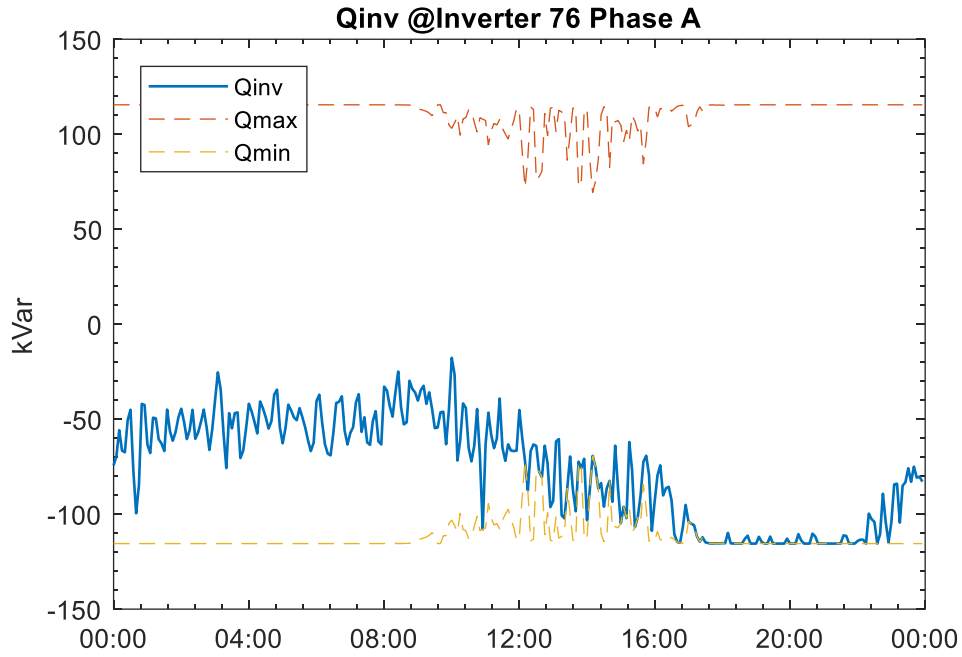

Figure 3.29 Reactive power at Inverter 76 A in a heavy load day

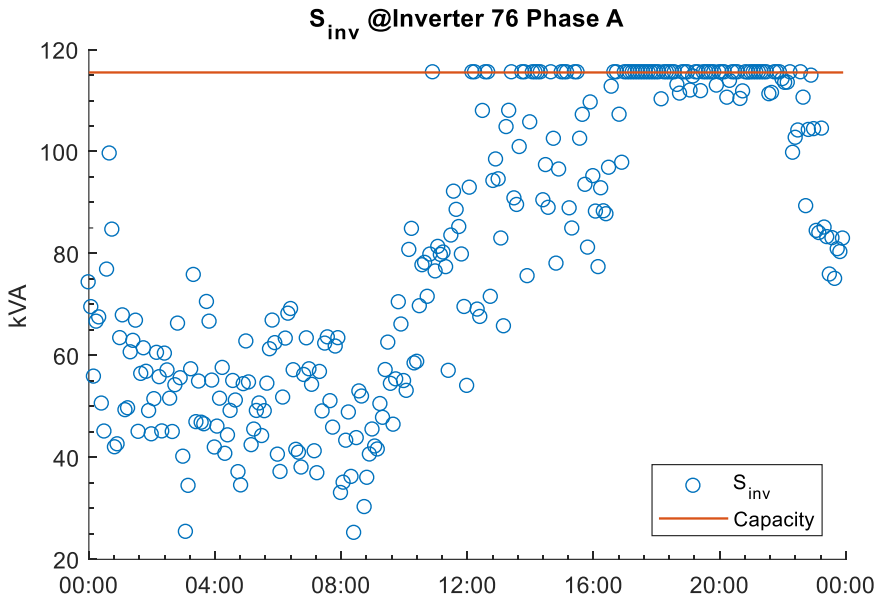

Figure 3.30 Apparent power at Inverter 76 A in a heavy load day

Figure 3.31 shows the power loss profile under both the proposed method and the conventional VVC during the day. In this figure, power loss of conventional case increases significantly after 16:00. This is due to the system net reactive load change with capacitors always on, as shown in Figure D7. The results indicate that the proposed VVC provides considerable power loss reduction compared to the conventional VVC scheme: the total energy loss during the day in this case is 31.25% lower than that of the conventional VVC scheme. Figure 3.32 shows VR4 Phase A tap operations under both the proposed VVC scheme and conventional scheme. As expected, with variability of system PV output and load, as shown in Figure 3.25, conventional VR control results in excessive tap operations. the proposed coordinated VVC scheme reduces the operation of VR and LTC significantly. Figure 3.33 shows the variance of system voltages after each control cycle. We can observe that the proposed coordinated VVC scheme has much less variance than conventional control

scheme. This indicates that the proposed method creates potential for conservation voltage reduction (CVR) application.

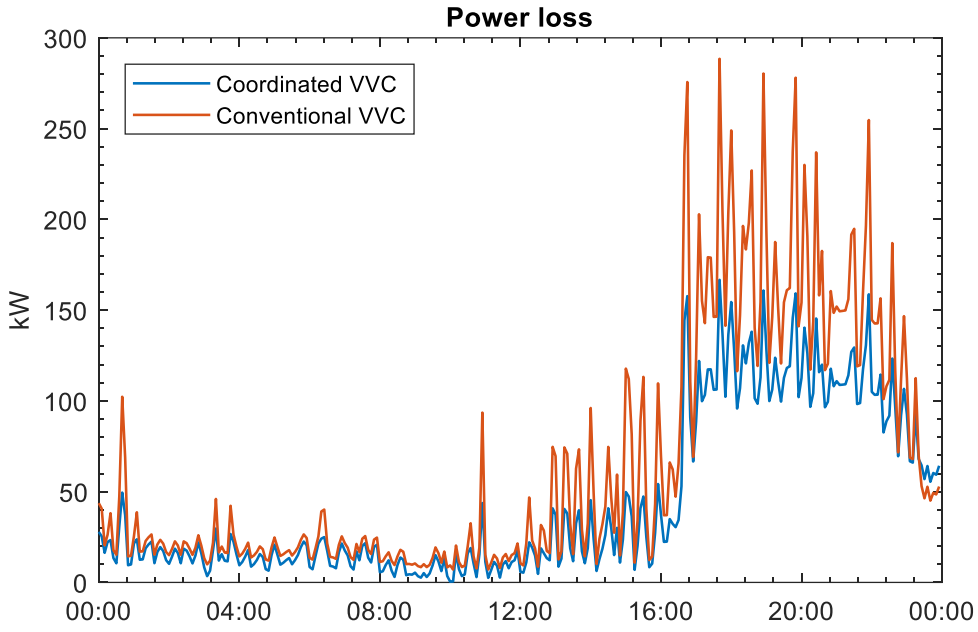

Figure 3.31 Power loss profile in a heavy load day

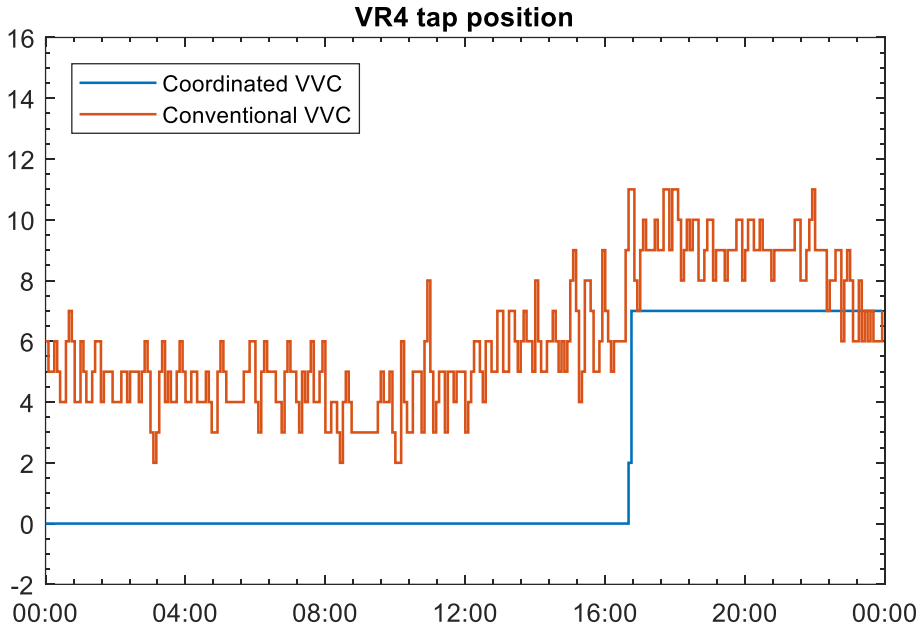

Figure 3.32 Comparison of VR phase A tap position profile in a heavy load day

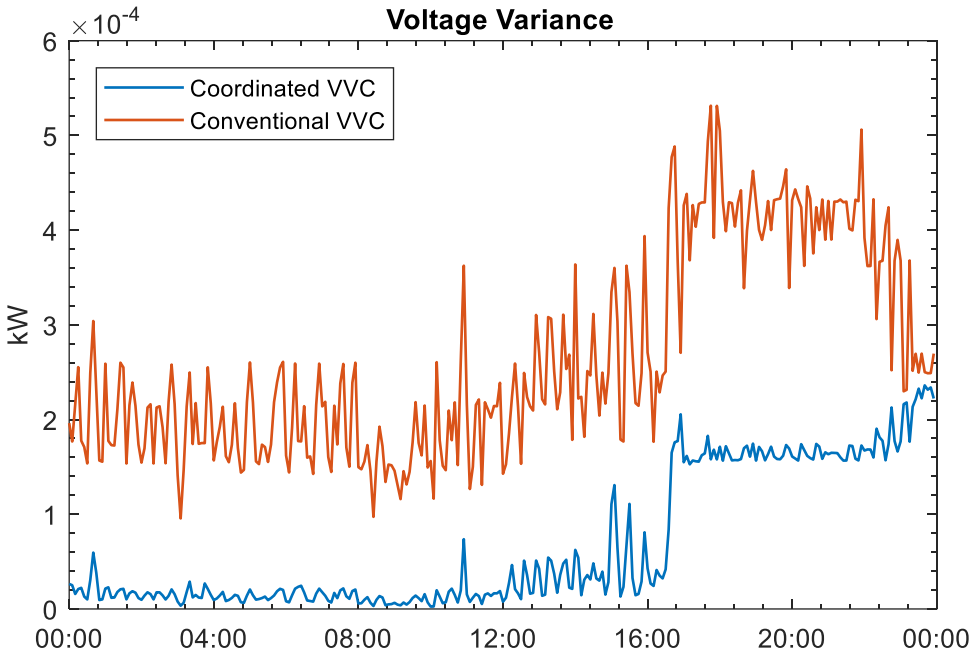

Figure 3.33 Comparison of voltage variance in a heavy load day

Finally, the computation time of the proposed coordinated VVC method is not high, 288 executions of the program (during 24-h simulation) takes 952.2s (3.31s per operating point on average, with same PC Tech Spec as simulations in Chapter 2). Even though this runtime is much higher than the results of 34 node system, it is still acceptable for 5 min interval real-time implementation.

Voltage Optimization

Take the situation at 16:35 for example, with the previous VR tap positions and the updated load and PV generation at 16:35, VVO application sees an under-voltage violation.

According to the two-level control scheme, VVO first estimates if the reactive power support from the smart inverters is sufficient to correct the voltage. As Figure 3.34 shows, the

node voltages move towards the acceptable ranges gradually and it takes nine iterations to bring the voltages within 0.95 – 1.05 p.u..

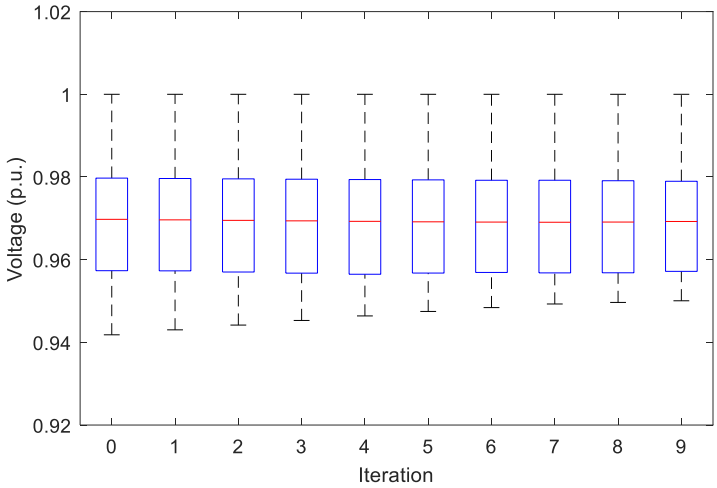

Figure 3.34 Voltage statistics in voltage optimization

Voltage Control

In the next control cycle, at 16:40, the system net load increased from 69% to 92%, the VVO application finds that reactive power from smart inverters is not sufficient to support the voltage. Therefore, the voltage control module, tap searching, is triggered.

Table 3.3 shows the tap positions found. The new tap positions bring the minimum system voltage from 0.92 p.u. to 0.95 p.u. To test if the proposed tap search is sufficient to get an optimal tap setting, searching with $\Delta Tap^{p} = \{0 \quad \pm 1 \quad \pm 2 \quad \pm 3 \quad \pm 4\}$ is performed. With a wider tap range searched, it returns the same results as shown in Table 3.3.

Table 3.3 Tap positions after searching

	Phase A	Phase B	Phase C
VR1	3	0	3
VR2	0	NA	NA
VR3	0	NA	0
VR4	2	0	0

Var Optimization

At 16:40, after the voltage violation is fixed by the voltage control module in VVO, the Var Optimization is triggered to determine the reactive power support from the smart inverters to minimize the power loss. The result of Var Optimization is shown in Table 3.4. The power loss returned is higher than the value in the last iteration on Figure 3.35, this is because there are inverters reach the limit of available Var. The power loss in Figure 3.35 does not consider the limit of available Var. In this case, $\beta(0)$ and γ are selected in the same way as in 34 node system. A larger $\beta(0)$ such that $|\Delta u|^{min} = 0.2\ kVar$ results in 32 iterations to converge. Figure 3.36 shows the voltage from the source node to one of the feeder ends, Node 114. 3-D plot, Figure 3.37, visualizes the reactive power injection on each node with load in the system. Nodes that are labeled with Node ID are the nodes with PV systems. We can observe that these nodes have reactive power going into the system, which indicates the inverters provides reactive power to minimize the system power loss.

Table 3.4 Results of Gradient VVC

	Iterations	Vmin (p.u.)	Vmax (p.u.)	Loss (kW)	Loss Reduction(kW)
Initialization		0.956	1.019	152.536	
Gradient Method	56	0.967	1.019	144.329	8.207

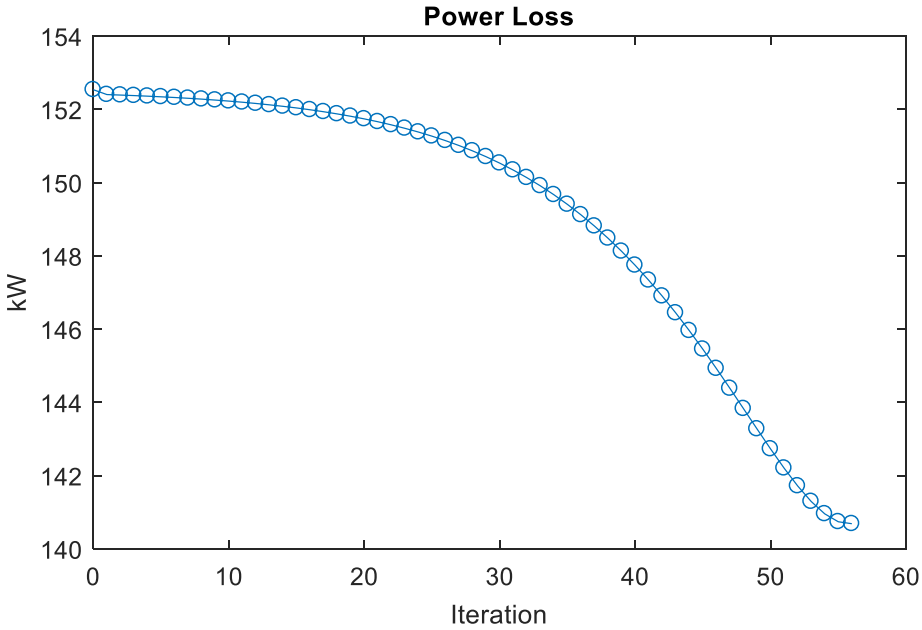

Figure 3.35 Power loss of gradient based Var Optimization

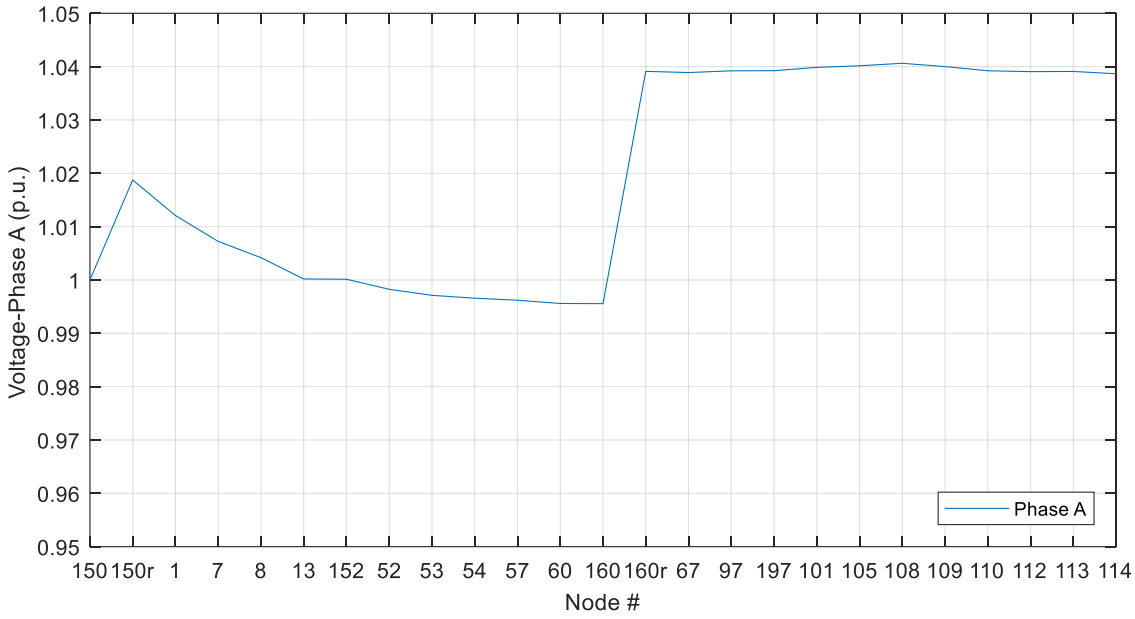

Figure 3.36 Phase A feeder voltage after Var Optimization

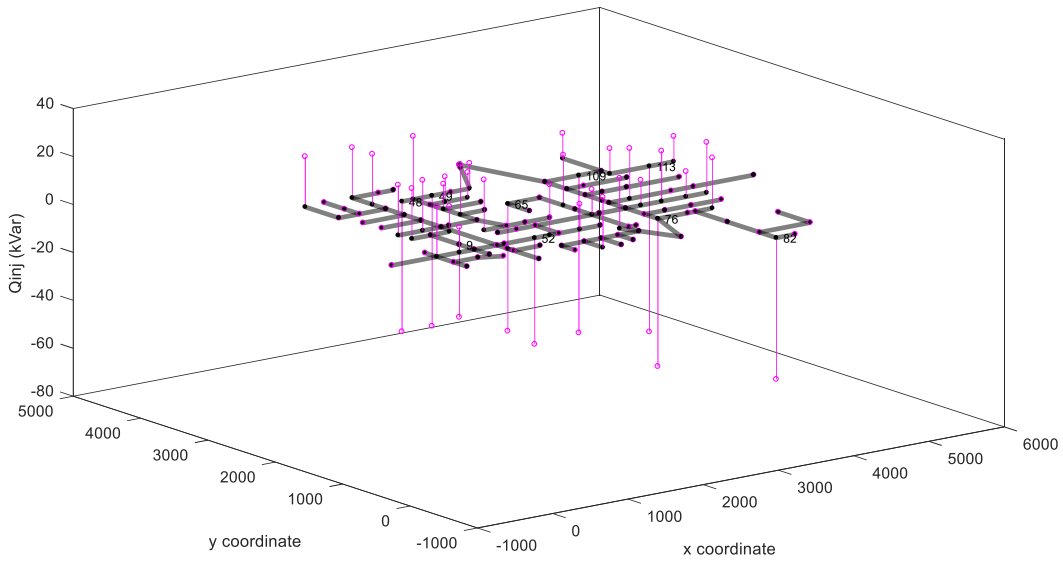

Figure 3.37 Q_{inj} on modified IEEE 123 node system after Var Optimization

Case 2: Light load day

Figure 3.38 represents a light load day which is used to create the PV generation and load profile. Figure 3.39 shows that the taps of VR4 remain unchanged in this light load day. And for other VRs in the system, it is the same case. This is due to that the system load and PV penetration are not significant enough to trigger the voltage control module to adjust the taps. Figure 3.40 confirms that the system maximum and minimum voltages are always within the range 0.95 – 1.05 p.u.. Figure 3.41 shows the Var support from the inverter at Node 76 phase A. Figure 3.42 shows the apparent power at the same inverter. The simulation show that Var support is adjusted throughout the day for loss reduction without violating the rating of the inverter.

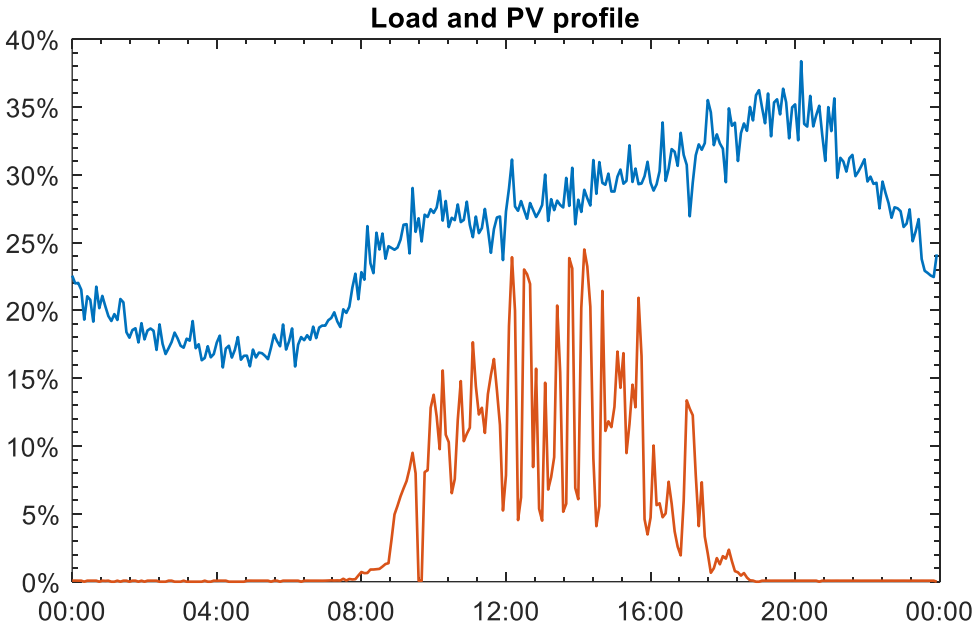

Figure 3.38 Normalized load and PV profile in a light load day

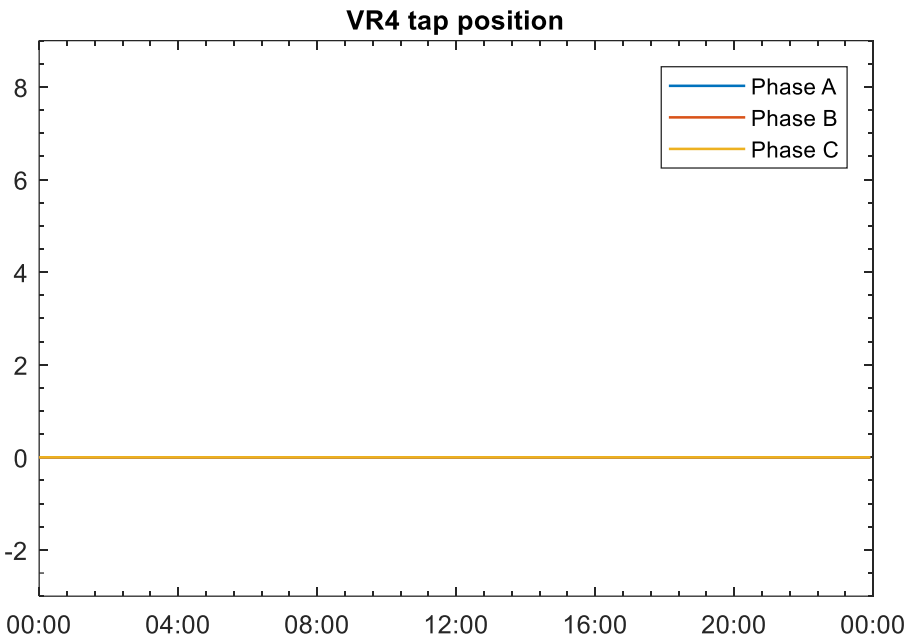

Figure 3.39 VR4 Tap positions for a light load day

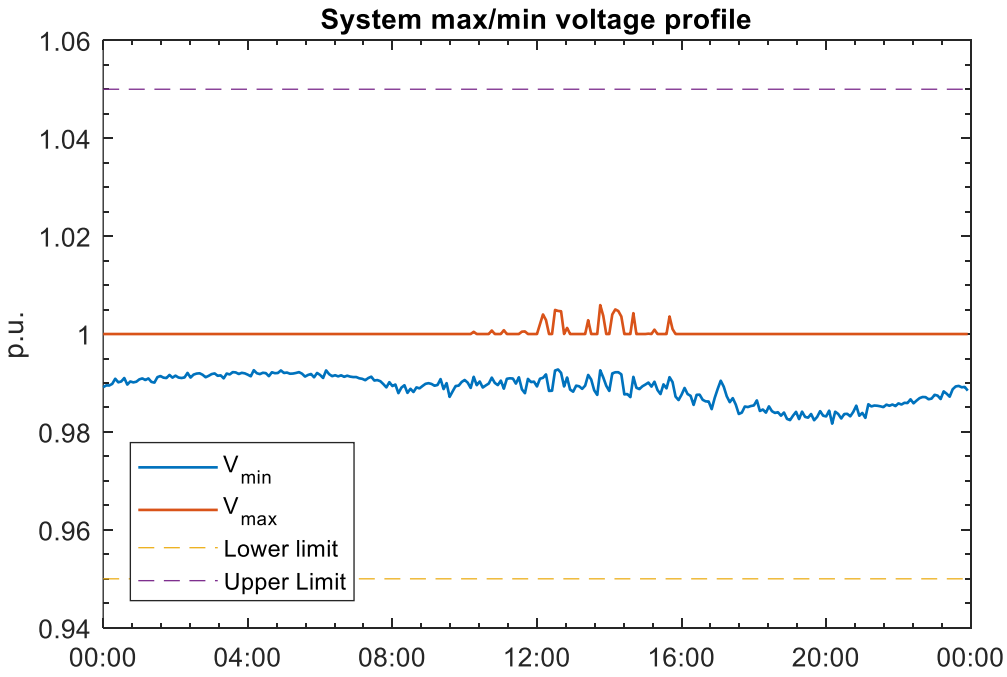

Figure 3.40 V_{max} and V_{min} profile in a light load day

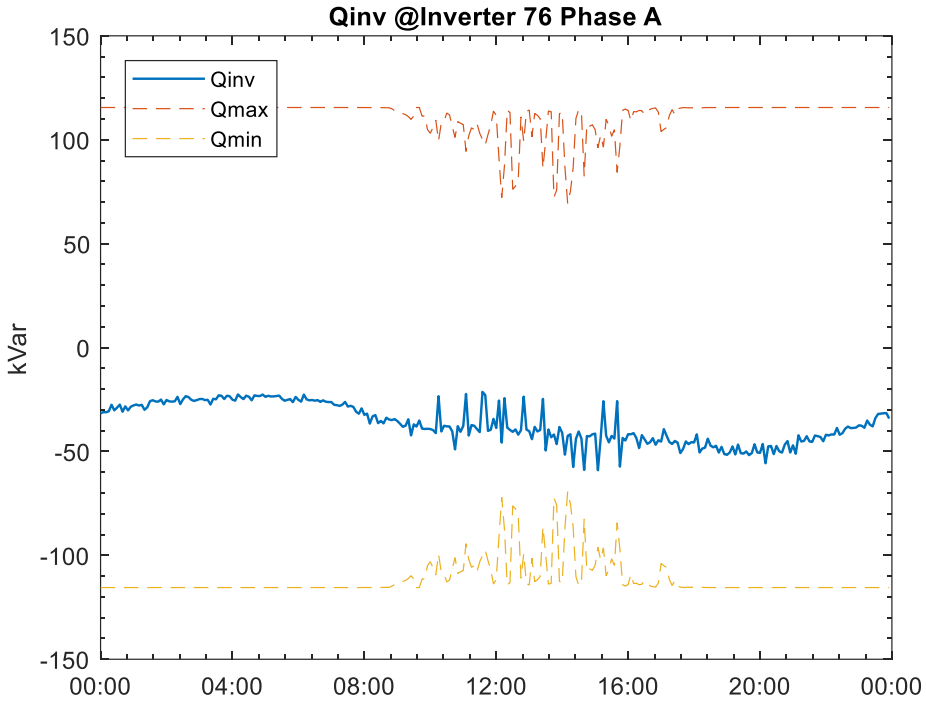

Figure 3.41 Reactive power at Inverter 76 A in a light load day

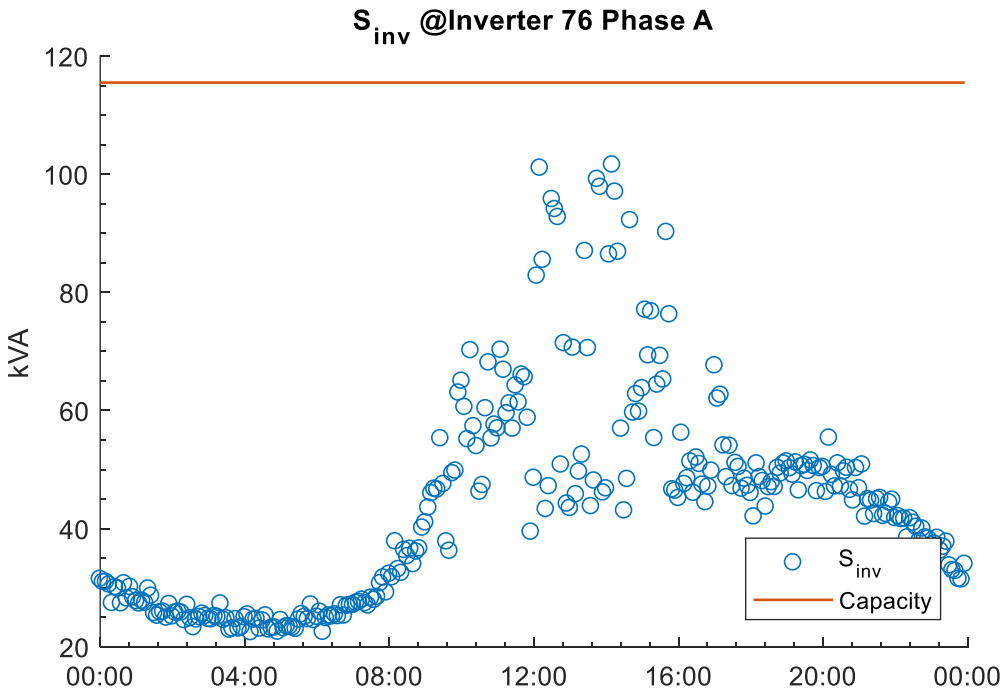

Figure 3.42 Apparent power at Inverter 76 A in a light load day

Figure 3.43 shows the power loss profile under both the proposed method and the conventional VVC during the day. The results indicate that the proposed VVC provides considerable power loss reduction compared to the conventional VVC scheme: the total energy loss during the day in this case is 57.55% lower than that of the conventional VVC scheme. Figure 3.44 shows the VR4 Phase A tap operations under both the proposed VVC scheme and conventional scheme. Figure 3.45 shows the variance of system voltages after each control cycle. We can observe that the proposed coordinated VVC scheme has much less variance than conventional control scheme. This indicates that the proposed method creates potential for conservation voltage reduction (CVR) application.

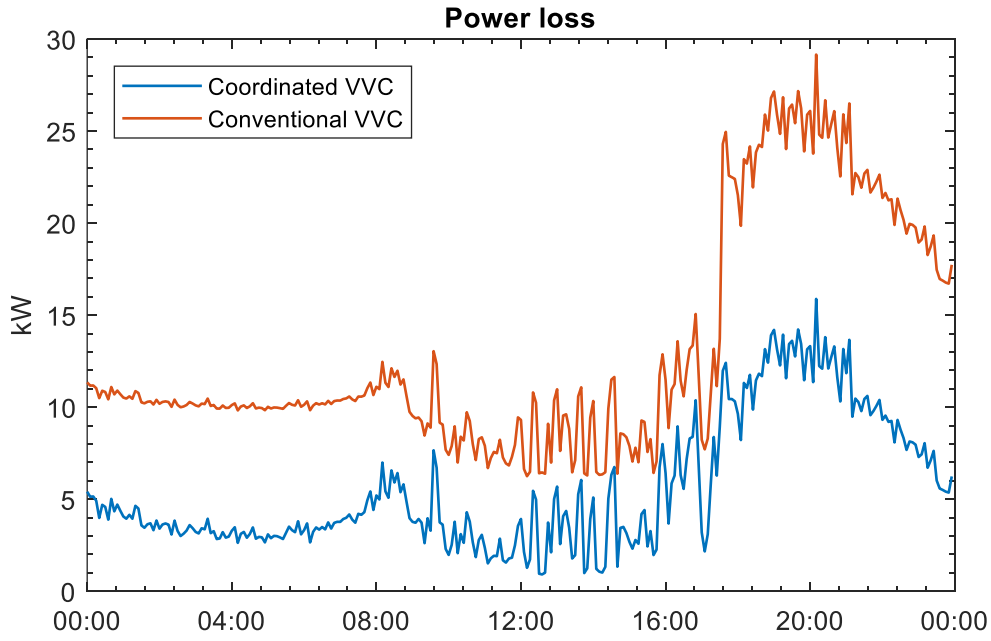

Figure 3.43 Power loss profile in a light load day

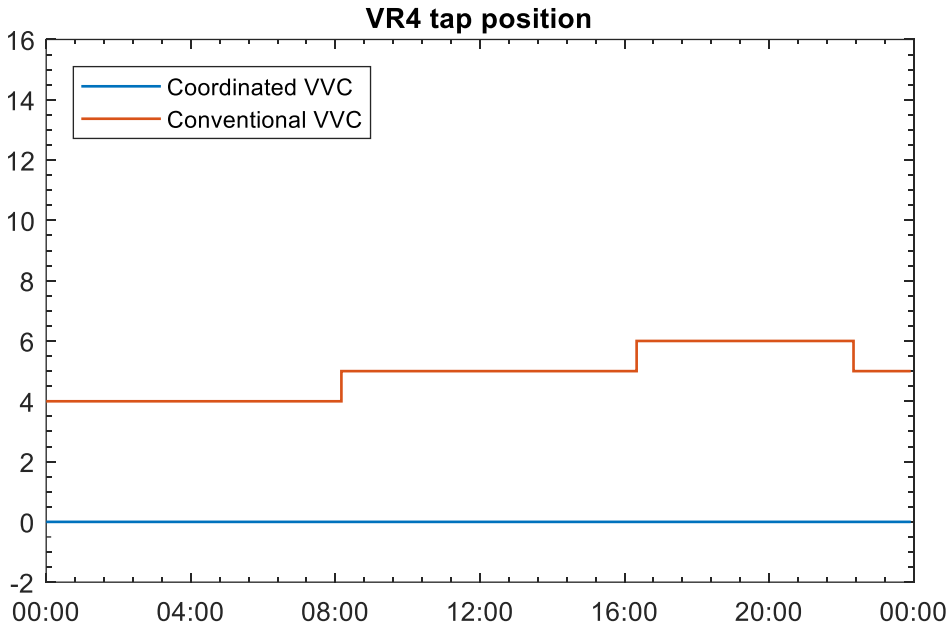

Figure 3.44 Comparison of VR4 Tap positions in a light load day

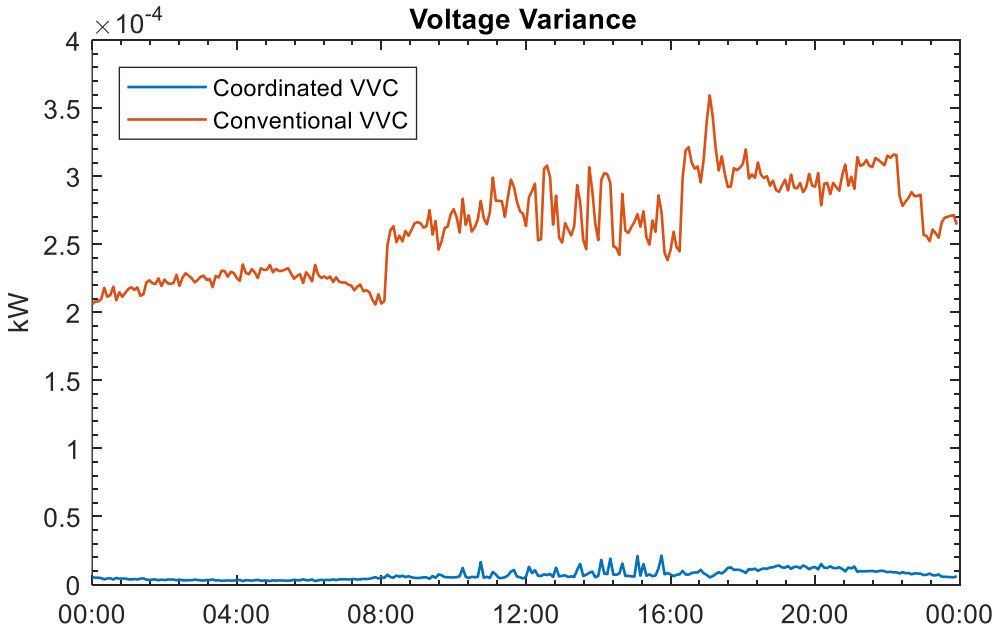

Figure 3.45 Comparison of voltage variance in a light load day

Finally, the computation time of the proposed coordinated VVC method is not high, 288 executions of the program (during 24-h simulation) takes 575.1s (2.00s per operating point

on average, with same PC Tech Spec as simulations in Chapter 2). Even though this runtime is much higher than the results of 34 node system, it is still acceptable for 5 min interval real-time implementation.

3.4 Conclusions

In this chapter, a two-level coordinated Volt/Var control is proposed. The FREEDM IEEE 34 node test feeder with full PV deployment and IEEE 123 node test feeder with partial PV deployment are used to test the performance of proposed VVC scheme. The results show that the method handles the three operational requirements for VVC effectively: maintaining the node voltages within limits while avoiding excessive device operations, and reducing power losses. The test results also show that proposed gradient method for Var compensation is very effective in determining the Var support from DRERs. Results based on a daily operation also verify that the method minimizes the operation of the LTC and VR by using Var support from DERs to respond to the voltage variations caused by variable PV output. Runtime results also show that the proposed VVC method is fast and therefore appropriate for practical implementation.

Chapter 4. Load Parameter Estimation for Real-time Volt/Var Control

Load modeling is important for power system studies. Distribution power flow analysis requires more detailed modeling of line sections and loads to represent the actual system, because these will affect the power flow results. Since this work formulates the VVC problem as an optimal power flow problem, load modeling for VVC needs to be investigated. This chapter first introduces the common load models used in power system analysis. Then, different parameter estimation techniques that can be used for load parameter estimation are discussed. In this chapter, a load model for small-size transformer (e.g. SST) is proposed. An on-line estimation approach is used to identify the parameters of the load model in real-time to support the VVO application. The proposed estimation approach is tested on IEEE 13 node system with detailed load modeling of 629 houses.

4.1 Load Models

Researchers has been realized the importance of load modeling for power systems analysis. Challenges of load modeling come from, diversity of components, uncertainty and lack of data [36]. In the last few decades, many load models were proposed based on the need of studies [36]-[38]. Basically, load models can be classified into two categories, static load model and dynamic load model.

1) Static load model

   In static load models, at every instant of time, the power, both real and reactive, is a function of voltage magnitude or voltage magnitude with frequency. These models are accurate enough for some static loads, for example electric heaters. And they are also used to approximate dynamic loads, for example induction motors [36].

- ZIP load model

  In this model, a load is assumed to have three components, constant impedance component, constant current component and constant power component, as shown by (4-1). For simplicity, the formulas are presented for real power only. This model is commonly used in both steady-state and dynamic studies.

  $$P = P_0(\alpha_Z \cdot V^2 + \alpha_I \cdot V + \alpha_P) \quad \text{where } \alpha_Z + \alpha_I + \alpha_P = 1 \qquad (4\text{-}1)$$

- Exponential model

  This model assumes that the load is exponentially related to voltage as shown by (4-2). The advantage of this model is that it has less parameters than the ZIP model.

  $$P = P_0\left(\frac{V}{V_0}\right)^{\alpha} \qquad (4\text{-}2)$$

- Frequency load model

  This model introduces a frequency dependent factor to relate the load change to frequency change, as shown in (4-3).

  $$P = P_0(\alpha_Z \cdot V^2 + \alpha_I \cdot V + \alpha_P) \cdot \left(1 + \alpha_f \left(f - f_0\right)\right)$$
  $$or \;\; P = P_0\left(\frac{V}{V_0}\right)^{\alpha} \cdot \left(1 + \alpha_f \left(f - f_0\right)\right) \qquad (4\text{-}3)$$

2) Dynamic load model

Dynamic load models are used in stability analysis. In these models, both real and reactive power is a function of voltage magnitude and time. Commonly used models include:

1) Exponential Recovery Model [39]

This model sees the power a response of a step voltage change, as shown in Figure 4.1. The respective mathematic representation can be found in (4-4) and (4-5). This model is used to represent a load that slowly recover over time, typically ranging from several seconds to tens of minutes, for example the power at substation transformer after a tap change.

$$T_p \frac{dP_r}{dt} + P_r = P_0 \left(\frac{V}{V_0} \right)^{\alpha^s} - P_0 \left(\frac{V}{V_0} \right)^{\alpha^t} \qquad (4\text{-}4)$$

$$P_l = P_r + P_0 \left(\frac{V}{V_0} \right)^{\alpha^t} \qquad (4\text{-}5)$$

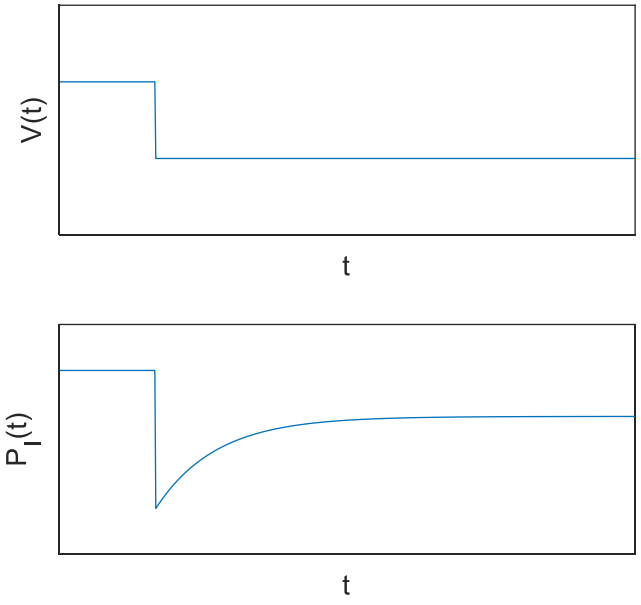

Figure 4.1 Step voltage change and power response of simple recovery model

2) Induction Motor (IM) Model [40]

This model is derived from the equivalent circuit of induction motor, considering the dynamics of rotor.

3) Composite Load Model [41]

This model is a combination of static model, recovery model and the IM model, as shown in (4-6). The model with only ZIP and IM components is the most commonly used model in US for dynamic studies[42].

$$P = \lambda_1 \cdot P_{ZIP} + \lambda_2 \cdot P_R + \lambda_3 \cdot P_{IM} \qquad (4\text{-}6)$$

4.2 Load Parameter Estimation

After a load model is selected, one needs to apply estimation techniques to obtain the parameters in the model. So far, the estimation approaches are classified into component-based approach and measurement-based approach.

1) Component based approach

   This approach involves several steps. First, the load characteristics of load components are obtained from experiments. Then for each class of load, the component models are aggregated to obtain a load class model. In the last step, load at a bus is the aggregation of class models based on the load mix data, where load mix is the contribution of each load class in percentage [43], [44].

2) Measurement based approach

   Due to increasing number of sources of the data, such as Power Quality (PQ) measurement, Digital Fault Recorders (DFR) and Phase Measurement Units (PMU), researchers tend to use the measurement based approach. This approach does not require intensive experiments and has the potential of providing real-time feedback of the changing characteristics of the load [45]. In this approach, parameters are estimated by fitting the measurements to the load structure, using identification and estimation techniques [36]. This work follows the measurement based approach to estimate the load parameters.

Two Types of Load Parameter Estimation Problem

1) Static parameter estimation

Static load parameter means the load parameter remains constant as time goes. For example, the α's in the static load model.

Suppose θ is constant but unknown, and each element in measurement vector y is a linear combination of parameter θ with the addition of some measurement noise, where θ is a vector. For each measurement, we have

$$\begin{aligned} y_1 &= H_{11}\theta_1 + \cdots + H_{1n}\theta_n + \upsilon_1 \\ &\vdots \qquad\qquad \text{or in matrix form } y = H \cdot \theta \\ y_k &= H_{k1}\theta_1 + \cdots + H_{kn}\theta_n + \upsilon_k \end{aligned} \tag{4-7}$$

The measurement residual is

$$\begin{aligned} \varepsilon_1 &= y_1 - H_{11}\hat{\theta}_1 - \cdots - H_{1n}\hat{\theta}_n \\ &\vdots \\ \varepsilon_k &= y_k - H_{k1}\hat{\theta}_1 - \cdots - H_{kn}\hat{\theta}_n \end{aligned} \tag{4-8}$$

By minimizing the square sum of the residuals $J = \sum_{i=1}^{k} \varepsilon_i^{\,2}$, we can obtain a least square estimator, $\hat{\theta} = H^L y$, where H^L is the left pseudo inverse of H. For the case that measurement error for each element in y is different. A weighted least square estimator $\hat{\theta} = \left(H^T R^{-1} H\right)^{-1} H^T R^{-1} y$ can be derived similarly, where R is the measurement covariance matrix [46].

2) Dynamic parameter estimation

In this type of problems, the parameter in load model is time dependent, for example P_r in exponential recovery model. Suppose the load parameter can be described as linear discrete system as follows:

$$\theta_k = F_{k-1}\theta_{k-1} + G_{k-1}u_{k-1} + \omega_{k-1} \qquad (4\text{-}9)$$

With the noise measurement described by

$$y_k = H_k\theta_k + v_k \qquad (4\text{-}10)$$

(4-9) is called state transition model and (4-10) is called observation model. For this type of problem, Kalman Filtering (KF) method can be used estimate the system parameters dynamically. When the transition model is non-linear, Unscented Kalman Filter (UKF) and Extended Kalman Filtering(EKF) methods can be applied [46], [47].

In general, methods that can be used to solve a parameter estimation can be classified into batch processing methods or recursive methods. Batch processing means the estimation is performed only once, based on all the measurements collected. The least square method presented above is an example of batch processing method. A recursive method estimates the parameter based on the measurement at current time instant and most recent estimate. (4-11) shows a general form of recursive estimation [48]. The current estimate is obtained by adjusting previous estimate by a gain multiplied by output estimation error.

$$\hat{\theta}_k = \hat{\theta}_{k-1} + K_k\left(y_k - \hat{y}_k\right) \qquad (4\text{-}11)$$

KF is one representation of this general form. Recursive methods are commonly used in on-line estimation.

Constant load parameter are used at transmission level or substation level, assuming at these voltage levels parameters do not change frequently, because the aggregation of significant number of individual loads masks the uncertainty. With integration of new components and control technologies in power system, more accurate model with time-

varying parameter are needed. [49] proposes a method to estimate time-varying parameter, assuming the parameters changes are very small, by feeding previous estimates to current sample time and formulating the estimation problem in each sample time as a weighted least square problem. There're also researchers applying Kalman Filtering based method to a catch the dynamics of parameters [50]. [51] uses recursive least square (RLS) method to calculated constant parameters for a few sliding windows. In [51], when a parameter change is detected, the recursive estimation result is dropped, and an adaptive search method is triggered to estimate the new parameter. In the following section, a load model at service transformer is proposed and a recursive method is adopted to realize an on-line load parameter estimation.

4.3 Load Modeling for VVC and Parameter Estimation

In the FREEDM architecture, each SST serves a few houses with voltage and power consumption monitored in real-time. Voltage at the secondary side of SST can be either fixed or varies as primary side voltage changes, depends on user configuration. In the partial PV deployment cases as shown in the revised IEEE 123 Node system, many loads are served by traditional transformers. And the size of these transformers is not big. The power consumed by the loads under SST or traditional transformer can be affected by the voltage change due to VVO. In the proposed VVC architecture, as shown in Figure 4.2, VVO slaves collect the power measurement in every control cycle, and the master models the loads as constant power sink, which does not show the load response to voltage change. Therefore, it is necessary to develop a load model at a transformer with parameters reflecting voltage sensitivity.

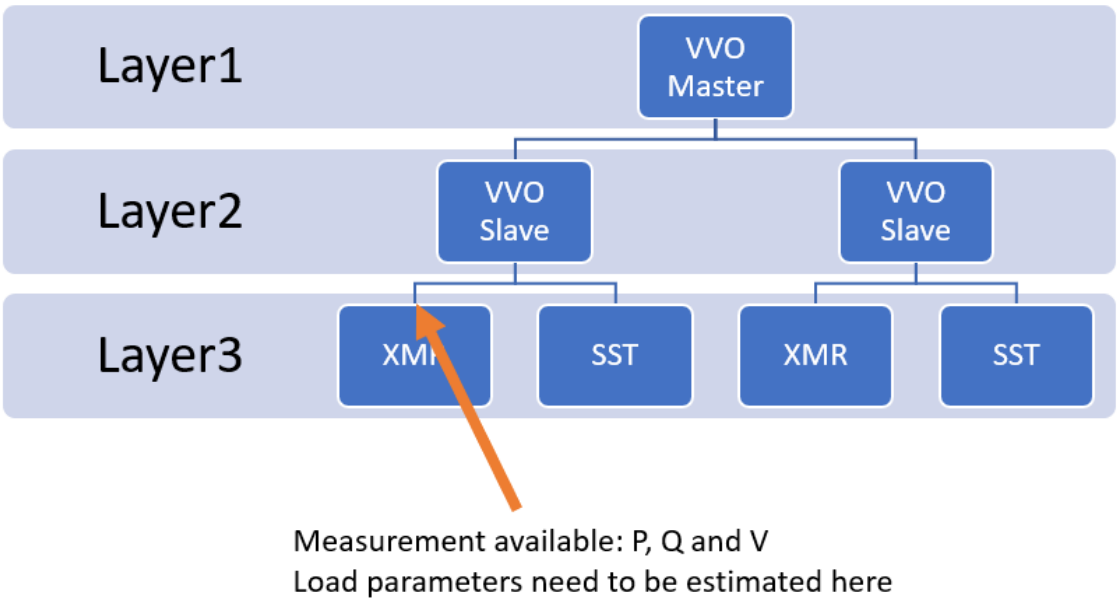

Figure 4.2 VVC architecture in system with partial SST deployment

Figure 4.3 shows the actual real power measurement of a single-family home from [52]. The black line is PV generation. The blue line is the power consumption. And the green line is the net load seen from gird. Figure 4.4 shows a zoom-in view of the load data from 18:30 to 0:00. From Figure 4.4, we can observe that there are large power changes due to major load device, such as ON/OFF status change of HVAC as marked in blue. There, are also small variations caused by the bus voltage variations.

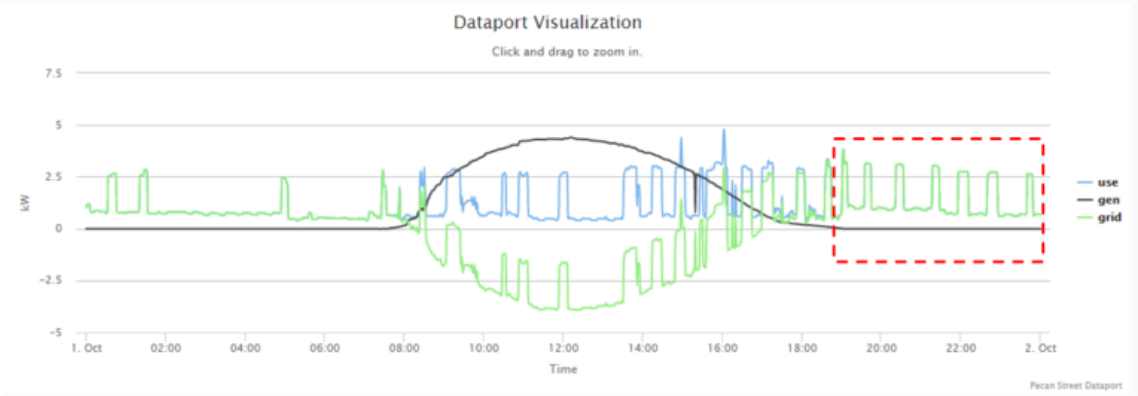

Figure 4.3 Actual real power measurement of a single-family home

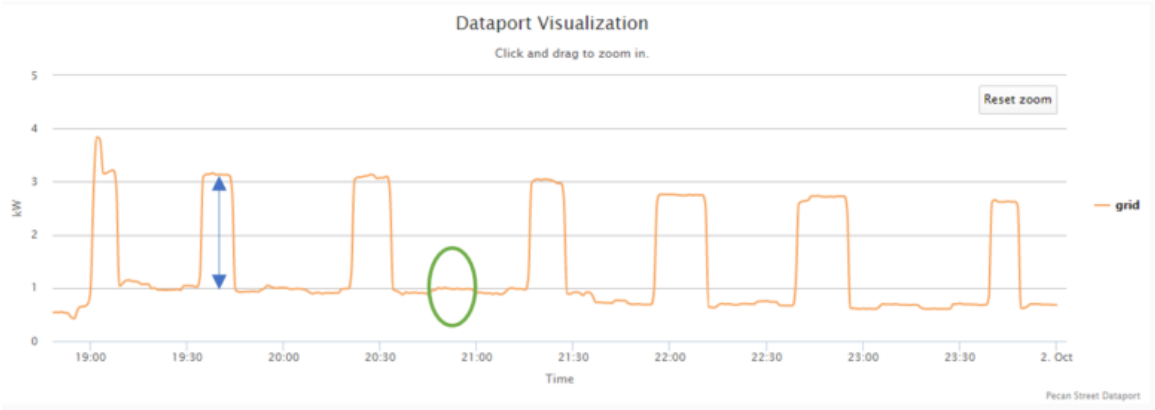

Figure 4.4 Zoom-in view of power measurement of a single-family home

In general, if neglect power loss, the power consumption at transformer is the summation of all the power consumption of all devices downstream as (4-12) shows.

$$P_{XMR}(t) = \sum_{m=1}^{M} P_m(t) \qquad (4\text{-}12)$$

where m is the index of devices and M is the total number of devices

Suppose each device is modeled by the static ZIP model, we have

$$P_m(t) = u_m(t) P_{m0} \left(\alpha_Z V(t)^2 + \alpha_I V(t) + \alpha_P \right) \qquad (4\text{-}13)$$

where $u_m(t)$ is binary, indicating the ON/OFF status of a device.

Substitute $P_m(t)$ in (4-12) by (4-13), and rearranging as shown in (4-14). We have (4-15), and parameters $Coeff_Z$, $Coeff_I$ and $Coeff_P$ depend on u_m only.

$$\begin{aligned} P_{XMR}(t) &= \sum_{m=1}^{M}\left[u_m(t)P_{m0}\left(\alpha_Z V(t)^2+\alpha_I V(t)+\alpha_P\right)\right] \\ &= \sum_{m=1}^{M}\left[\left\{u_m(t)P_{m0}\alpha_Z\right\}\cdot V(t)^2+\left\{u_m(t)P_{m0}\alpha_I\right\}\cdot V(t)+\left\{u_m(t)P_{m0}\alpha_P\right\}\right] \\ &= V(t)^2\cdot\sum_{m=1}^{M}\left\{u_m(t)P_{m0}\alpha_Z\right\}+V(t)\cdot\sum_{m=1}^{M}\left\{u_m(t)P_{m0}\alpha_I\right\}+\sum_{m}^{M}\left\{u_m(t)P_{m0}\alpha_P\right\} \end{aligned} \quad (4\text{-}14)$$

$$P_{XMR}(t) = Coeff_Z(t)\cdot V(t)^2 + Coeff_I(t)\cdot V(t) + Coeff_P(t) \quad (4\text{-}15)$$

In Figure 4.3, we found that $u_m(t)$ is almost constant for a single house in a few minutes. With only a few houses connected to the transformer, after aggregation, the device status vector $u(t)=\left[u_1(t) \quad \cdots \quad u_M(t)\right]$ remains the same for a short period. This is confirmed by the GridLab-D simulation in next section. Therefore, when the transformer serves a limited number of houses, we have (4-16) valid for small time interval

$$P_{XMR}(t) = Coeff_Z\cdot V(t)^2 + Coeff_I\cdot V(t) + Coeff_P \quad (4\text{-}16)$$

This static parameter model can be solved by least square method, which performs batch processing for all the data collected in the small interval. However, the challenge of batch processing is that the duration of the small interval is unknown. Therefore, the recursive method is adopted, in which each estimate is an adjustment of previous estimate. At the instant when *Coeff* changes, with a proper configuration of the gain in (4-11), the recursive method gradually converge to the new *Coeff* [48]. One advantage of recursive method is that only previous estimation and present measurements are stored for estimation in current

simulation step. This will save memory greatly compared with the batch processing method, such as least square.

The simulation in next section utilizes the recursive estimation tool within System Identification Toolbox in MATLAB.

4.4 Results of On-line Load Parameter Estimation on IEEE 13 system

Figure 4.5 shows the Simulink model of the proposed load parameter estimation. The recursive estimator gives the estimation of the parameters in real-time. Based on (4-16), $H(t)=\begin{bmatrix} V(t)^2 & V(t) & 1 \end{bmatrix}$ is the linear model's input, $P_{XMR}(t)$ as the model output $y(t)$, and the estimate is $\hat{\theta}(t)=\begin{bmatrix} \hat{Coeff}_Z(t) & \hat{Coeff}_I(t) & \hat{Coeff}_P(t) \end{bmatrix}^T$.

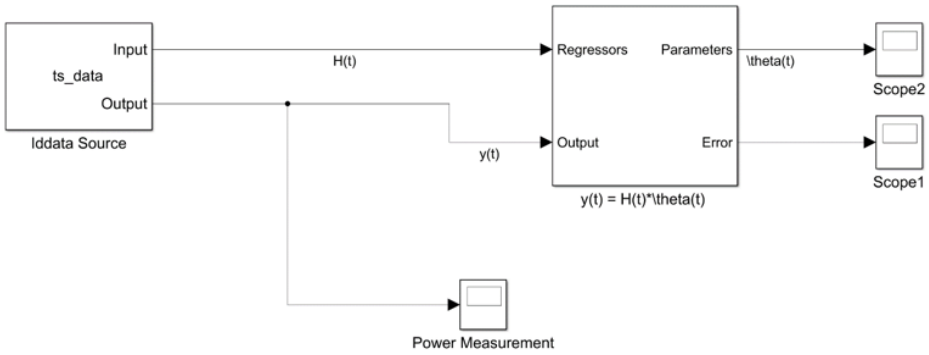

Figure 4.5 Simulink diagram for online load parameter estimation

The voltage and power measurement are obtained from GRIDLAB-D [53] simulation of an IEEE 13 Node Test Feeder with detailed load model of houses. Since the IEEE 13 Node Test Feeder does not have a small transformer serving residential loads. The measurement at a small transformer is created by aggregating the real power meter readings of four different houses connected to the same service transformer. Detail of the load model in the houses can be found in [54]. In real-time VVC, the load and voltage at the transformer are measured in

real-time. The sampling rate can be much faster than the control cycle used in Volt/Var Optimization. In the case studies, the measurements data are fed to the estimation module every 5s. In MATLAB Simulink simulation, this 5s is represented by a 0.01s simulation step.

In this study, two cases, a winter day and a summer day, are simulated to test the proposed load parameter estimation method.

Case 1: Winter day

In this case, GridLab-D simulation uses the weather data on January 1st, 2000 in Seattle, WA.

First, a time-series 24h simulation in GridLab-D is performed to create measurement data, which are the model input and output data for parameter estimation. Figure 4.6 shows the aggregated power measurements of four houses connected to the same service transformer in GridLab-D. This aggregated power is used to represent $P_{XMR}(t)$, the power consumption at a transformer. Figure 4.7 shows the voltage on the secondary side of the service transformer, which is used to represent the voltage at the transformer.

Then, time-domain data are created from the GridLab-D measurements and imported to the recursive estimation tool by the "Iddata Source" block in Simulink, as shown in Figure 4.5.

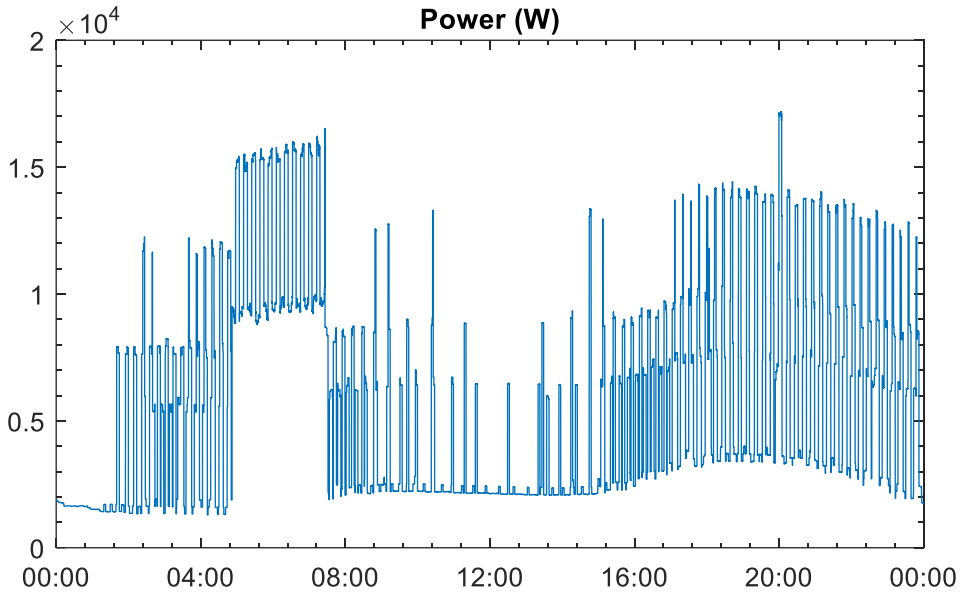

Figure 4.6 Power measurement at transformer in a winter day

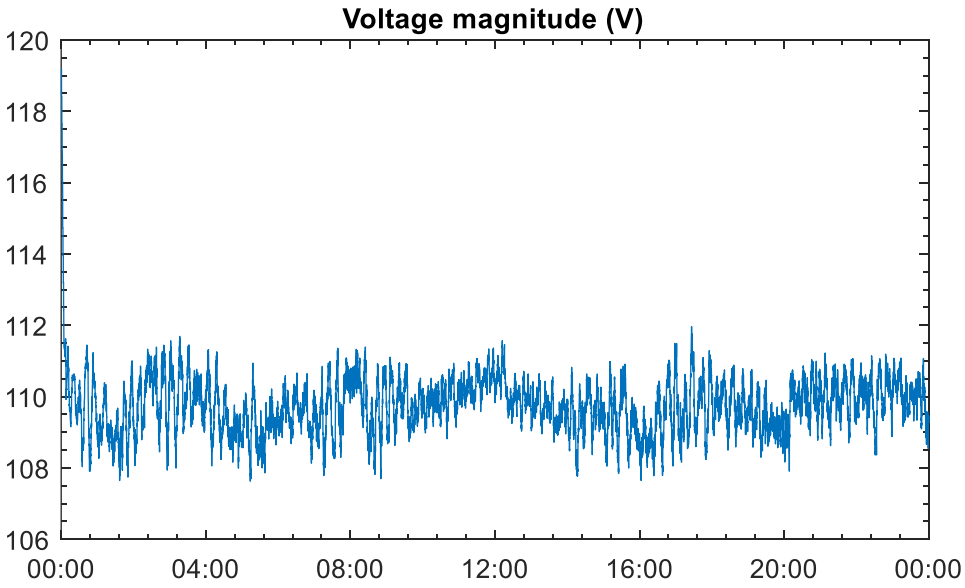

Figure 4.7 Voltage measurement at transformer in a winter day

Figure 4.8 shows the estimation results of the parameters. Figure 4.9 shows the estimation error of each simulation step (0.01s in Simulink, and 5s in GridLab-D), where the spikes indicate that the first few estimations after a parameter change is not very accurate.

Practically, we won't send the estimated parameter at each simulation step. For VVC, the parameters are sent every 5 min.

Here, the estimation error of the recursive estimator is calculated by

$$Eor_{est}(t) = y(t) - H(t) \cdot \hat{\theta}(t)$$

However, the recursive method always converges after several iterations. This can be observed in a zoom-in view of the results. In Simulink, $y(t)$ varies around 1700W from 10.76s to 11.18s, as shown in Figure 4.10. Figure 4.11 and Figure 4.12 show that the estimated parameters gradually move to a stable value and the corresponding error converges to almost zero in several iterations before 10.9s.

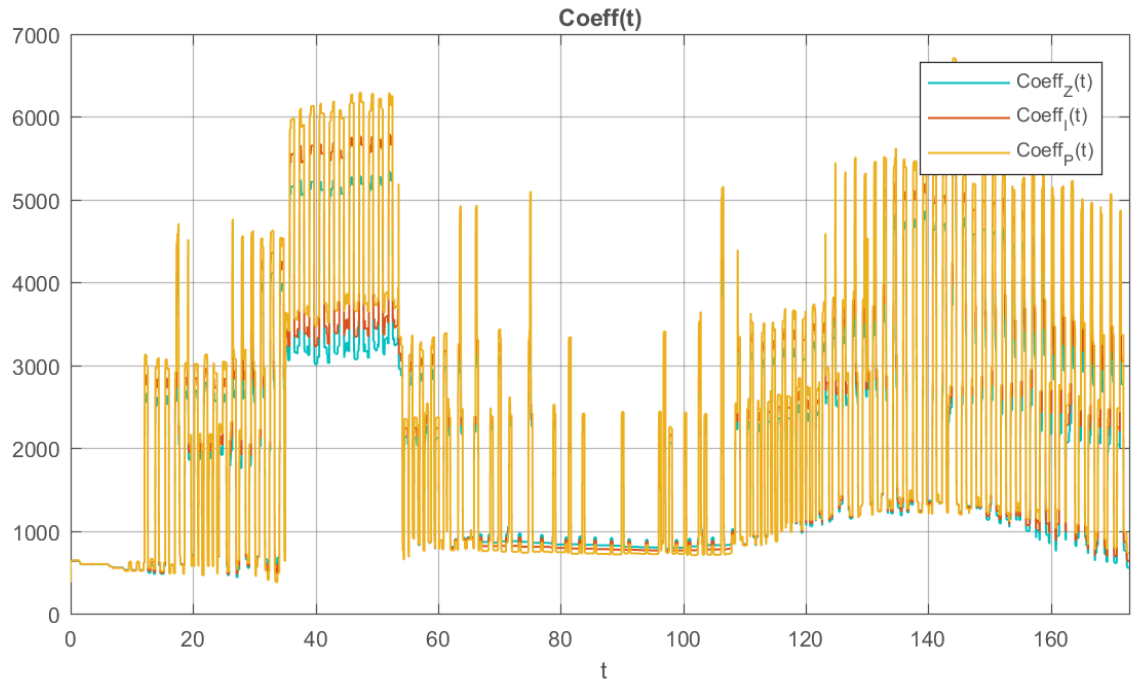

Figure 4.8 Estimated load parameter in a winter day

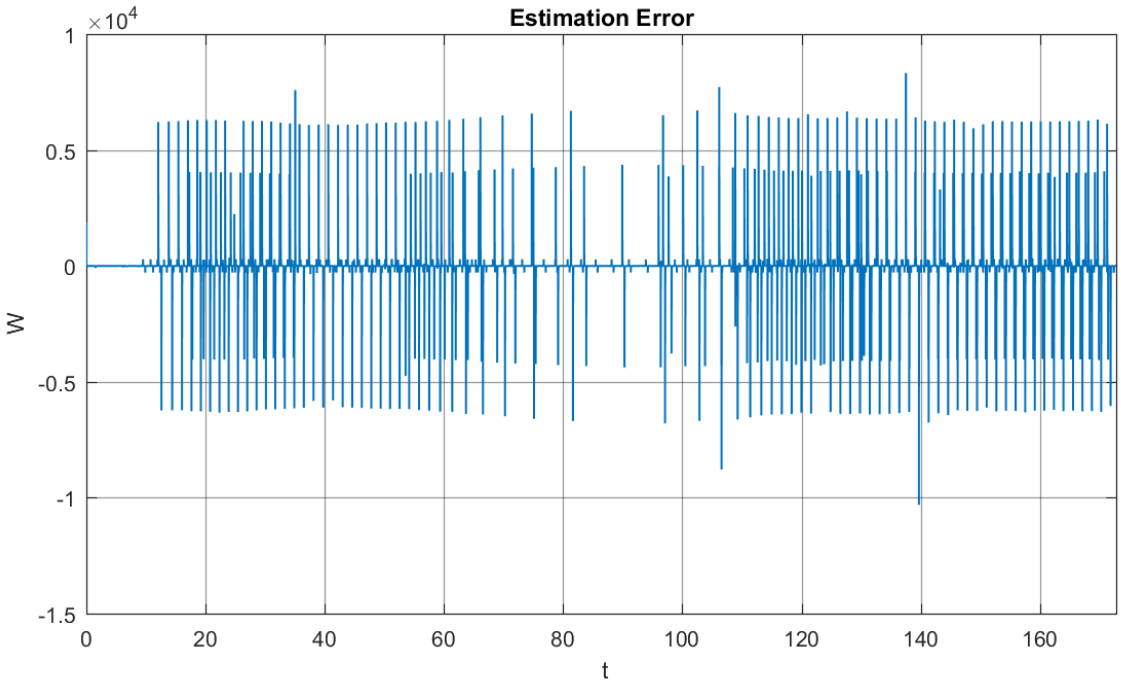

Figure 4.9 Estimation error of recursive estimator

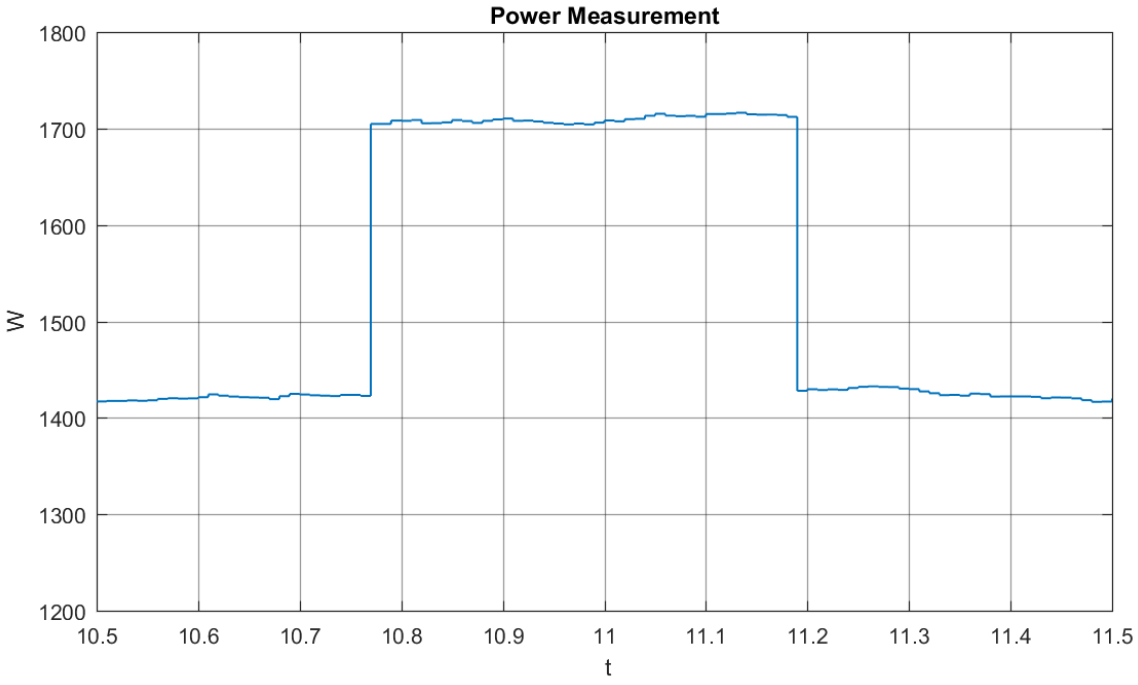

Figure 4.10 Power measurement in selected interval in a winter day

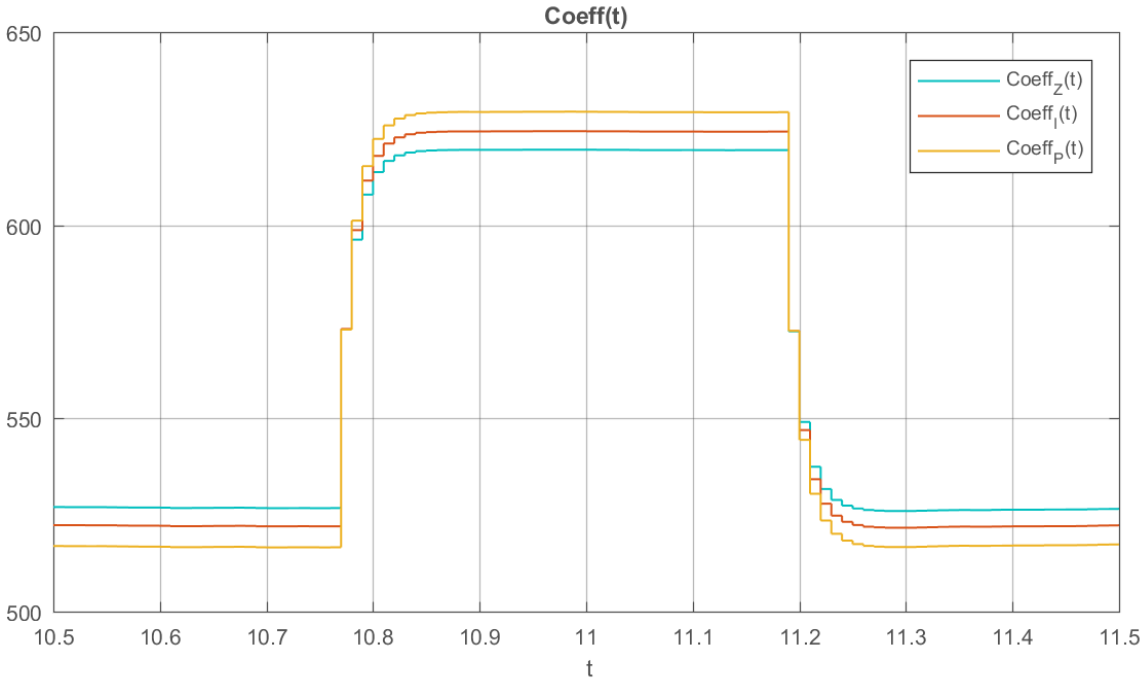

Figure 4.11 Estimated parameter in selected interval in a winter day

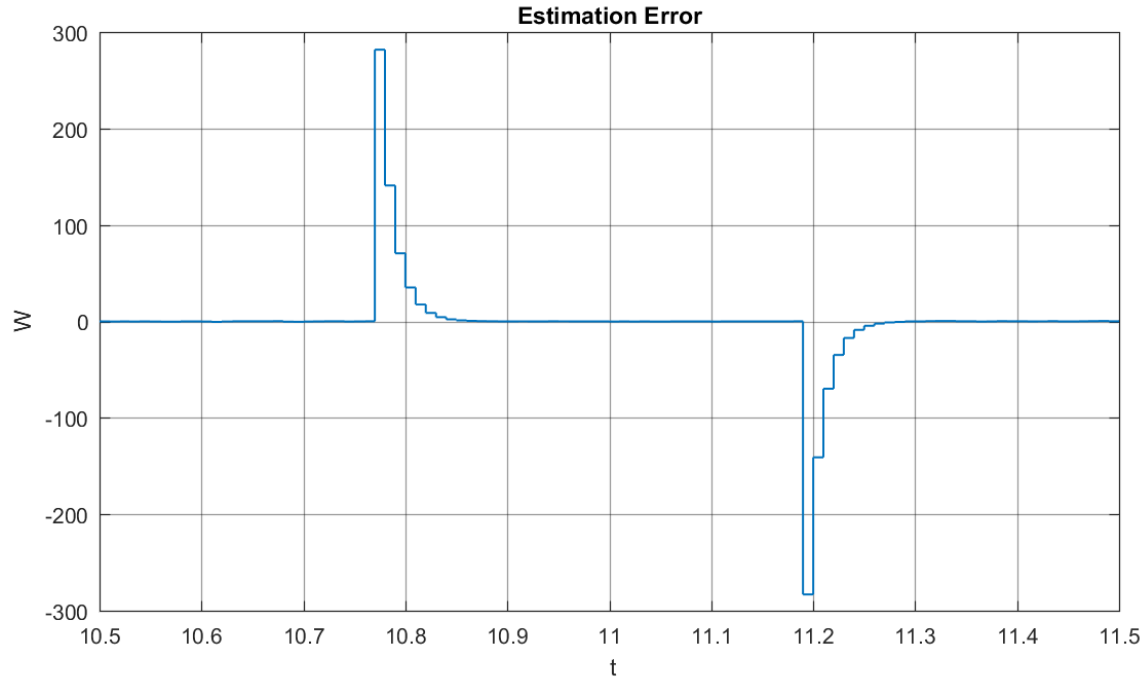

Figure 4.12 Estimation error in selected interval in a winter day

Comparison with LS method

To test the performance of the recursive method, a least-square method is simulated to compare with the results of recursive method. Since the intention of the load parameter estimation is to support system level application Volt/Var Control, the estimation results are sent to VVO slaves every 5min. Therefore, a least square with 5min window-size is adopted to estimate the parameters. Figure 4.13 show the actual measurement (blue), estimated power using the parameters from recursive method (red), and estimated power using the parameters from LS method (green). Data for actual measurement and recursive estimation on this figure are obtained by sampling with 5 min interval from the data with 5s sampling rate. The results show that most of the time the blue line overlaps the red one, while the green line does not track the blue line well. We define the error for each method as

$$Eor_{\mathrm{R}}(t) = \left| y_{mea}(t) - \hat{y}_{\mathrm{Re}c}(t) \right| \qquad (4\text{-}17)$$

$$Eor_{LS}(t) = \left| y_{mea}(t) - \hat{y}_{LS}(t) \right| \qquad (4\text{-}18)$$

This histogram of the two errors can be found in Figure 4.14. The large error of recursive method is due to that sampling with 5 min interval takes values from the estimation result before the recursive method converges. And large error of the leas square comes from the parameter change within the 5-min interval. Table 4.1 shows the comparison of mean and variance of the errors. The recursive method has a smaller mean and small variance, which indicates a better performance than LS method.

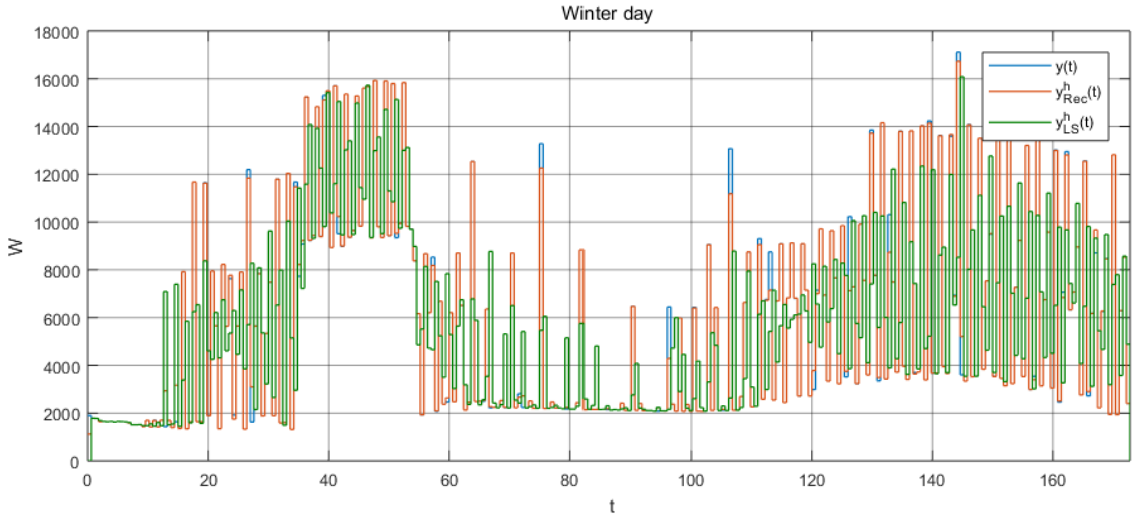

Figure 4.13 Comparison of estimated power of load in a winter day

Table 4.1 Statistics of error of LS method and Recursive method

Method	**Mean**	**Variance**
LS	2323.19	5.66e+6
Recursive	93.6	1.21e+4

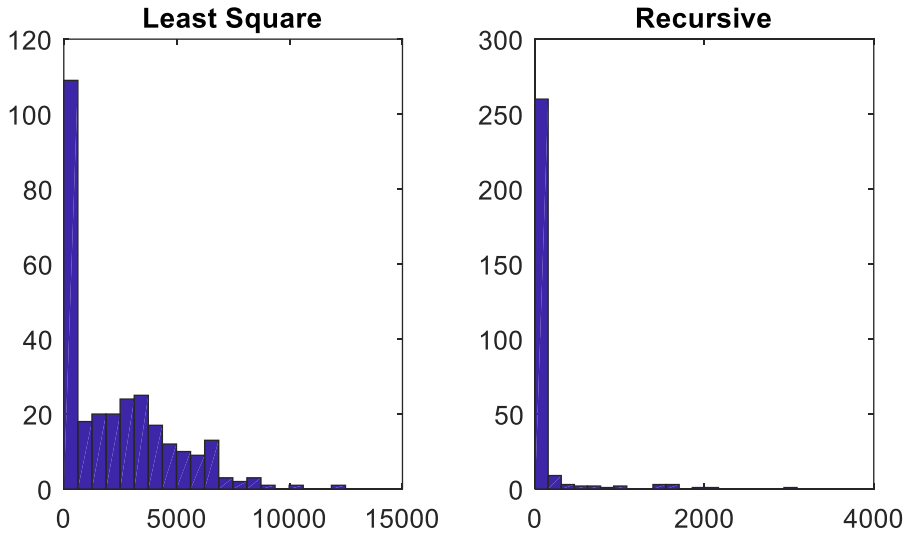

Figure 4.14 Histograms of error of LS method and Recursive method

Case 2: Summer day

In this case, GridLab-D simulation uses the weather data on July 1st, 2000 in Seattle, WA. Figure 4.15 and Figure 4.16 show the measurement data from GridLab-D for a summer day.

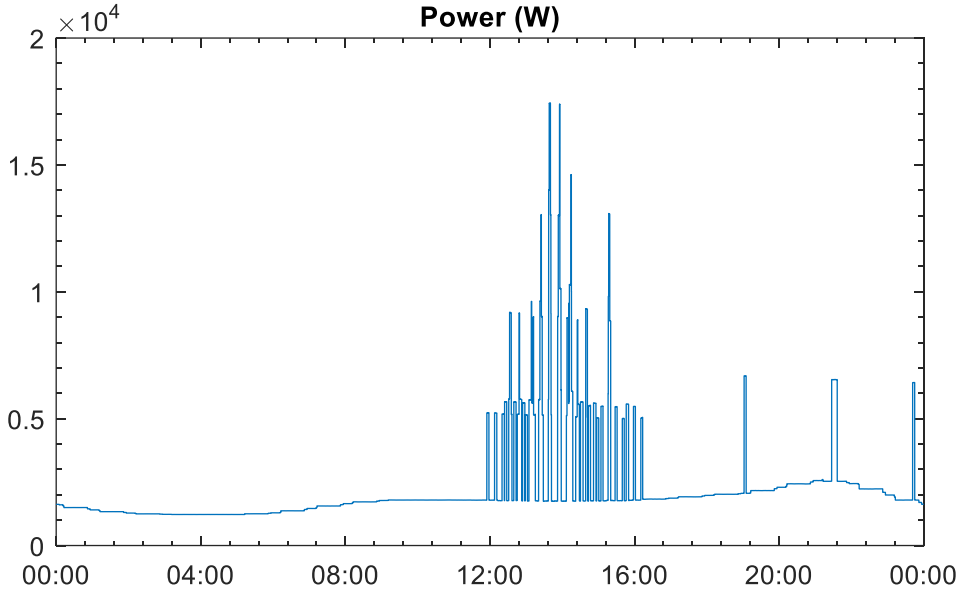

Figure 4.15 Power measurement at transformer in a summer day

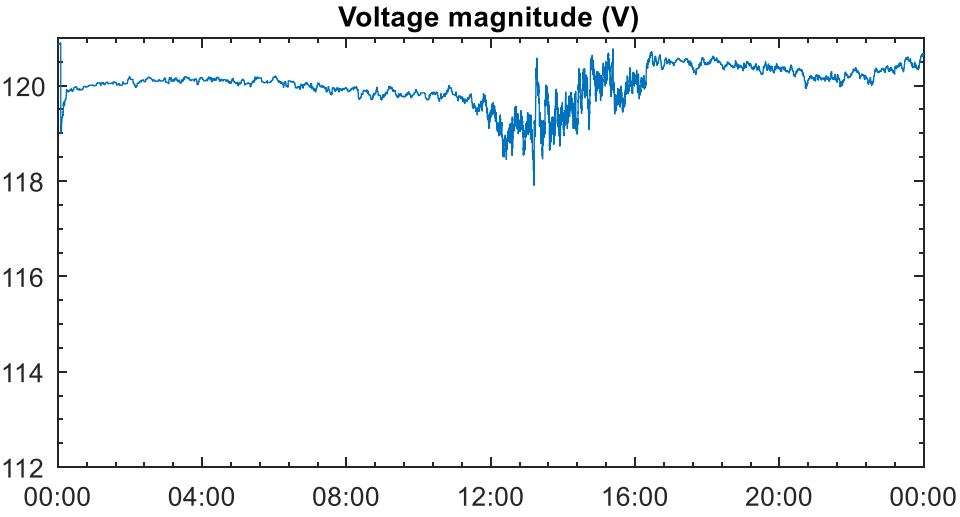

Figure 4.16 Voltage measurement at transformer in a summer day

Figure 4.17 and Figure 4.18 show the estimated parameters and estimation error of the recursive estimator. Similar as the case for winter day, the spikes occur at the beginning of parameter changes and the error converges to a very small value in a few iterations.

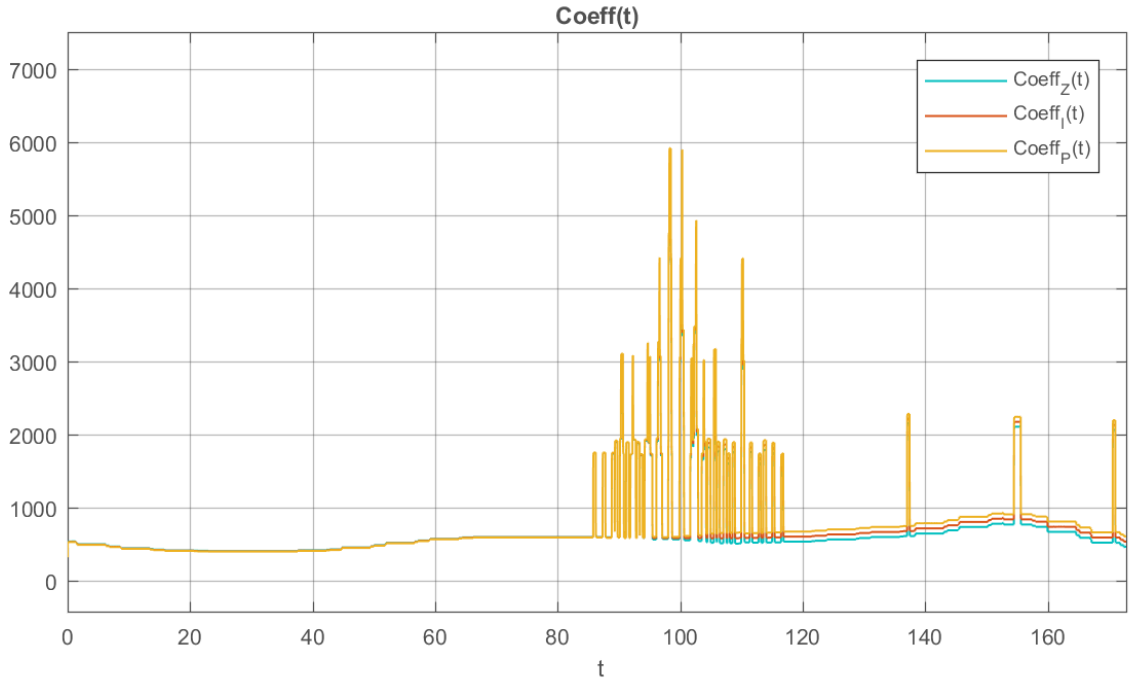

Figure 4.17 Estimated load parameter in a summer day

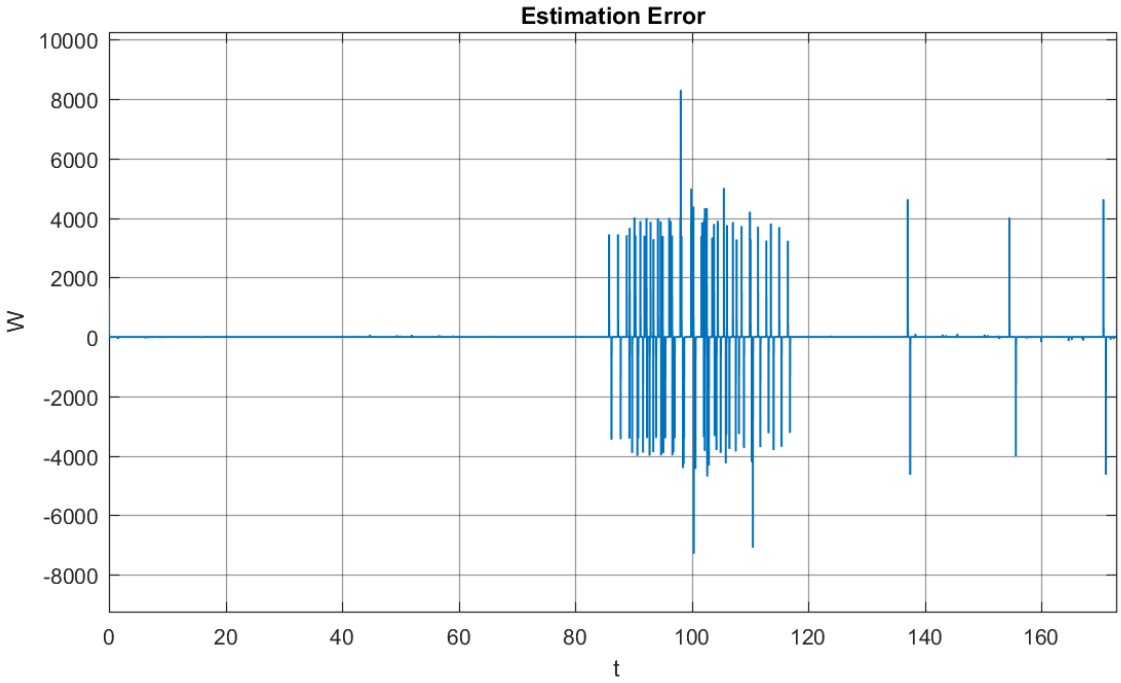

Figure 4.18 Estimation error of recursive estimator

Comparison with LS method

Figure 4.19 show the actual measurement (blue), estimated power using the parameters from recursive method (red), and estimated power using the parameters from LS method (green). Similar as the winter day case, Figure 4.19 shows that most of the time the blue line overlaps the red one, while the green line does not track the blue line well. And the histogram of errors of the two methods can be found in Figure 4.20. As Table 4.2 shows, the mean and variance of the recursive method is much less than the LS method, which indicates a much better performance than the LS method.

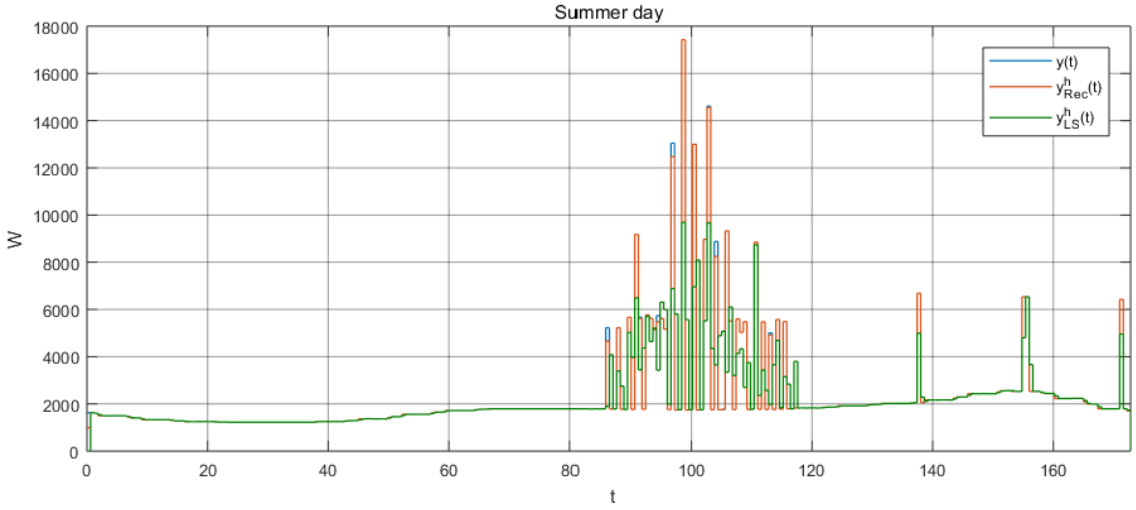

Figure 4.19 Comparison of estimated power of load in a summer day

Table 4.2 Statistics of error of LS method and Recursive method

Method	**Mean**	**Variance**
LS	414.8	1.37e+6
Recursive	10.01	5.24e+3

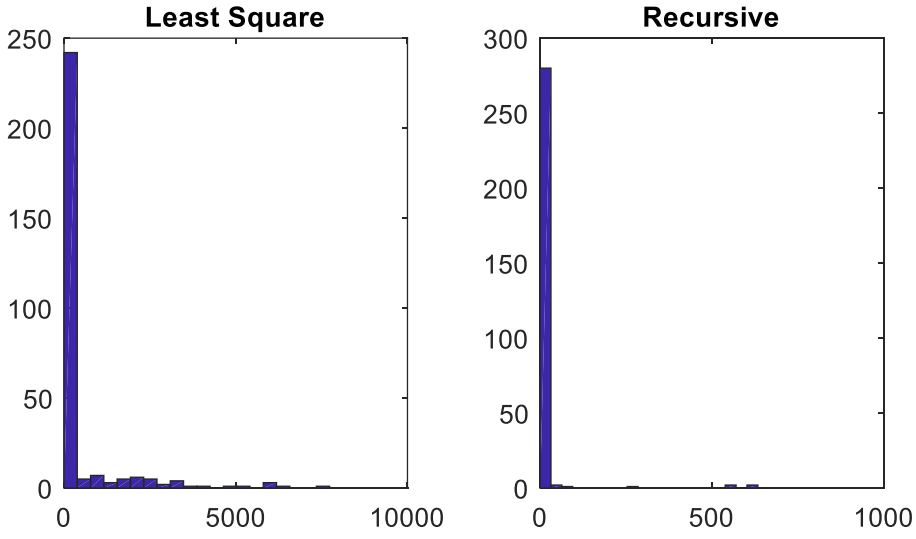

Figure 4.20 Histograms of error of LS method and Recursive method

4.5 Verification of the proposed load model

In previous section, a load model at a small transformer, as shown in (4-16), is proposed. To test if the load model proposed can give a good indication of power change due to voltage, the load parameters estimated in a day with CVR is used to estimate the power consumption for a no-CVR day with voltage profile given. (CVR is voltage reduction technique used to shave the peak power demand and reduce power consumption [55]) The assumption for this verification process is that device status changes have the same pattern in both CVR case and no-CVR case.

To perform the above estimation process, IEEE 13 Node Test Feeder is simulated with the same date, weather and load models in GridLab-D for both CVR case and no-CVR case. The CVR day data are fed to the online estimation module in MATLAB Simulink, to obtain a daily profile of the load parameters. Then, the estimated power consumption for no-CVR case is estimated by

$$\hat{y}_{noCVR}(t) = H_{noCVR}(t) \cdot \hat{\theta}_{CVR}(t) \qquad (4\text{-}19)$$

A percentage estimation error of power consumption in no-CVR case is defined by

$$Error\%(t) = \left| \frac{y_{noCVR}(t) - \hat{y}_{noCVR}(t)}{y_{noCVR}(t)} \right| \qquad (4\text{-}20)$$

Figure 4.21 shows the profile of $Error\%$. Figure 4.22 is a zoom-in view of the box plot of Error%, where outliers larger than 450% are not shown. This figure shows that most of the time the error is small, within 1%.

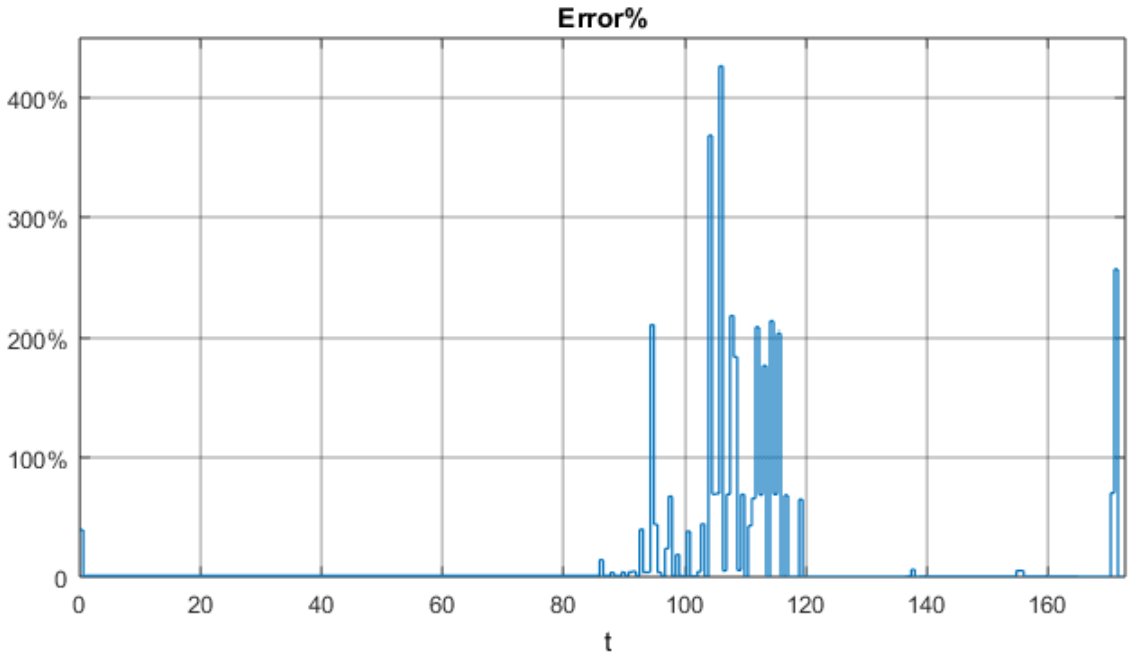

Figure 4.21 Error% of estimated power of load for no-CVR case

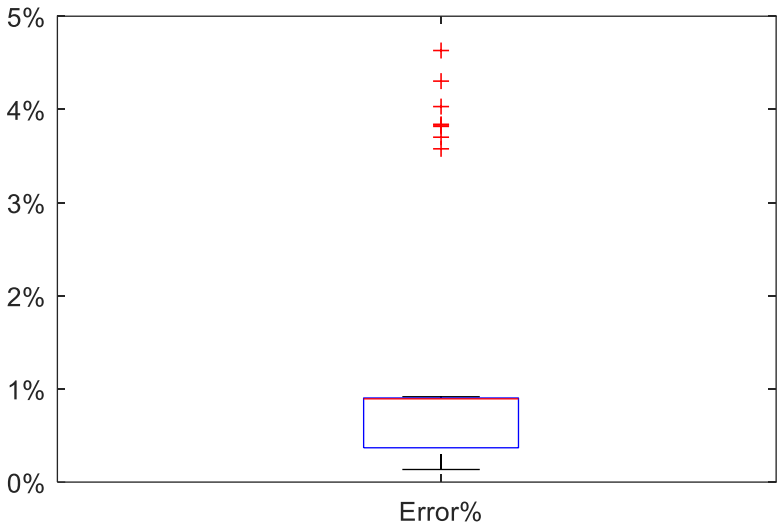

Figure 4.22 Zoomed-in box plot of Error%

We can observe from Figure 4.21 that some of the errors are very large. This is due to the violation of the assumption for verification process, which means the device ON/OFF status in no-CVR case is not exactly the same as in CVR case. Figure 4.23 shows the power

measurement mismatch between no-CVR case and CVR case. We can find that there are some large mismatches. This is reasonable because with the control model of HVAC and water heater in GridLab-D, CVR would change the operation pattern of those devices. Therefore, the parameters change in different time instants for two cases.

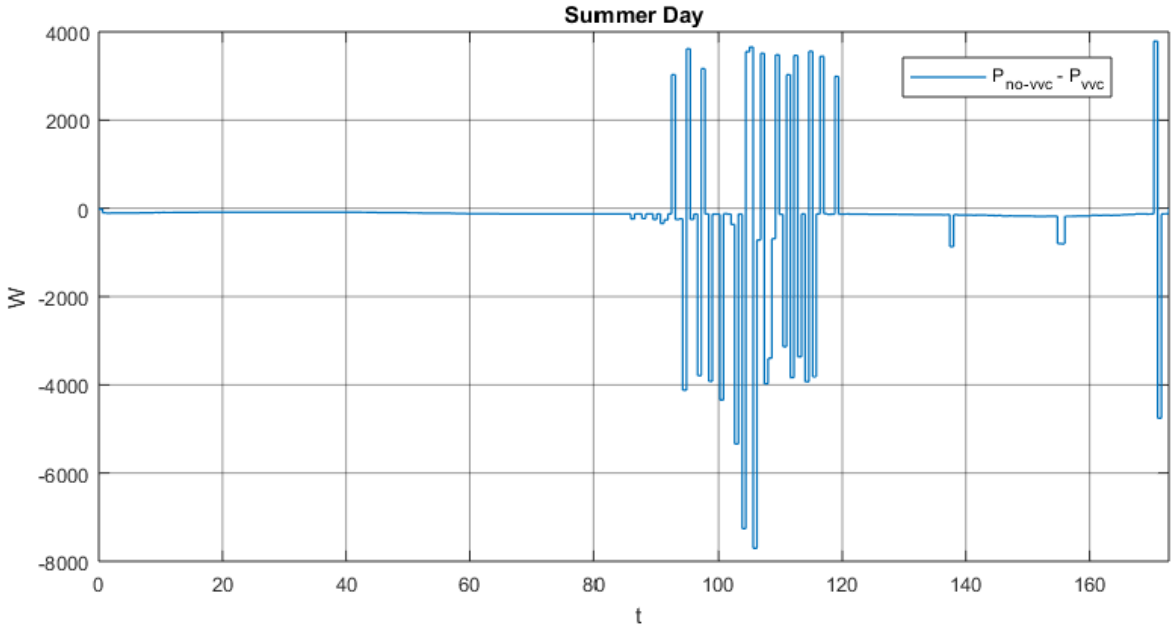

Figure 4.23 Difference between measured of no-CVR case and CVR case

Figure 4.24 shows the absolute estimation error in a selected time interval calculated by $Error = \left| y_{noCVR}(t) - \hat{y}_{noCVR}(t) \right|$. During this time interval the error converge to large value because a huge mismatch between $y_{CVR}(t)$ and $y_{noCVR}(t)$, as shown in Figure 4.25. The error shown in Figure 4.26 is the estimation error calculated by $Eor_{CVR}(t) = \left| y_{CVR}(t) - \hat{y}_{CVR}(t) \right|$. Figure 4.26 shown that the estimation error converges to small value which indicates the convergence of recursive method.

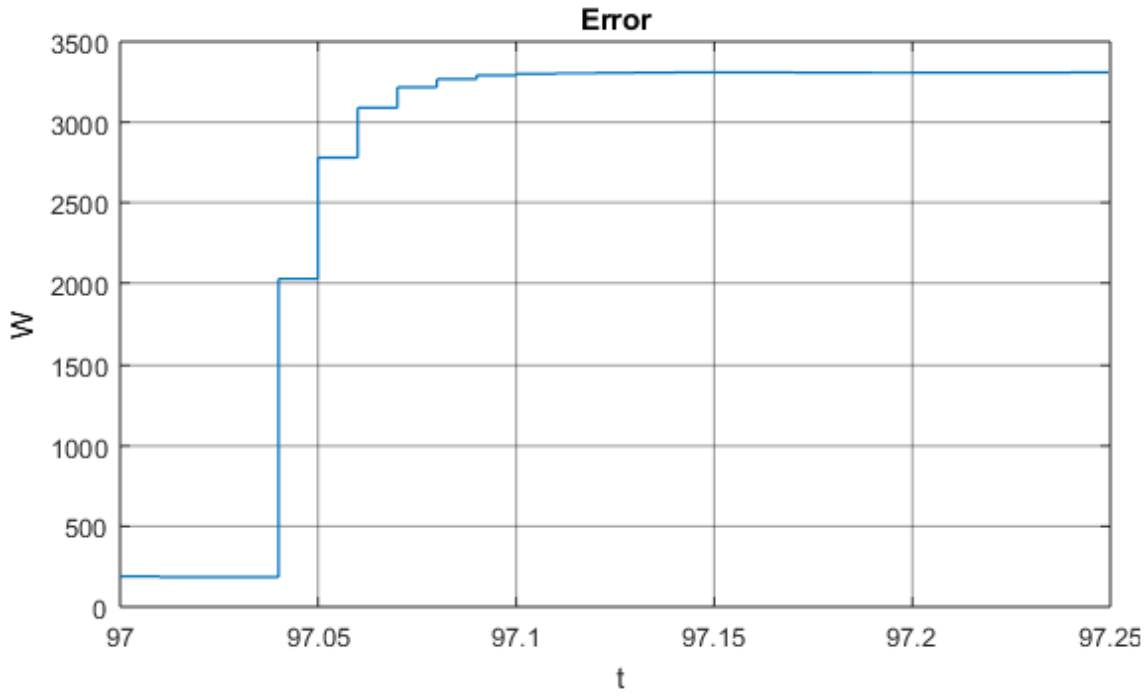

Figure 4.24 Estimation error of power of load for no-CVR case in selected time interval

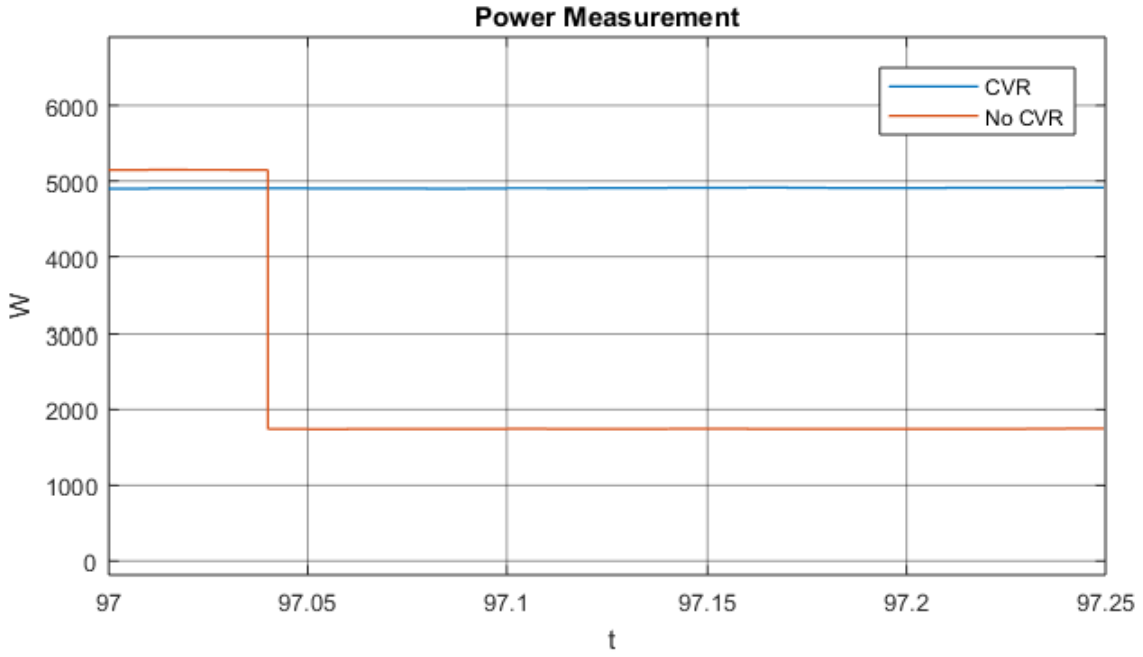

Figure 4.25 Power measurement of CVR case and No CVR case in selected time interval

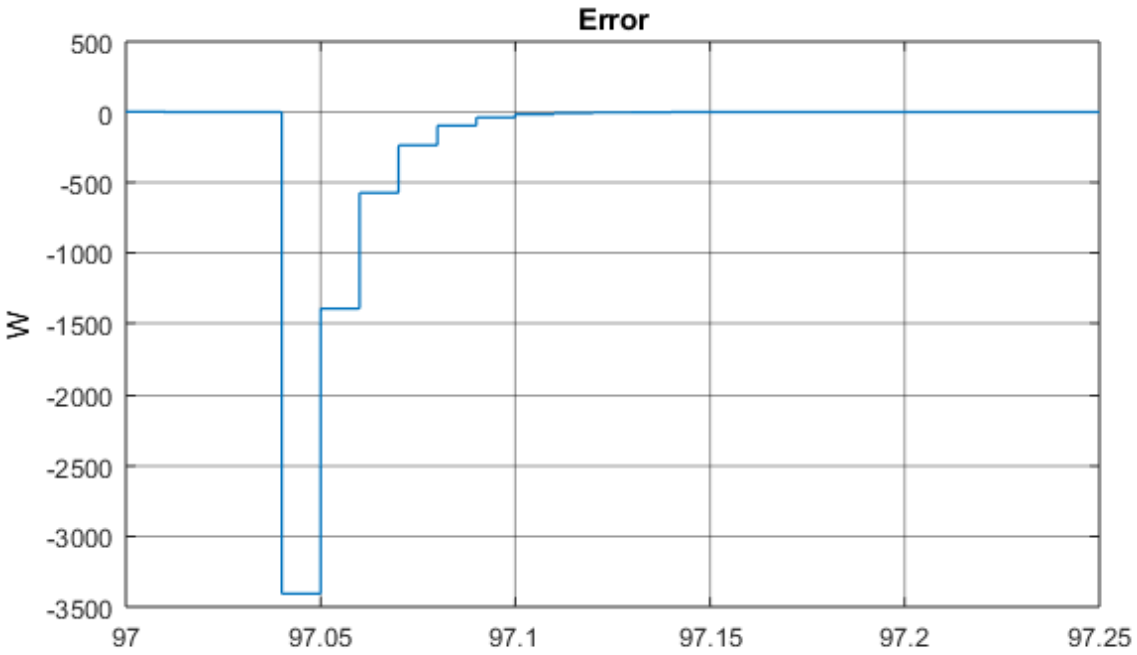

Figure 4.26 Estimation error of recursive estimator in selected time interval

4.6 Conclusion

This chapter proposes a load model at a small transformer. The model is static for short time interval and the parameters can be estimated online effectively by recursive methods. The estimation process only needs measurement data locally from the transformer, and does not need any private load information inside the houses. Simulation results show its better performance compared with LS method. The estimated parameters can be used to estimate power demand change due to system voltage variations. Therefore, the proposed online load parameter can be used in CVR performance estimation with voltage profile change given. One possible use of the proposed online load parameter estimation is to feed the estimated parameter to online VVC to improve the model accuracy of VVC.

Chapter 5. Implementation of Real-time VVO on FREEDM Systems

This chapter introduces the current progress of real-time VVO implementation on FREEDM systems. First, the architecture of the implementation of the proposed VVO is presented. Then the requirements for the proposed VVO is discussed. At last, test cases are presented.

5.1 Integrated Volt/Var Control Architecture

Integrated Volt/Var Control refers to the Volt/Var Optimization (VVO) as one of the main functions in Distribution Management Systems (DMS). Figure 5.1 shows a generic architecture of a centralized DMS, which are using by vendors nowadays.

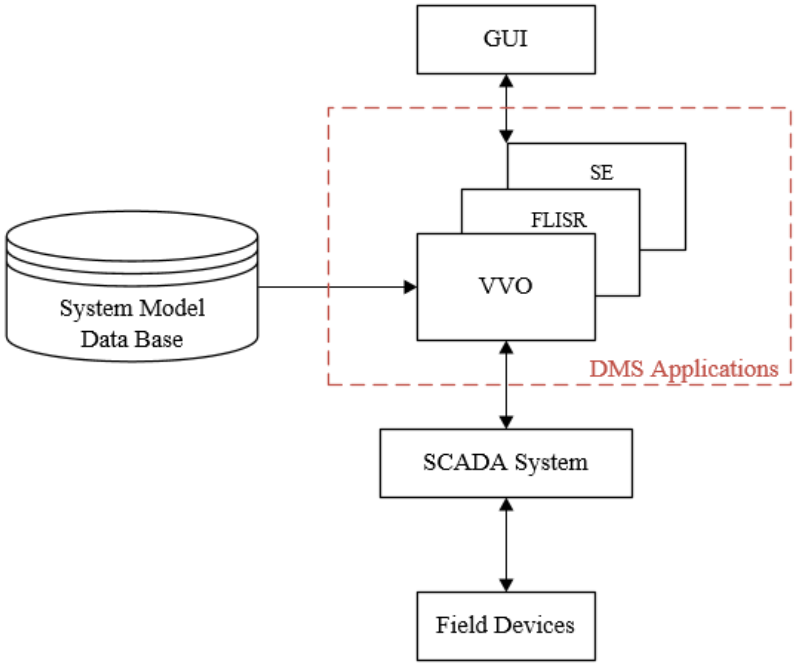

Figure 5.1 A generic architecture of a centralized DMS

The DMS applications and system model data base are located at the control center. For various DMS applications including VVO, both the system model and real-time data from

the feeder are needed as input. At the control center managing multiple substations, the user can configure the parameters for the DMS applications through the GUI. The output of the DMS applications can be either actual control commands to be sent to the field devices or just a recommendation for the operators. In this centralized DMS, the SCADA system at the control center communicates with the field devices directly.

With an increasing number of DERs and smart meters in large distribution networks, more real-time monitoring data become available for DMS applications. In a large centralized control network, huge data may be exchanged at the control center, increasing both the communication requirement and processing power requirement. In the proposed VVO schemes, the field devices, SSTs, smart inverters, are controlled in a master-slave decentralized fashion to address those issues. A decentralized communication network as shown in Figure 5.2 is utilized in FREEDM systems to implement the proposed decentralized VVC scheme. For each group of SSTs, a VVO slave is assigned to collect the real-time monitoring data and to forward the data to the VVO master at the substation. Each slave also receives data from the master, determines the control commands for each SST in that group based on the data received, and finally sends the control commands to SSTs.

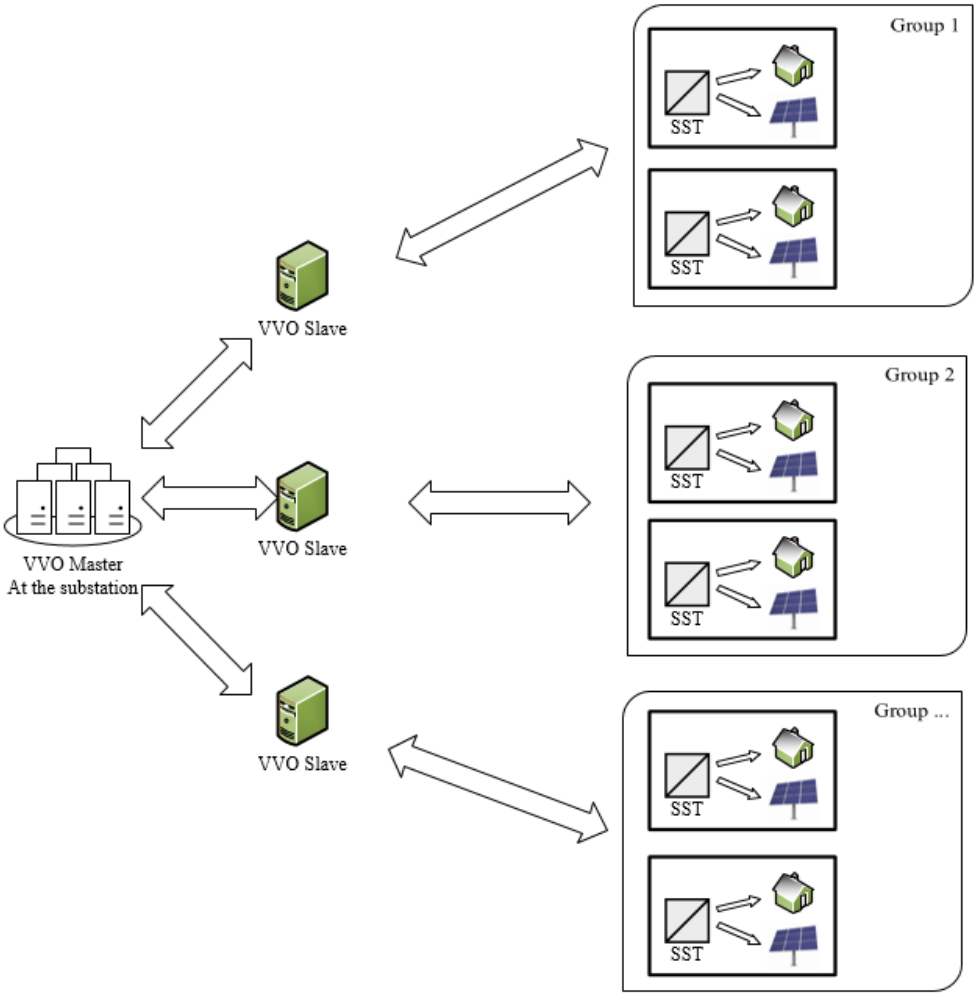

Figure 5.2 Architecture of the proposed VVO scheme

In this work, the proposed VVC scheme is implemented on the open source operating system, DGI, which can launch various DMS applications as show in Figure 5.1 based on a user defined scheduler. The VVO master and other DMS applications are programmed as sub-routines of DMS applications on the DGI system installed at the substation. In the field, each VVO slave is programmed as a sub-routine of DGI on a microprocessor which manages a group of SSTs.

5.2 Basic Requirements for the Proposed VVO scheme

To implement the proposed VVO to control the actual devices in a smart distribution system, requirements in the following aspects need to be considered:

- Data requirement

  Since the proposed VVO is a model based approach, the VVO application should have access to the system model data base as Figure 5.3 shows. In the proposed VVO scheme, the master VVO needs feeder impedance and topology data, and the slaves need the capacity of the SSTs.

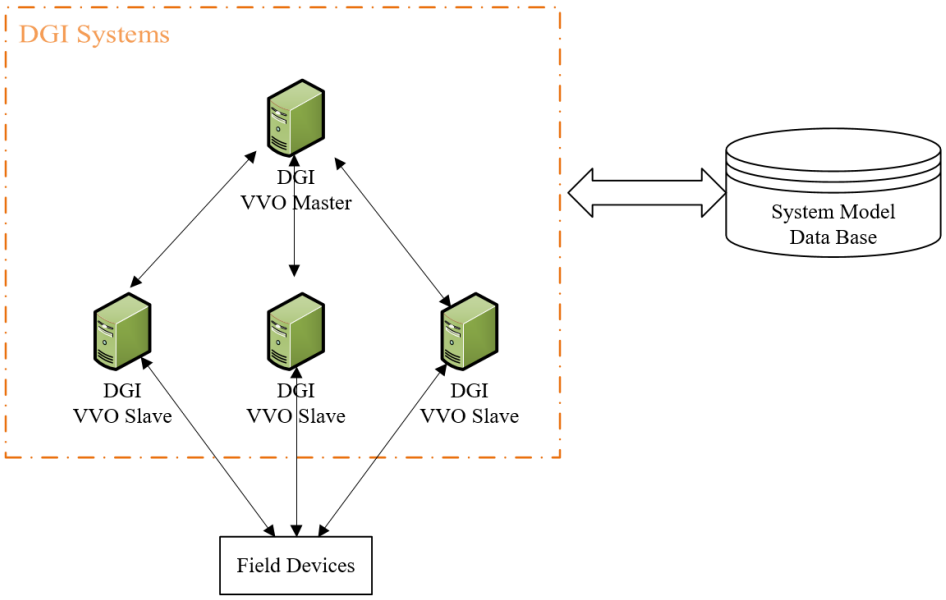

Figure 5.3 Architecture of proposed VVO

As shown in section 1.2, both voltage magnitude and angle are needed to formulate the optimization problem. However, the available monitoring data at SSTs are voltage magnitude, real and reactive power injection without measurement of voltage angle. For FREEDM systems with SSTs installed at all the nodes, the system

is fully monitored. In the simulation in previous chapter, a power flow solver is used to convert those power injection values into system states in phasor voltages. However, in reality due to the error of measurement and the unavailability of measurement at some locations in the system, state estimation (SE) technique is needed to provide an accurate and efficient estimation of the states of the system. Therefore, the real-time monitoring data required by the VVO application with SE should be the measurements that are sufficient to perform an effective state estimation in real-time. The minimum data requirement for SE can be identified by observability analysis [56].

- Communication requirement
    - Communication interface

      For the slaves to have access to the real-time monitoring data at field devices and to send control command to field devices, a communication interface is needed.
    - Throughput and Bandwidth

      Based on the master/slave topology of the communication network, the VVO master listens to different ports to receive packets from all slaves and sends packets to all slaves via ports as well. Therefore, the number of slaves in the system will influence the bandwidth (maximum possible data rate) requirement for the VVO master. Depending on the network topology, the amount of monitoring data and the amount of control commands, the estimation of throughput (actual data exchanged) at VVO slaves and VVO

master become complicated. At the slaves, communication to field devices might use different network protocols, such as DNP3 and IEC 61850. The diversity of communication protocols adds more complexity to estimate the throughput.

- Data Synchronization

  Since the formulation of VVO is based on the system states at a certain operating point, ideally input should belong to the same operating point in each run of VVO. However, for real-time implementation, data from different VVO slaves arriving at master VVO may not belong to the system states at the same instant. Therefore, investigation of latency and missing data is needed to make sure the input for VVO master represents the true system operating condition.

- Processing power requirement

  As proposed in previous chapter, the VVO master solves the optimization problem and the slaves allocate the reactive power injection of SST based on master's solution. Therefore, the master needs much stronger processing power than the slaves in the field.

5.3 Accomplishment

So far, the proposed VVC schemes has not been implemented in FREEDM systems completely. For testing purpose, only the Var Optimization function has been implemented as one subroutine in DGI. The real-time VVC has been tested on two systems, Hardware-In-the-Loop (HIL) test system, Green Energy Hub (GEH) system.

The implementation process involves in the following steps:

1) Source code conversion

   The proposed VVC schemes are developed and simulated in MATLAB. However, the implementation requires the VVC program to be part of the DGI. Therefore, the first step is to convert the MATLAB scripts into C++. Since the gradient VVC algorithm has intensive matrix operation, Armadillo library [57] (a C++ library for matrix operation) is utilized in the VVC C++ source code.

2) Integration on DGI

   As mentioned before, DGI is an open source operating system which can carry many applications including VVC. The intelligence of FREEDM systems is composed of many microprocessors with DGI, so-called DGI nodes. The architecture of the DGI node is shown in Figure 5.4. DGI works as a Round-Robin scheduler to schedule multiple applications. In the Round-Robin scheduler on DGI, time slices are assigned to each real-time application in equal portions and in circular order. After integrate source code of VVC as another module in DGI, the timing configuration needs to be configured properly, such that the time slice, “Phase”, assigned for VVC is long

enough to make VVC execute once and make sure the time for one cycle, “Round”, are configured properly as well.

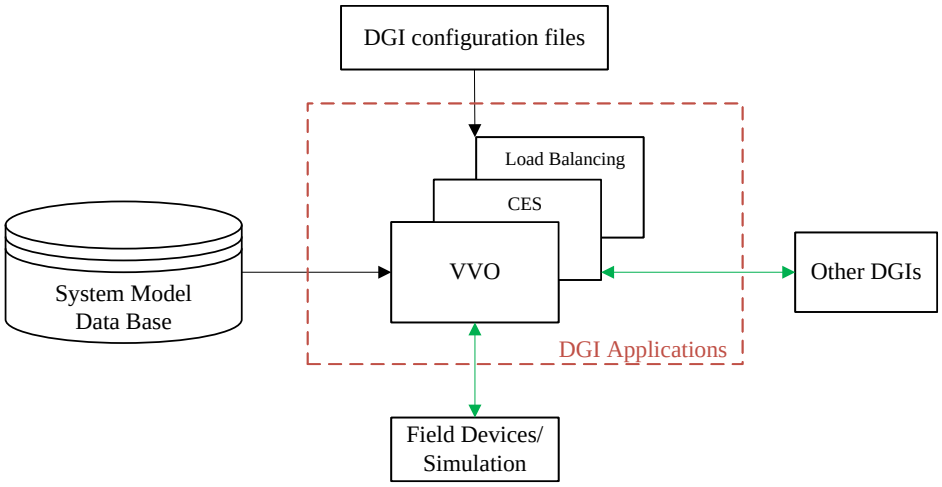

Figure 5.4 DGI architecture

3) Communication Configuration

Each DGI has the access to system model information, and bidirectional communication capability with field devices and other DGIs. To realize the data exchange between DGIs, the messages are structured in Google’s Protocol Buffers. Then DGIs can send/receive Google’s Protocol Buffers messages via TCP/IP protocol. As long as the Google Protocol file corresponding to VVO is configured, messages can be sent with a few simple commands inside the VVO module on DGI. To realize the data exchange between DGI and simulation system or field devices, each DGI has an “adapter” to configure the signals coming from/going to various devices and simulations. This adapter maps the signals to the names that DGI can recognize.

5.3.1 Hardware-In-the-Loop Test System

In this section, the VVO implementation on FREEDM HIL testbed is presented. The HIL system is a small system with 7 SSTs simulated in RSCAD. Same as the FREEDM Notional System, SST is the only VVC devices in the system. Based on sensitivity analysis, the SSTs are divided into three groups, as shown in Figure 5.5. For each group, a VVO slave is assigned. Therefore, four DGI nodes are needed to implement the proposed VVO, one for the master and three for the slaves, as shown in Figure 5.3.

Figure 5.6 shows the hardware system of HIL test bed. DGI - RSCAD interface is shown in the dashed box. The RSCAD simulation, instead of communicating directly to DGI, relies on a server to collect all signals and forward them to DGI nodes.

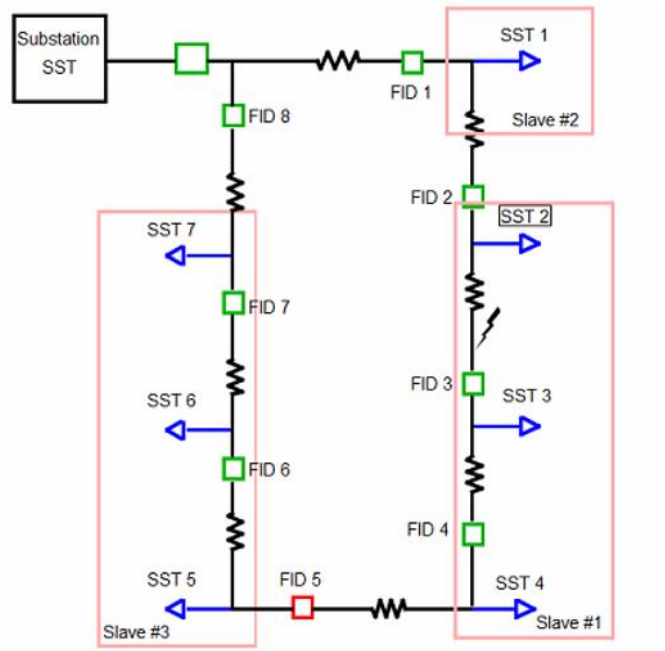

Figure 5.5 FREEDM HIL System

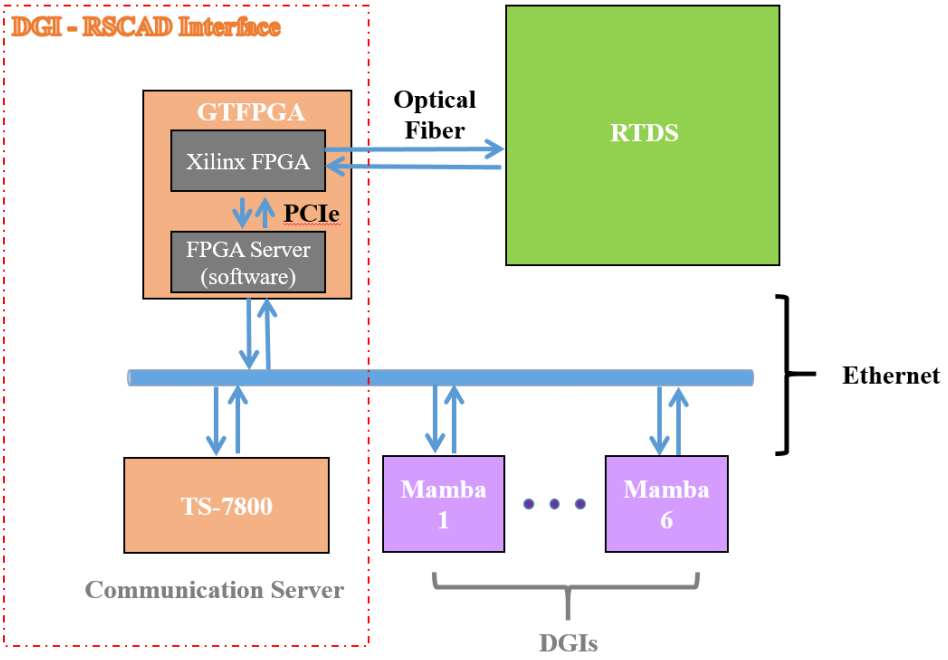

Figure 5.6 Hardware system of HIL Testbed [58]

To test if the proposed VVO can respond to real-time load change, a load profile is scheduled in the HIL system. Figure 5.7 shows how the system power loss, voltages and reactive power injection of SST2 change as the VVO adjust the control to follow load changes. The results indicate that the proposed VVO can adjust the reactive power injection of SST to reduce system power loss when load changes.

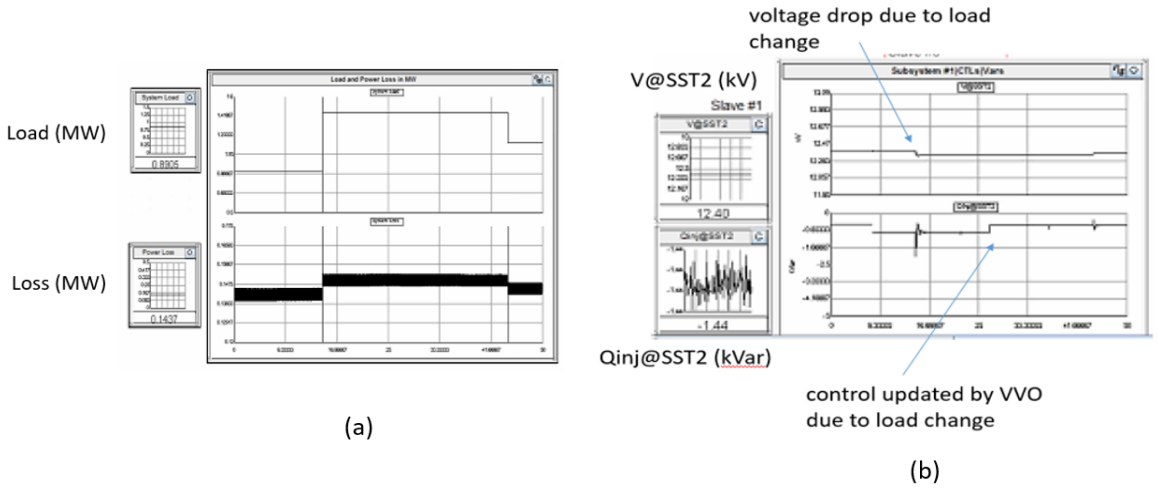

Figure 5.7 Results of VVO implementation on FREEDM HIL Testbed

5.3.1 Green Energy Hub Test System

In this section, the VVO implementation on FREEDM GEH testbed is presented. The GEH system, which is also an actual system located at NCSU, has 3 SSTs connected in series. Same as the FREEDM Notional System, SST is the only VVC devices in the system. Figure 5.8 shows the Hardware setup for GEH testbed. Due to the small size of the network, only one slave is used to control all the SSTs. The communication between VVC application on DGI and SSTs are realized by MQTT protocol. In this system, each SST is attached with a microprocessor and has the capability to publish/subscribe to MQTT broker. On the other hand, the DGI node with VVO slave has Paho MQTT client [59] installed such that it can communicate via MQTT broker. In the communication structure, as shown in Figure 5.8, VVO slave can subscribe the real and reactive load measurements that published by the SSTs, in the meanwhile SSTs can subscribe the control command published by VVO slave.

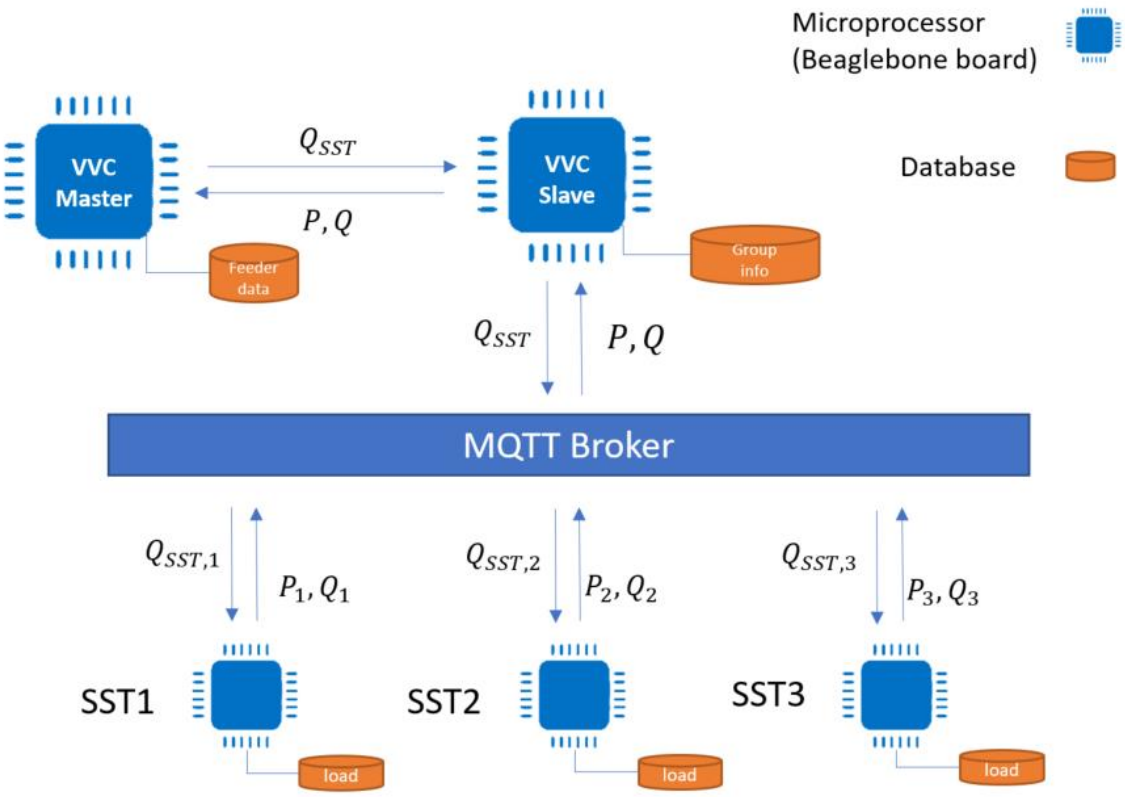

Figure 5.8 Hardware system of GEH Testbed

Figure 5.9 is a screenshot of the SCADA panel of GEH system, which shows the real-time power injection at each SST in numerical values. The meter plot at the bottom shows the system real-time load in kW. The three meter plots above it show the control command Q_{SST} that each SST received. As the load changes, the VVO on DGI generate control commands to minimize power loss, and it also adjust the commands as the load changes.

Figure 5.9 SCADA monitoring of GEH system

Chapter 6. Conclusion and Future Work

6.1 Conclusion

In this work, two VVC methods are proposed for smart distribution systems with DRER. The first one is a two-phase Volt/Var optimization performed in every control cycle, for example every 5 min. Simulation results demonstrate the effectiveness on regulating voltage and minimizing power loss as the system PV generation and load changes. The runtime also shows the feasibility to be implemented in real-time. To address the excessive tap operation issue in the first method, a two-level coordinated VVC scheme is proposed. With smart inverters and SSTs used for voltage regulation in a fast control loop, this method reduces the tap changes significantly. Results on full-PV deployment system and partial-PV deployment system show that the coordinated VVC scheme is effective and good for practical implementation. Simulation result also shows the scalability of the coordinated scheme by test on a large system, IEEE 123 system.

To investigate the load response to voltage variation due to VVC, a load model for small distribution transformers is proposed. Recursive method is adopted to estimate the parameters online. Simulation results demonstrate that the parameter calculated online is effective to estimate the demand change due to system voltage variation.

At last, the current progress of implantation of proposed VVO scheme is presented. The Var Optimization with master-slave architecture has been implemented successfully in two FREEDM testbeds, which confirms the capability of proposed schemes in practical implementation.

6.2 Future Work

The coordinated VVC scheme has been tested for different size of network and different PV penetration level in simulation. However, from implementation point of view, several functions within the coordinated VVC scheme have not been implemented on DGI, which includes the tap searching module and the module which optimize Var to correct voltage violation. Besides, communication requirements still need assessment for different size of network. This is because as the network size increases the number of slaves increases as well, which will affect the throughput and bandwidth requirement.

The VVC schemes proposed are to be implemented in real-time. Therefore, it should have the capability to deal with topology change of the network. A potential approach is to utilize the information from state estimation.

The online load parameter estimation proposed enables the VVC application to estimate the expected demand change due to VVC online. Therefore, those parameters can be used to form a more accurate load model in VVC algorithm and demand reduction could be formulate as another objective considered. The proposed load model and online load parameter estimation are tested on GridLab-D data which is still simulated data. Tests on field measurement data are still needed. Besides, since the load model proposed is for small transformers, online load parameter estimation need more tests to see how small the transformer should be.

REFERENCES

[1] "ANSI C84.1-2011 electric power systems and equipment : Voltage ratings (60 hertz)," 2011.

[2] G.G. Karady, A.Q. Huang and M. Baran, "FREEDM system: An electronic smart distribution grid for the Future," in *PES Transmission and Distribution Conference and Exposition (T&D)*, May 2012, pp. 1-6.

[3] T. Gönen, *Electric power distribution system engineering*, 2nd ed., CRC Press, 2008.

[4] Don Wareham. *Step Voltage Regulators*, 2013 [Online]. available: http://www.cscos.com/wp-content/uploads/NY1839-Eaton-Regulators-D.Wareham.pdf.

[5] GE Grid Solution. *DTR Transformer Tap Changer Controller*, 2013 [Online]. available: https://www.gegridsolutions.com/multilin/catalog/dtr.htm.

[6] GE Grid Solution. *Multilin Voltage Regulator Controller*, 2017 [Online]. available: http://www.gegridsolutions.com/multilin/catalog/dgcv.htm.

[7] J.J. Grainger and S. Civanlar, "Volt/var control on distribution systems with lateral branches using shunt capacitors and voltage regulators part I: The overall problem," *IEEE Transactions on Power Apparatus and Systems*, vol. PAS-104, no. 11, pp. 3278-3283, November 1985.

[8] B.A.d. Souza and Almeida, Angelo M F de, "Multiobjective optimization and fuzzy logic applied to planning of the volt/var problem in distributions systems," *IEEE Transactions on Power Systems*, vol. 25, no. 3, pp. 1274-1281, August 2010.

[9] B. Uluski. *Volt/VAR Control and Optimization Concepts and Issues*, 2011 [Online]. available: http://cialab.ee.washington.edu/nwess/2012/talks/uluski.pdf.

[10] A. Borghetti, F. Napolitano and C.A. Nucci, "Volt/var optimization of unbalanced distribution feeders via Mixed Integer Linear Programming," in *Power Systems Computation Conference*, August 2014, pp. 1-7.

[11] Z. Shen, "Centralized and Decentralized Volt/Var Control Schemes for the FREEDM System,"PhD dissertation, North Carolina State University , 2013.

[12] M.E. Baran and I.M. El-Markabi, "A multiagent-based dispatching scheme for distributed generators for voltage support on distribution feeders," *IEEE Transactions on Power Systems*, vol. 22, no. 1, pp. 52-59, February 2007.

[13] S. Deshmukh, B. Natarajan and A. Pahwa, "Voltage/VAR control in distribution networks via reactive power injection through distributed generators," *IEEE Transactions on Smart Grid*, vol. 3, no. 3, pp. 1226-1234, Sept 2012.

[14] Y. Shi, Z. Shen and M.E. Baran, "A decentralized Volt/Var Optimization scheme for smart distribution systems," in *Power Energy Society Innovative Smart Grid Technologies Conference (ISGT)*, Sept 2016, pp. 1-5.

[15] DNV GL. *Short-term forecasting* [Online]. available: https://www.dnvgl.com/services/short-term-forecasting-3848.

[16] Cooper Power Systems by Eaton. *Integrated Volt/VAR Control*, 2014 [Online]. available: http://www.cooperindustries.com/content/dam/public/powersystems/resources/library/1100_EAS/B110014011.pdf.

[17] Electrical Technology. *SCADA System for Electric Distribution*, 2015 [Online]. available: http://www.electricaltechnology.org/2015/09/scada-systems-for-electrical-distribution.html.

[18] J.J. Grainger, S. Civanlar and K.N. Clinard, "Optimal voltage dependent continuous-time control of reactive power on primary feeders," *IEEE Power Engineering Review*, vol. PER-4, no. 9, pp. 59-60, Sept 1984.

[19] X. Feng and W. Peterson. Volt/VAR Optimization Reduces Losses, Peak Demands. *Electric Energy T&D Magazine*,2010(Feb), pp. 22-25.

[20] D.G. Luenberger and Y. Ye, *Linear and Nonlinear Programming*, 2nd ed., Springer, 2016.

[21] J. Nocedal, *Numerical Optimization*, 2nd ed. New York, Springer, 2006.

[22] R.A. Jabr, "Minimum loss operation of distribution networks with photovoltaic generation," *IET Renewable Power Generation*, vol. 8, no. 1, pp. 33-44, January 2014.

[23] X. Hu and R. Eberhart, "Solving Constrained Nonlinear Optimization Problems with Particle Swarm Optimization," in *6th World Multiconference on Systemics, Cybernetics and Informatics*, 2002, pp. 203–206.

[24] Z. Michalewicz and M. Schoenauer, "Evolutionary algorithms for constrained parameter optimization problems," *Evolutionary Computation*, vol. 4, no. 1, pp. 1–32, March 1996. http://dx.doi.org/10.1162/evco.1996.4.1.1.

[25] "1547a-2014 - IEEE standard for interconnecting distributed resources with electric power systems - amendment 1," *IEEE*, May 2014.

[26] 2015, "IEEE 1547 Standards for
Grid Integration of DER Overview and Current Activity," in *IEEE PES Seattle Chapter Meeting*, Jun 2015.

[27] A.J. Wood, B.F. Wollenberg and G.B. Sheblé, *Power Generation, Operation, and Control*, 3rd ed., Wiley, 2013.

[28] G. Ozdemir, S. Emiroglu and M. Baran, "Supervisory control for coordinating Volt/Var control devices on a distribution system," in *Power Energy Society Innovative Smart Grid Technologies Conference (ISGT)*, Sept 2016, pp. 1-5.

[29] M.E. Baran, E.A. Staton and J.W. Gajda, "A Distribution Feeder Simulator," in *the LASTED International Conference High Technology in the Power Industry*, Orlando, Florida, USA, 1997.

[30] N. Deeb and M. Shahidehpour, "Linear reactive power optimization in a large power network using the decomposition approach," *IEEE Transactions on Power Systems*, vol. 5, no. 2, pp. 428-438, June 1990.

[31] Z. Shen and M.E. Baran, "Gradient based centralized optimal Volt/Var control strategy for smart distribution system," in *PES Innovative Smart Grid Technologies Conference (ISGT)*, February 2013, pp. 1-6.

[32] Distribution System Analysis Subcommittee, "IEEE 34 node test feeder,". http://ewh.ieee.org/soc/pes/dsacom/testfeeders/.

[33] Y. Shi and M.E. Baran, "Assessment of Volt/Var control schemes at power distribution level," in *North American Power Symposium (NAPS)*, October 2015, pp. 1-5.

[34] G.K. Ari and Y. Baghzouz, "Impact of high PV penetration on voltage regulation in electrical distribution systems," in *Clean Electrical Power (ICCEP)*, Oct 10, 2011.

[35] Distribution System Analysis Subcommittee, "IEEE 123 node test feeder,". http://ewh.ieee.org/soc/pes/dsacom/testfeeders/.

[36] A. Arif, Z. Wang, J. Wang, B. Mather, H. Bashualdo and D. Zhao, "Load modeling - A review," *IEEE Transactions on Smart Grid*, vol. PP, no. 99, pp. 1-1 2017.

[37] F.S. Chassin, E.T. Mayhorn, M.A. Elizondo and Shuai Lu, "Load modeling and calibration techniques for power system studies," in *North American Power Symposium*, 2011, pp. 1-7.

[38] EPRI, "Advanced load modeling,", Sep 25, 2002. https://www.epri.com/#/pages/product/1007318/.

[39] D. Karlsson and D.J. Hill, "Modelling and identification of nonlinear dynamic loads in power systems," *IEEE Transactions on Power Systems*, vol. 9, no. 1, pp. 157-166, February 1994.

[40] Kundur and Prabha, *Power system stability and control*, 1st ed. New York, McGraw-Hill, 1994.

[41] S.Z. Zhu, Z.Y. Dong, K.P. Wong and Z.H. Wang, "Power system dynamic load identification and stability," in *International Conference on Power System Technology*, 2000, pp. 18 vol.1.

[42] J.V. Milanovic, K. Yamashita, S.M. Villanueva, S.Ž Djokic and L.M. Korunović, "International industry practice on power system load modeling," *IEEE Transactions on Power Systems*, vol. 28, no. 3, pp. 3038-3046, August 2013.

[43] W.W. Price, K.A. Wirgau, A. Murdoch, J.V. Mitsche, E. Vaahedi and M. El-Kady, "Load modeling for power flow and transient stability computer studies," *IEEE Transactions on Power Systems*, vol. 3, no. 1, pp. 180-187, February 1988.

[44] J.Y. Lim, P.S. Ji, A. Ozdemir and C. Singh, "Component-based load modeling including capacitor banks," in *Power Engineering Society Summer Meeting*, 2001, pp. 1204 vol.2.

[45] Z.Y. Dong, A. Borghetti, K. Yamashita, A. Gaikwad, P. Pourbeik and J.V. Milanović, "CIGRE WG C4.605 recommendations on measurement based and component based load modeling practice,", October 1, 2012.

[46] D. Simon, *Optimal state estimation*. Hoboken, NJ, Wiley-Interscience, 2006.

[47] P. Zarchan and H. Musoff, *Fundamentals of Kalman Filtering: A Practical Approach*, 4th ed. Washington, DC, American Institute of Aeronautics and Astronautics, Inc, 2015.

[48] L. Ljung, *System Identification*, 2nd ed. Upper Saddle River, NJ, Prentice-Hall, 2006.

[49] C. Wang, Z. Wang, J. Wang and D. Zhao, "Robust time-varying parameter identification for composite load modeling," *IEEE Transactions on Smart Grid*, vol. PP, no. 99, pp. 1-1 2017.

[50] A. Rouhani and A. Abur, "Real-time dynamic parameter estimation for an exponential dynamic load model," *IEEE Transactions on Smart Grid*, vol. 7, no. 3, pp. 1530-1536, May 2016.

[51] S. Pandey, A.K. Srivastava, P. Markham and M. Patel, "On-line estimation of steady-state load models considering data anomalies," *IEEE Transactions on Industry Applications*, vol. PP, no. 99, pp. 1-1 2017.

[52] Anonymous *DATAPORT FROM PECAN STREET* [Online]. available: https://dataport.cloud/.

[53] David P. Chassin, Jason C. Fuller and Ned Djilali, "GridLAB-D: An agent-based simulation framework for smart grids," *Journal of Applied Mathematics*, vol. 2014, pp. 1-12 2014. http://dx.doi.org/10.1155/2014/492320.

[54] GridLab-D. *Residential module user's guide* [Online]. available: http://gridlab-d.sourceforge.net/wiki/index.php/Residential_module_user's_guide.

[55] K.P. Schneider, J.C. Fuller and D. Chassin, "Evaluating conservation voltage reduction: An application of GridLAB-D: An open source software package," in *Power and Energy Society General Meeting*, July 2011, pp. 1-6.

[56] A. Abur, *Power system state estimation : theory and implementation*, CRC Press, 2004.

[57] C. Sanderson and R. Curtin, "Armadillo: A template-based C++ library for linear algebra," *The Journal of Open Source Software*, vol. 1, no. 2, Jun 10, 2016.

[58] I. Leonard, HIL Test Bed Communication, Oct.

[59] Eclipse Paho. *Embedded MQTT C/C++ Client Libraries* [Online]. available: https://www.eclipse.org/paho/clients/c/embedded/.

APPENDICES

Appendix A – Calculation of the gradient $\nabla f_u = \frac{\partial f}{\partial u}$

By the chain rule to the optimization problem represented by (1-1) to (1-4), we have the following

$$\frac{\partial f}{\partial u} = \frac{\partial f}{\partial g} \cdot \frac{\partial g}{\partial u} \qquad \text{(A-1)}$$

$$\frac{\partial f}{\partial x} = \frac{\partial f}{\partial g} \cdot \frac{\partial g}{\partial x} \qquad \text{(A-2)}$$

here $\frac{\partial f}{\partial u}$ and $\frac{\partial f}{\partial x}$ are row vectors. Equation (A-2) can be written as

$$\frac{\partial f}{\partial g} = \frac{\partial f}{\partial x} \cdot \left[\frac{\partial g}{\partial x} \right]^{-1} \qquad \text{(A-3)}$$

Substituting $\frac{\partial f}{\partial g}$ in (A-1) by (A-3), the gradient of power loss with respective to reactive power injection of SSTs, $\frac{\partial f}{\partial u}$, can be calculated, if $\frac{\partial g}{\partial x}$, $\frac{\partial f}{\partial x}$, and $\frac{\partial g}{\partial u}$ are known.

$\frac{\partial g}{\partial x}$ is the Jacobian matrix of power flow equations:

$$\frac{\partial g}{\partial x} = \begin{bmatrix} \frac{\partial \Delta P}{\partial \theta} & \frac{\partial \Delta P}{\partial V} \\ \frac{\partial \Delta Q}{\partial \theta} & \frac{\partial \Delta Q}{\partial V} \end{bmatrix} = J \qquad \text{(A-4)}$$

$\frac{\partial g}{\partial u}$ can be derived from (1-6):

$$\frac{\partial g}{\partial u} = \begin{bmatrix} \frac{\partial \Delta P}{\partial Q_{inj}} \\ \frac{\partial \Delta Q}{\partial Q_{\text{inj}}} \end{bmatrix} = \begin{bmatrix} 0 \\ I \end{bmatrix} \qquad \text{(A-5)}$$

$\frac{\partial f}{\partial x}$ can be obtained directly since *f* is function depends on *x* only [27].

$$\frac{\partial f}{\partial x} = \begin{bmatrix} \frac{\partial f}{\partial \theta} \\ \frac{\partial f}{\partial V} \end{bmatrix} \qquad \text{(A-6)}$$

The elements in (A-6) is the gradient of the objective function with respect to the node voltage magnitude and angle, $\frac{\partial f}{\partial \theta_i}$ and $\frac{\partial f}{\partial V_i}$. The calculation of those elements is shown as the following

$$\frac{\partial f}{\partial \theta_i} = 2 \cdot \sum_{j}^{i \neq j} G_{ij} V_i V_j \sin\left(\theta_i - \theta_j\right) \qquad \text{(A-7)}$$

$$\frac{\partial f}{\partial V_i} = 2 \cdot \sum_{j}^{i \neq j} G_{ij} \left[V_i - V_j \cos\left(\theta_i - \theta_j\right) \right] \qquad \text{(A-8)}$$

Hence, $\frac{\partial f}{\partial u}$ can be calculated by

$$\frac{\partial f}{\partial u} = \left(\frac{\partial f}{\partial x} \cdot \left[\frac{\partial g}{\partial x} \right]^{-1} \right) \cdot \frac{\partial g}{\partial u} \qquad \text{(A-9)}$$

Appendix B – Sensitivity Analysis on FREEDM IEEE 34 System

Table B.1 shows the sensitivity of power loss with respect to Var injection at nodes with SST. Average gradient is calculated by averaging the gradient of each phase at a node. K-means clustering technique is used to grouping the SSTs with similar gradient. The original data from Table B1 was adjusted as the following to make the grouping reflets both geographical proximity and gradient cluster.

1) Node 806 and 810 has almost zero gradient, therefore distance is adjusted to be almost same and gradient are changed to zero.
2) All distances were scaled such that they are not over-weighted in K-means clustering.

Table B2 shows the actual input of K-means and the clustering results. Node 856 is moved manually into Cluster "5" because of geographical proximity. The final clustering results can be found in Figure 2.18.

Table B1 Raw data to be clustered

Node ID	Distance from substation (ft)	Averaged sensitivity
806	4310	0.001217
810	42344	0.006709
820	153950	0.023203
822	167690	0.023195
824	114300	0.017312
826	117330	0.017301
828	115140	0.035231
830	135580	0.027843
858	177840	0.03014
834	183670	0.030145
844	185300	0.03014
846	188940	0.033438
848	189470	0.030126
860	185690	0.030137
836	188370	0.030129
840	189230	0.030126
838	193510	0.026143
864	179460	0.023648
890	183500	0.025213
856	159430	0.020929

Table B2 Input and output of K-means clustering with 6 clusters

Node ID	Adjusted distance	Adjusted sensitivity	Cluster ID
806	**0.431**	**0**	2
810	**0.42344**	**0**	2
820	1.5395	0.023203	1
822	1.6769	0.023195	1
824	1.143	0.017312	4
826	1.1733	0.017301	4
828	1.1514	0.035231	5
830	1.3558	0.027843	5
858	1.7784	0.03014	6
834	1.8367	0.030145	3
844	1.853	0.03014	3
846	1.8894	0.033438	3
848	1.8947	0.030126	3
860	1.8569	0.030137	3
836	1.8837	0.030129	3
840	1.8923	0.030126	3
838	1.9351	0.026143	3
864	1.7946	0.023648	6
890	1.835	0.025213	6
856	1.5943	0.020929	**1**

Appendix C – Results of two-phase VVC schemes on FREEDM IEEE 34 System

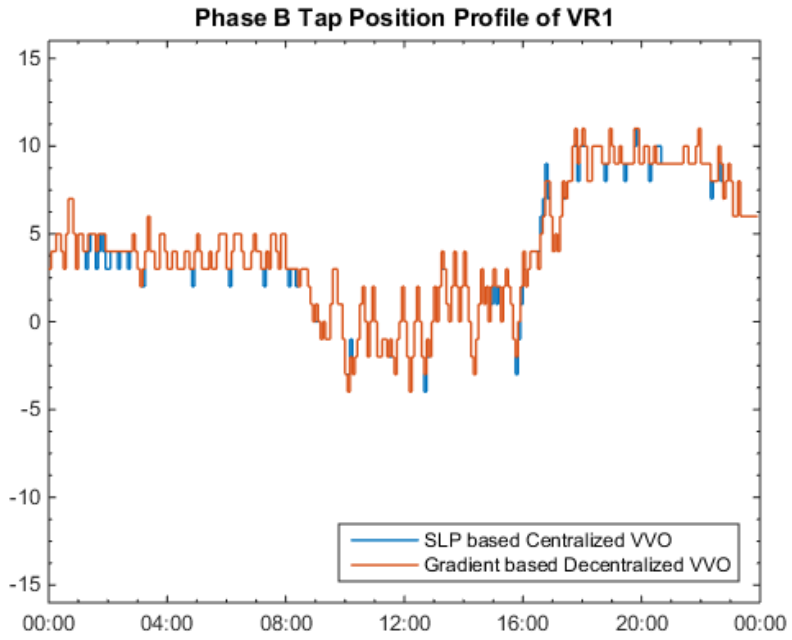

Figure C1 VR phase B tap positions during 24 hours

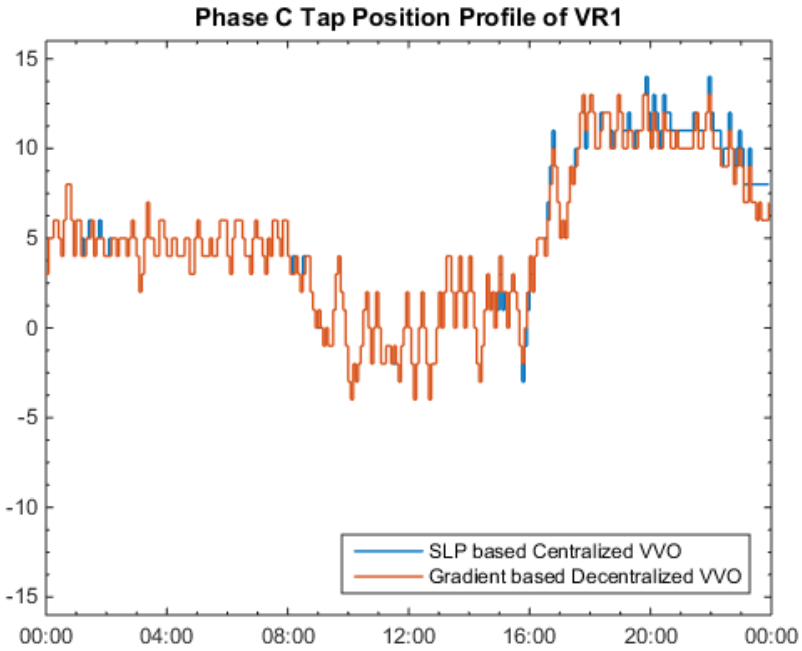

Figure C2 VR phase C tap positions during 24 hours

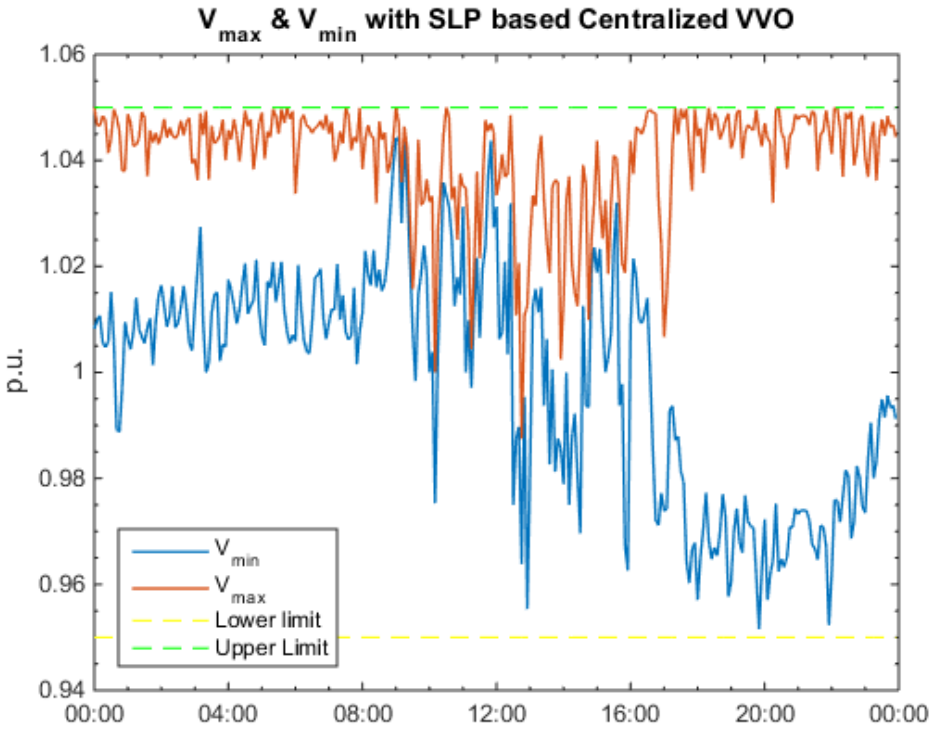

Figure C3 *Vmax* and *Vmin* profile of FREEDM IEEE 34 System

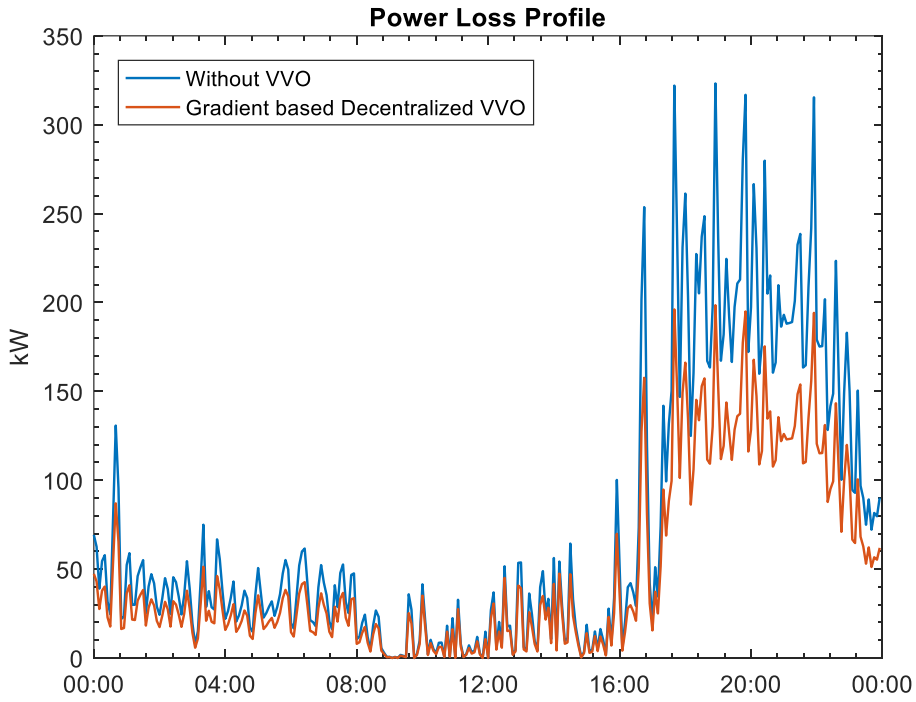

Figure C4 Power loss of FREEDM IEEE 34 system during 24 hours

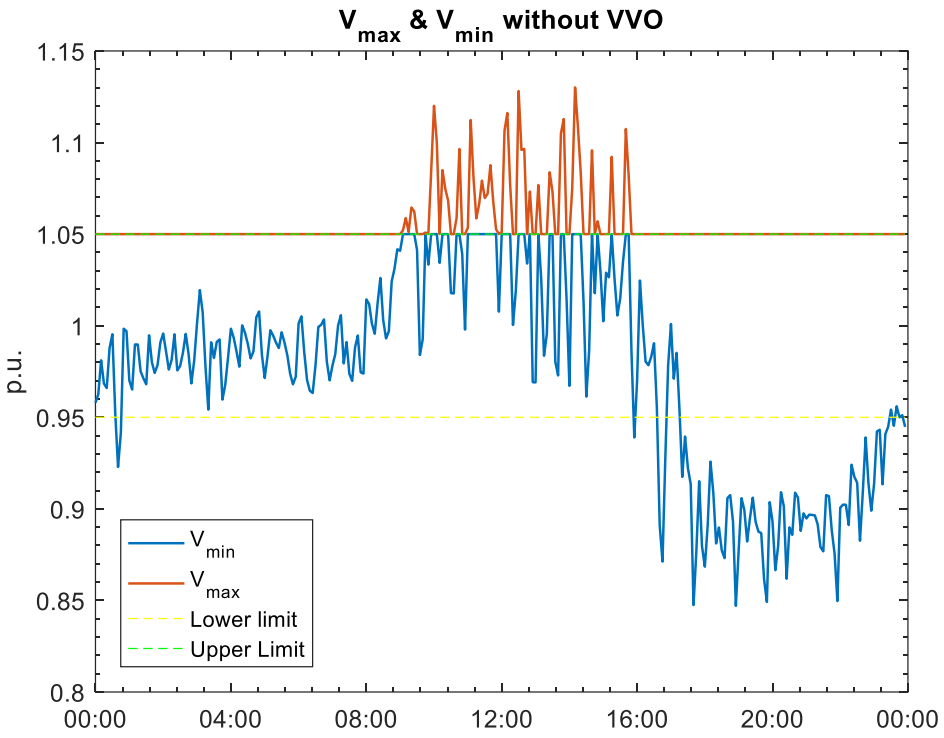

Figure C5 *Vmax* and *Vmin* profile of FREEDM IEEE 34 System

Appendix – D Results of coordinated VVC on modified IEEE 123 system

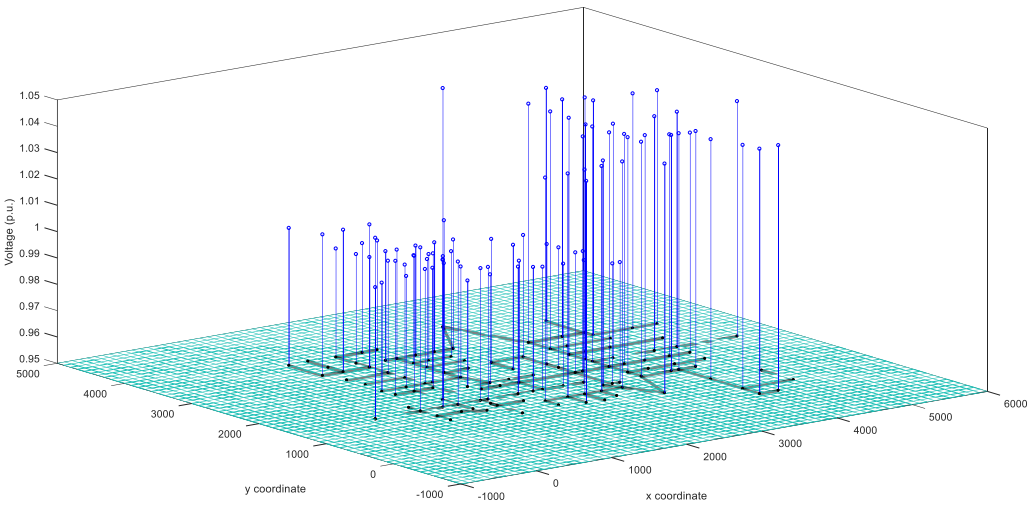

Figure D1 Feeder voltage after Var Optimization

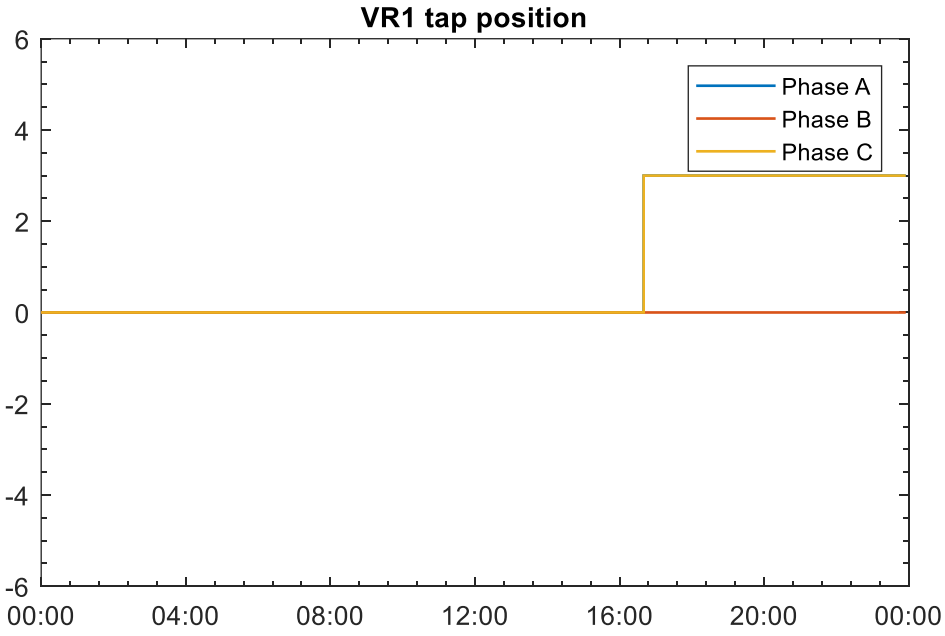

Figure D2 VR1 tap position with Coordinated VVC in a heavy load day

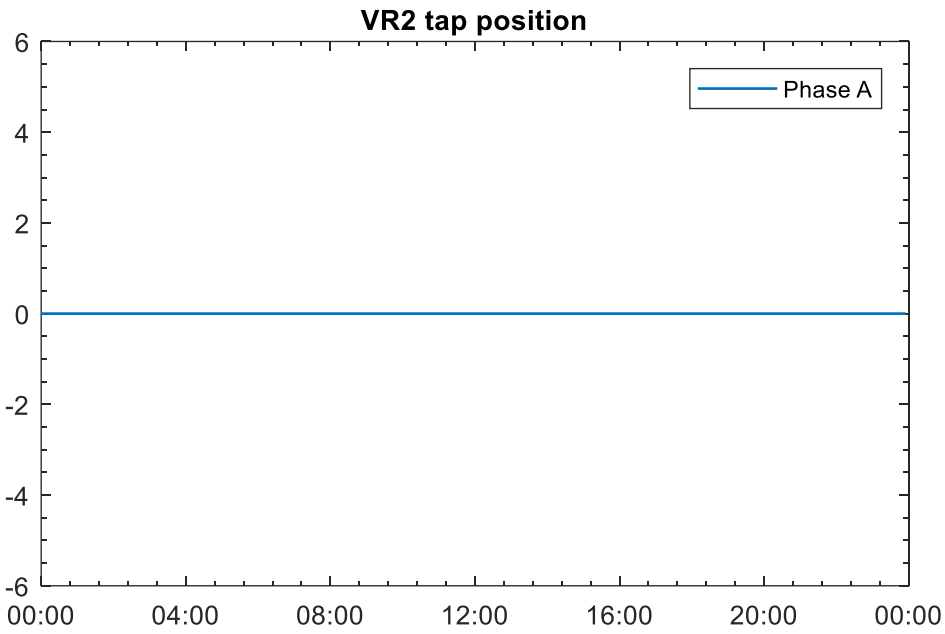

Figure D3 VR2 tap position with Coordinated VVC in a heavy load day

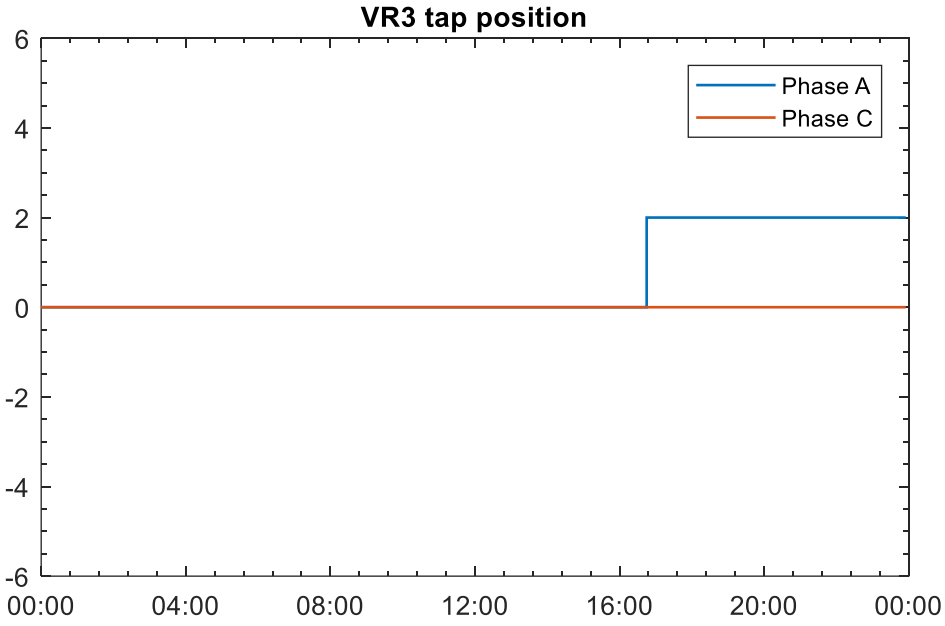

Figure D4 VR3 tap position with Coordinated VVC in a heavy load day

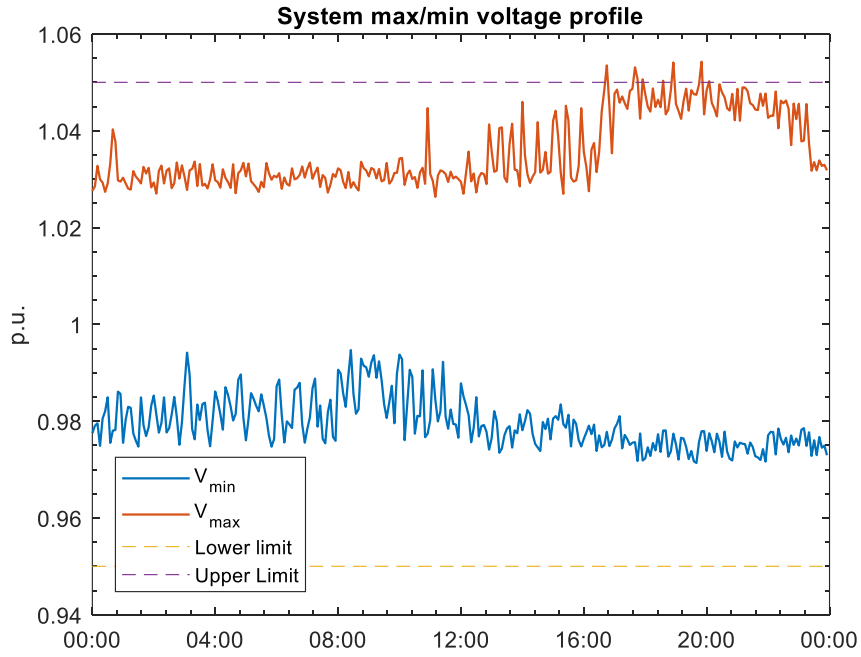

Figure D5 V_{max} and V_{min} profile of modified IEEE 123 system with conventional VVC in heavy load day

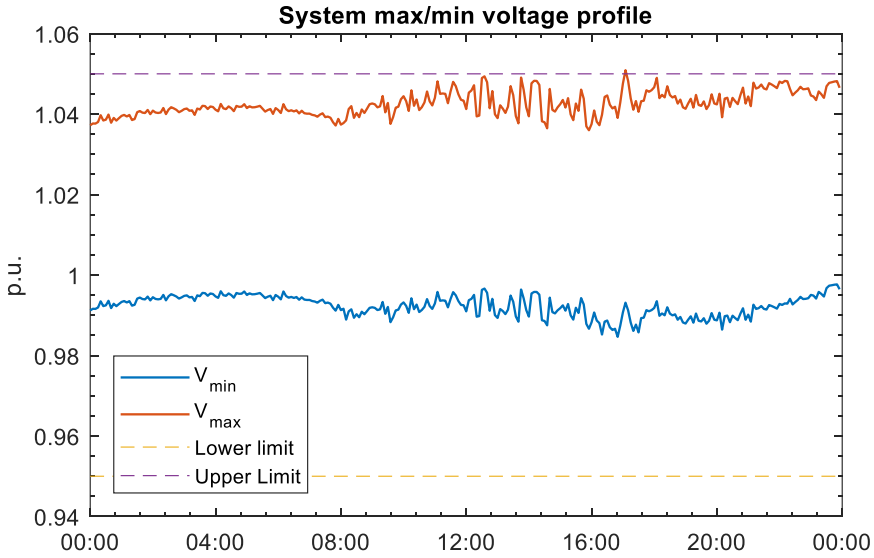

Figure D6 V_{max} and V_{min} profile of modified IEEE 123 system with conventional VVC in light load day

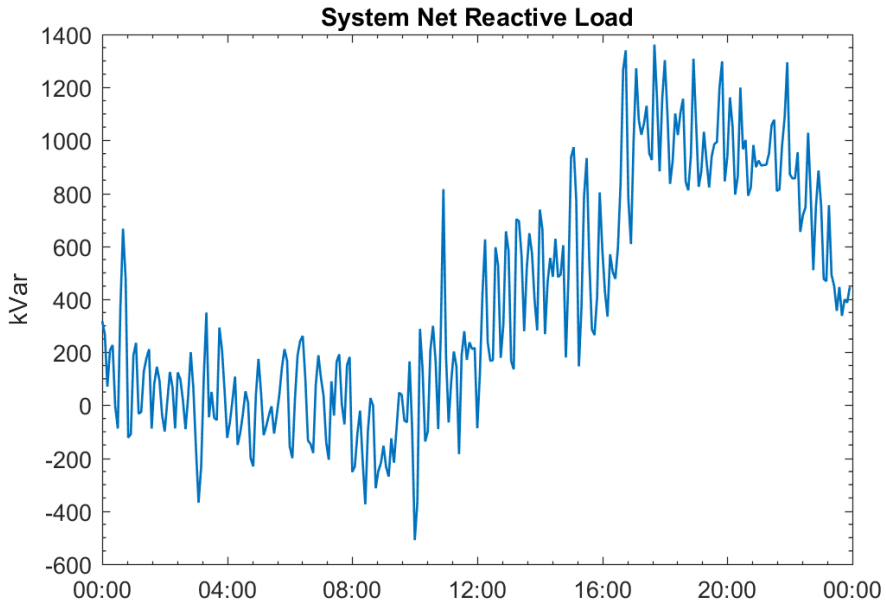

Figure D7 Total net reactive load of IEEE123 systems in heavy load day